TOPOLOGICAL AND DYNAMICAL FEATURES OF CATIONIC DETERGENT MICELLES IN AQUEOUS SOLUTION

A Doctoral Thesis

by

TOSHIYUKI SHIKATA

Submitted to

the Faculty of Science, Osaka University

1988

TOPOLOGICAL AND DYNAMICAL FEATURES OF CATIONIC DETERGENT MICELLES IN AQUEOUS SOLUTION

A Doctoral Thesis

by

Toshiyuki Shikata

Submitted to

the Faculty of Science, Osaka University

October, 1988

Approvals

October, 1988

TOPOLOGICAL AND DYNAMICAL FEATURES
OF CATIONIC DETERGENT MICELLES
IN AQUEOUS SOLUTION

A Doctoral Thesis

by

Toshiyuki Shikata

This thesis is approved as to style and content by

小高忠男
Member-in-Chief

幸本明夫
Member

高本俊夫
Member

蒲池幹治
Member

足立桂一郎
Member

ACKNOWLEDGMENTS

This thesis is written on the basis of my work carried out from 1985 to 1988 at the Department of Physical Chemistry, Niigata College of Pharmacy.

First, I wish to express my sincere appreciation to Professor Hirotaka Hirata, Department of Physical Chemistry, Niigata College of Pharmacy, who led me to this study on fantastic viscoelastic aqueous detergent systems and has always been giving me tolerant guidance and encouragement.

I next want to express my gratitude to Professor Tadao Kotaka, Department of Macromolecular science, Faculty of Science, Osaka University, for his guidance, encouragement, and valuable suggestions. I had gotten a lot of physical and chemical instruction from Professor Kotaka during my Bachelor and Graduated Courses from 1981 to 1985 in his laboratory.

I also express my gratitude to Dr. Hiroshi Watanabe, Kotaka's Laboratory, Department of Macromolecular science, Osaka University, for his good instruction in rheology and valuable discussions.

I also express my gratitude to Associate Professor Keiichiro Adachi and Mr. Shinsaku Uemura, Kotaka's Laboratory, Department of Macromolecular Science, Osaka University, for their encouragement and valuable suggestions.

Thanks are also due to Mr. Eiichi Takatori and Professor Kunihiro Osaki, Institute of Chemical Research, Kyoto University, for their contribution to Chapter VI concerning

the nonlinear viscoelastic behavior, valuable discussion and friendly cooperation.

I am indebted to Miss Yuko Sakaiguchi for her contribution to Chapter III. Thanks are also due to all the members of Niigata College of Pharmacy for their friendship.

I thank the Yukawa Scholarship Association, Faculty of Science, Osaka University, which had kindly provided me a scholarship on this study for six months in 1988.

Finally, I would like to acknowledge the constant encouragement of my wife, Mari, from the bottom of my heart.

Niigata

October, 1988

T. Shikata

Toshiyuki Shikata

CONTENTS

Chapter I

Introduction

I-1 Background

Detergent or surfactant molecules usually consist of hydrophilic and hydrohobic groups. When their hydrophilic portions are cationic such as ammonium and pyridinium salts, they are called cationic surfactants. When the parts are anionic groups such as carboxylate and sulfonate, they are called anionic surfactants. On the other hand, surfactant bearing no ionizable groups are called nonionic or neutral surfactants.

These surfactants are generally soluble or molecularly dispersed in water only to a certain limited extent, but they form intermolecular aggregates called micelles when their concentration exceeds a certain threshold called the critical micelle concentration (CMC).[1-5] Physical properties of the surfactant solutions such as viscosity, osmotic pressure, electric conductivity, and interfacial free energy change dramatically at this CMC.[1-5] The surfactant molecules aggregate to form micelles of a spherical shape with the hydrohobic parts being barried inside and the hydrophilic parts being arranged on the surface of the micelles.[1-5] In fact, the shape and aggregation number of the surfactant molecules in the micelles were determined by several experimental techniques such as osmotic pressure, the vapor

pressure and light scattering measurements on aqueous solutions of low surfactant concentrations and existence of the micelles of spherical shape was confirmed.[1-5]

In 1951, Debye and Anacker[6] found that a cationic surfactant, cetyltrimethylammonium bromide (CTAB), formed micelles each composed of over 4000 molecules in aqueous KBr solution. From the angular dependence of scattered light intensities from such a solution, they concluded that such large micelles were rod-like and rather stiff.[6]

Similar rod-like micelles have been identified in aqueous solutions of not only cationic surfactants but also some other anionic and nonionic surfactants.[7-10] Moreover, micelles of other various shapes such as disc-like, prolate, or oblate ellipsoids have been reported for several other surfactants.[11-13] We are intrigued particularly in cationic surfactant systems which are known to form rod-like or thread-like micelles in aqueous media.

When the concentration C_D of such a surfactant is increased in an aqueous medium containing a simple salt such as NaCl, spherical micelles are first formed at the concentration above CMC; CMC decreases with increasing concentration of the salt. Then, the molar mass of the micelles begins to rapidly increase as the detergent concentration is further increased beyond another critical concentration. From light scattering and nuclear magnetic resonance experiments,[4-6,14-18] it was confirmed that enormously long rod-like or thread-like micelles are formed at

this other critical concentration. Since the shape of the micelles transforms from sphere to rod, this phenomenon is sometimes called sphere-rod transition and the critical concentration, the second critical micelle concentration (CMC_{II}).[14]

The sphere-rod transition is also detected as a dramatic increase in solution viscosity.[21,22] In 1970s, Ozeki and Ikeda discussed the relation between the flexibility and molar mass of the rod-like micelles in dilute aqueous dodecylammonium chloride (DDAC) solutions with added NaCl.[22] They employed a wormlike cylinder model proposed by Yamakawa and Fujii[23,24] to estimate the persistent length of the micelles. They concluded that the persistent length varies from about 45 nm to about 25 nm when the molar mass M increases beyond 10^6, and the flexibility of the micelles alters depending on M.[22]

On the other hand, studies on moderately concentrated surfactant solutions started in this 1980s.[25-30] Candau et al.[25-27] have investigated aqueous solutions of CTAB with KBr up to the concentrations as high as 0.42 mol l^{-1} using static and dynamic light scattering techniques. They showed that the concentration C_D dependence of scattered light intensities and the mutual diffusion constant estimated from the dynamic light scattering data follow the power laws,[31] called the scaling theory, established for semidilute solutions of linear chain polymers.[25-27]

Imae and Ikeda have discussed static light scattering from

aqueous solutions of tetradecyltrimethylammonium bromide (TTAB) with NaBr with varying the detergent and salt concentrations, C_D and C_S.[28-30] They applied the scaling theory to analyze their light scattering data in terms of blobs[31] for entangled networks consisting of the rod-like micelles. They found that for the radius of gyration ξ_G of a blob with the molar mass M_ξ, which is a unit of the entanglement mesh with a size ξ called the correlation length,[31] a power law of the form $\xi_G \sim M_\xi^{0.54}$ holds independently of the salt concentration C_S of NaBr.[29] These results imply that the long flexible rod-like or thread-like micelles are entangling each other, just like flexible polymers are at semidilute conditions.[31]

This success of the scaling theory in semidilute rod-like or thread-like micellar solutions makes one think that the rod-like or thread-like micelles have very large (average) molar masses and are quite stable or very hard to break. However, the micelles are stabilized by intermolecular forces among the surfactant molecules but not by chemical bonds as in polymer molecules so that they should be in a state of the dynamic association-dissociation equilibrium with a certain characteristic time.

So far, rheological studies on aqueous solutions of cationic surfactants had been restricted only to viscosity measurement.[18,22] However, aqueous solutions of a few kinds of cationic surfactants have been known to exhibit very striking viscoelasticity even at very low concentrations.[32-35]

For example, in aqueous solutions of cetyltrimethylammonium salicylate (CTASal) with the concentration of 10^{-3} mol l^{-1}, bubbles recoil after cessation of stirring up.[35] Although the solutions exhibited these interesting rheological features, they had not attracted rheologists' attention for a long time until 1980s, Hoffmann et al. began to examine dynamic viscoelastic properties of several cationic surfactant systems quantitatively.[36-40]

Hoffmann et al. carried out dynamic viscoelastic measurement on aqueous solutions of alkyltrimethylammoium salicylate or alkylpridinium salicylate with varying detergent C_D and salt C_S concentrations.[36-40] Figure I-1 shows a typical example representing the frequency ω dependence of storage G' and loss G" moduli for an aqueous cetylpridinium salicylate (CPySal) solution with C_D = 5.0 x 10^{-2} mol l^{-1}.[37] The G' curve reaches a plateau in the high frequency region and the G" curve exhibits a maximum and a minimum. These features of the curves are just similar to those of concentrated polymer systems.[41] They concluded that there might be a temporary network formed by the rod-like micelles.[36-40] They also found that the rheological data such as the maximum relaxation time of the systems changed quite complicatedly with the detergent C_D and with the salt C_S concentrations.[36-40] Therefore, they could not clarify what is the origin of the elasticity of the systems and what is the most essential factor controlling the maximum relaxation time of the systems, although they collected not only a large body

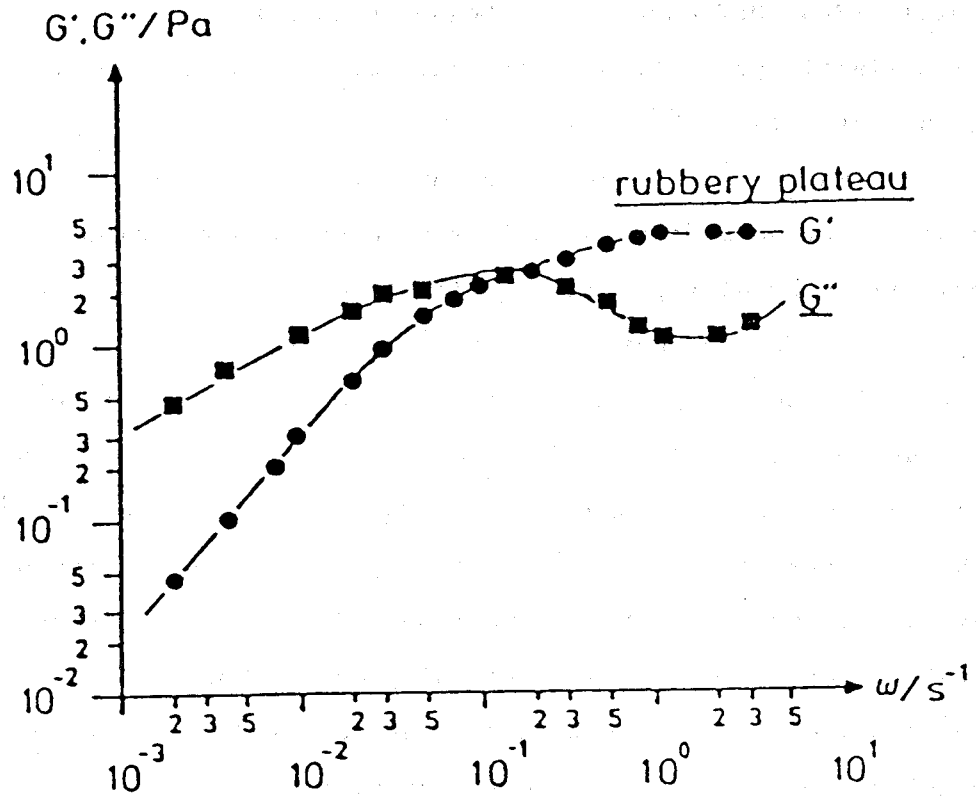

Figure I-1. Frequency ω dependence of the storage G' and loss G" moduli for the aqueous solution of cetylpyridinium salicylate (CPySal) with concentration C_D = 5.0 x 10^{-2} mol l^{-1} at 25°C.[37]

of interesting rheological data[36-40] but also data of the static and dynamic light scattering[42-44] and of small angle neutron scattering[42-44] for the same cationic detergent systems.

I-2 Scope of This Doctoral Thesis

The success of the scaling theory in semidilute aqueous cationic micellar systems implies that there might be a fully developed entanglement network among the rod-like or thread-like micelles of the surfactants in their solution just like in a polymeric system. In fact, some of the unique features of the rheological and other properties well correspond to the those of fully entangling polymeric systems. Therefore, the dynamics of aqueous cationic micellar systems should be understood from the dynamics of polymeric systems. However, the thread-like micellar systems must also have essentially different characteristics never identified in the polymeric systems.

A purpose of this thesis is to find out these essential features of the cationic thread-like micellar systems from experimental results of their unique rheology and to discuss these features on the well established basis of polymer rheology.

Then, we should first understand the rheological properties of cationic surfactant micellar systems through systematic investigation by adequately varying parameters, and

must clarify which factors essentially govern their viscoelastic properties. Moreover, we should identify the structure of the thread-like micelles which a cationic detergent forms, and also elucidate the superstructure termed the entanglement network composed of such thread-like micelles responsible for their viscoelasticity. Differences in topological interactions among the thread-like micelles and among polymer molecules are also discussed to clarify the essential dynamical features of the micellar systems different from those of polymer systems.

In attempts to solve these problems, we have carried out a series of systematic studies on aqueous solutions of a cationic detergent, cetyltrimethylammonium bromide, CTAB. This material was chosen because aqueous CTAB solutions with an aromatic salt or acid show the most pronounced viscoelastic behavior among all the aqueous cationic detergent systems so far studied.

This doctoral thesis consists of the following seven chapters.

Chapter II summarizes the methods and principles used for physical measurements.

In Chapter III, the results of electron microscopy are described to clarify the structures and the shape of the micelles formed in the aqueous viscoelastic detergent systems consisting of CTAB complexed with sodium salicylate (NaSal) and with salicylic acid (HSal). Nuclear magnetic resonance (NMR) measurements were also carried out on deuterium oxide

(D_2O) solutions (CTAB:NaSal/D_2O and CTAB:HSal/D_2O) of CTAB with NaSal or HSal to obtain molecular level information on the structure of the thread-like micelles in the viscoelastic solutions.

In Chapter IV, dynamic viscoelastic behavior of aqueous solutions (CTAB:NaSal/W) of CTAB with NaSal is fully investigated with varying the concentrations C_D of CTAB and C_S of NaSal. This system exhibits three types of viscoelastic behavior dependent on C_S when C_D is kept constant. The viscoelastic behavior of CTAB:NaSal/W systems discussed in comparison with that of concentrated polymer systems. The role of the free salicylate ions in the bulk aqueous phase on the viscoelastic properties of CTAB:NaSal/W systems is also discussed and an idea explaining the relaxation mechanism of CTAB:NaSal/W systems is proposed.

In Chapter V, dynamic viscoelastic properties of an aqueous system (CTAB:HSal/W) of CTAB with HSal are examined with varying the detergent and acid concentrations, C_D and C_A. Then, the results for this system are compared with those of the former CTAB:NaSal/W system, and distinct differences in viscoelastic features between the two systems are identified.

In Chapter VI, nonlinear viscoelastic behavior of the CTAB:NaSal/W and the CTAB:HSal/W systems such as shear stress relaxation at finite strain, steady shear flow and stress response at inception of steady shear flow are examined to obtain more detailed and meaningful information about their rheological properties, which can never be obtained through

the dynamic measurement. Results for these systems are compared each other and also compared with those of concentrated polymer systems to elucidate an essential difference in relaxation mechanisms of these micellar systems and of polymer systems.

Finally in Chapter VII, the principal results and conclusions derived from the present investigation are summarized.

REFERENCES

1) MacBain, J. W. Trans. Faraday Soc. 1913, 9, 99.

2) Hartley, G. S. Aqueous Solutions of Paraffin-Chain Salt; :Paris, 1936.

3) Debye, P. J. Phys. Colloid Chem. 1949, 53, 1.

4) Shinoda, K.; Nakagawa, T.; Tamamushi, B.; Isemura, T. Colloidal Surfactants. Some Physico-chemical Properties; Academic Press: New York, 1963.

5) Mukerjee, P.; Mysels, K. J. Critical Micelles Concentration of Aqueous Surfactant Systems; NSRDS-NBS 36, U.S. Government Printing Office: Washington, DC, 1971.

6) Debye, P.; Anacker, E. W. J. Phys. Colloid Chem. 1951, 55, 644.

7) Mazer, N. A.; Benedek, G. B.; Carey, M. C. J. Phys. Chem. 1976, 80, 1075.

8) Young, C. Y.; Missel, P. J.; Mazer, N. A.; Benedek, G. B.; Carey, M. C. J. Phys. Chem. 1978, 82, 1375.

9) Corti, M.; Degiorgio, V. Ann. Phys. 1978, 3, 303.

10) Robson, R. J.; Deniss, E. A. J. Phys. Chem. 1977, 81, 1075.

11) Mandel, A. B.; Ray, S.; Biswas, A. M.; Moulik, S. P. J. Phys. Chem. 1980, 84, 856.

12) Leibner, J. E.; Jacobus, J. J. J. Phys. Chem. 1977, 81, 130.

13) Tanford, C.; Nozaki, Y.; Rhode, M. F. J. Phys. Chem. 1977, 81, 1555.

14) Ozeki, S.; Ikeda, S. J. Colloid Interface Sci. 1982, 87, 424.

15) Hayashi, S.; Ikeda, S. J. Phys. Chem. 1980, 84, 744.

16) Jacobs, P. T.; Anacker, J. Colloid Interface Sci. 1973, 43, 105.

17) Maeda, H.; Ozeki, S.; Ikeda, S.; Okabayashi, H.; Matsushita, K. J. Colloid Interface Sci. 1980, 76, 532.

18) Ozeki, S. Hyomen 1982, 20, 632.

19) Kushner, L. M.; Hubbard, W. D.; Parker, R. A. J. Res. Natl. Bur. Stand. 1957, 59, 113.

20) Ikeda, S.; Ozeki, S.; Tsunoda, M. J. Colloid Interface Sci. 1980, 73, 27.

21) Ozeki, S.; Ikeda, S. Bull. Chem. Soc. Jpn. 1981, 54, 552.

22) Ozeki, S. Thesis: Nagoya University, 1981.

23) Yamakawa, H.; Fujii, M. Macromolecules 1973, 6, 407.

24) Yamakawa, H,; Fujii, M. Macromolecules 1974, 7, 649.

25) Candau, S. J.; Hirsch, E.; Zana, R. J. Colloid Interface Sci. 1985, 105, 521.

26) Candau, S. J.; Hirsch, E.; Zana, R. J. Phys.(Les Ulis, Fr.) 1984, 45, 1263.

27) Candau, S. In Surfactant Solutions; Zana, R. Ed.; Marcel Dekker: New York, 1987.

28) Imae, T.; Kamiya, R.; Ikeda, S. J. Colloid Interface Sci. 1985, 108, 215.

29) Imae, T.; Ikeda, S. J. Phys. Chem. 1986, 90, 5216.

30) Van De Sande, W.; Persoons, A. J. Phys. Chem. 1985, 89, 404.

31) De Gennes, P. G. Scaling Concept in Polymer Physics; Cornell University Press: Ithaca, New York, 1979.

32) Bungenberg de Jong, H. G.; Booij, H. L. Biocolloids and Their Interaction; Springer Verlag: Wien, 1956.

33) Lindman, B.; Wennerström, H. Phys. Rep. 1979, 1, 1.

34) Wennerström, H.; Ulmius, J.; Johansson, L. B. A.; Lindblom, G.; Gravsholt, S. J. Phys. Chem. 1979, 83, 2232.

35) Gravsholt, S. J. Colloid Interface Sci. 1976, 57, 576.

36) Hoffmann, H.; Rehage, H.; Platz, G.; Schorr, W.; Thurn, H.; Ulbricht, W. Colloid Polym. Sci. 1982, 260, 1042.

37) Hoffmann, H.; Rehage, H.; Reizlein, K.; Thurn, H. ACS Symp. Ser. 1985, 272, 41.

38) Hoffmann, H.; Rehage, H. Rheol. Acta 1982, 21, 561.

39) Rehage, H.; Hoffmann, H. Faraday Discuss Chem. Soc. 1983, 76, 363.

40) Hoffmann, H.; Löbl, M.; Rehage, H. In Physics of Amphiphiles: Micelles, Vesicles and Microemulsions; Degiorgio, V., Corti, M. Eds.; Elsevier: Amsterdam, 1985.

41) Ferry, J. D. Viscoelastic Properties of Polymers, 3rd ed.; Wiley: New York, 1980.

42) Hoffmann, H.; Platz, G.; Rehage, H.; Schorr, W. Adv. Colloid Interface Sci. 1982, 17, 257.

43) Hoffmann, H.; Kalus, J.; Thurn, H. Ber. Bunsenges. Phys. Chem. 1983, 87, 1120.

44) Kalus, J.; Hoffmann, H. J. Chem . Phys. 1987, 87, 714.

Chapter II

Experimental Methods and Principles

II-1 Introduction

In this study, measurements of dynamic viscoelasticity, steady shear flow, and stress relaxation at finite strain were carried out on aqueous solutions of cetyltrimethylammonium bromide (CTAB) complexed with sodium salicylate (NaSal) or salicylic acid (HSal). Transmission electron microscopic (TEM) observation was made out on the same systems to see directly structures of micelles and of higher order structures formed by the micelles. Proton nuclear magnetic resonance (NMR) measurement was carried out on deuterium oxide (D_2O) solutions of CTAB and NaSal or HSal to obtain information on the micelle structure of the CTAB:NaSal and CTAB:HSal complexes. In this chapter, the methods used in these experiments are described in detail along with their basic principles.

II-2 Materials

CTAB was purchased from Wako Pure Chemical Industries, Ltd., Osaka, and purified by recrystallization from methanol-acetone mixture. The chemical formula and physical characteristics of CTAB are listed in Figure II-1 and Table

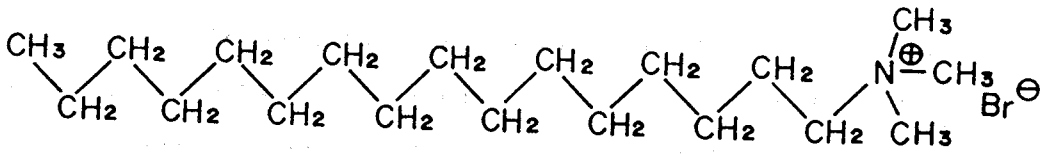

Figure II-1. A chemical formula representing a cationic detergent, cetyltrimethylammonium bromide (CTAB).

Table II-1. Physical properties of cetyltrimethylammonium bromide (CTAB).

molecular weight	364.48
melting point	237 - 243 ^{o}C
Kraft point	25^{o}C
critical micelle concentration	9.2 x 10^{-4} mol l^{-1} at 25^{o}C

concentration/mol l^{-1}	structures of aqueous solutions of CTAB
CMC < C < 0.3	spherical micelles
0.3 < C < 0.7	spherical and cylindrical micelles
0.7 < C	hexagonal liquid crystal

II-1, respectively. Sodium salicylate (NaSal), salicylic acid (HSal) and sodium bromide (NaBr) were of special grade and also purchased from the same company, and used without further purification. Water was distilled by a routine method.

We used deuterium oxide D_2O as a solvent instead of water to eliminate the NMR signal of protons in water molecules, because the ^1H signal of water was so strong that the objective signals could not be identified. The solutions were coded as CTAB:NaSal/D_2O and CTAB:HSal/D_2O.

II-3 Rheological Measurements

II-3-1 Dynamic Viscoelastic Measurement

For dynamic and steady flow measurements, we used a laboratory rheometer (model MR-3, Rheology Engineering, Kyoto) of a cone-and-plate type assembly schematically shown in Figure II-2. Three sets of cone and plate were used. The radius R and the angle β between the cone and plate were 16.0 mm and 3.0 ^{o}, 16.0 mm and 4.0 ^{o}, and 9.0 mm and 3.0 ^{o}, respectively.

When a linear viscoelastic material is subjected to a sinusoidal strain $\gamma(t) = \gamma_0 \sin\omega t$ at frequency ω, its stress response $\sigma(t)$ has the same frequency but has the phase difference δ. This situation can be written as

$$\gamma(t) = \gamma_0 \sin\omega t \qquad \text{(II-1)}$$

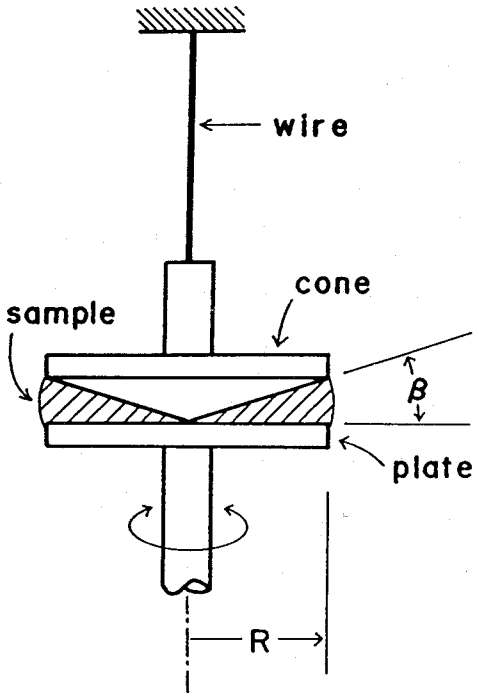

Figure II-2. Schematic illustration of the cone-and-plate geometry.

$$\sigma(t) = \sigma_0 \sin(\omega t + \delta) \qquad \text{(II-2)}$$

where γ_0 and σ_0 are the amplitudes of strain and stress, respectively. Then, the storage G' and loss G" moduli are defined as follows.[1]

$$G' = (\sigma_0 / \gamma_0) \cos\delta \qquad \text{(II-3)}$$

$$G'' = (\sigma_0 / \gamma_0) \sin\delta \qquad \text{(II-4)}$$

In dynamic measurement, the plate is subjected to a sinusoidal oscillation with an amplitude θ_{p0} and angular frequency ω. The displacement of the plate imposes a strain on the sample in the annular gap between the cone and plate. The torque on the cone generated by the sample is measured with a built-in electromagnetic transducer. The relation between displacement $\theta_p(t)$ of the plate and that $\theta_c(t)$ of the cone for the linear viscoelastic material can be written as follows

$$\theta_p(t) = \theta_{p0} \sin \omega t \qquad \text{(II-5)}$$

$$\theta_c(t) = \theta_{c0} \sin(\omega t + \psi) \qquad \text{(II-6)}$$

where ψ is the phase difference between the plate and cone, which is different from δ defined in eq II-2. The observed quantities such as θ_{p0}, θ_{c0} and ψ and the material parameters, γ_0, σ_0 and δ may related through the well known

Markovitz equation.[2]

$$1 + (1/P)e^{-i\psi} + (i/\eta^*)(A\omega - C/\omega) + \cdots = 0 \qquad \text{(II-7)}$$

Here, $P = \theta_{p0}/\theta_{c0}$ and $\eta^* = G''/\omega - iG'/\omega$ is a complex viscosity, with $i = \sqrt{(-1)}$. The instrumental constants A and C are defined by

$$A = 3I\beta / 2\pi R^3 \qquad \text{(II-8)}$$

$$C = \kappa A / I \qquad \text{(II-9)}$$

where I is the momentum of inertia of the cone systems including the detector arm and other attachments and κ is the torsion constant of the wire. Consequently, the storage G' and loss G" moduli can be estimated from the data of P and ψ as follows.

$$G' = (1 - \cos\psi/P)(A\omega^2 - C)/\{(\sin\psi/P)^2 + (1 - \cos\psi/P)^2\} \qquad \text{(II-10)}$$

$$G'' = -(\sin\psi/P)(A\omega^2 - C)/\{(\sin\psi/P)^2 + (1 - \cos\psi/P)^2\} \qquad \text{(II-11)}$$

II-3-2 Steady Shear Flow Measurement

In steady flow measurement, the plate is subjected to a steady rotation of angular velocity $\dot{\Omega}$ by using a built-in large torque motor. The apparent shear rate $\dot{\gamma}$ can be

calculated as follows.[1,3]

$$\dot{\gamma} = \dot{\Omega} / \beta \qquad \text{(II-12)}$$

The shear stress σ and the apparent viscosity η are obtained from the displacement θ_c of the cone as functions of the shear rate $\dot{\gamma}$.[2,4]

$$\sigma = 3\kappa \theta_c \beta / 2\pi R^3 \qquad \text{(II-13)}$$

$$\eta = \sigma / \dot{\gamma} \qquad \text{(II-14)}$$

II-3-3 Stress Relaxation Measurement

Shear stress relaxation measurement at finite strain was made by Mr. Takatori and Professor Osaki at Institute of Chemical Research, Kyoto University, who used a stress relaxation meter also of a cone-and-plate type assembly.[4] In stress relaxation measurement, the plate is subjected to a stepwise angular displacement θ_p. Then, the strain γ is calculated as

$$\gamma = \theta_p / \beta \qquad \text{(II-15)}$$

The shear stress σ when the strain γ is applied at $t = 0$ and kept constant for $t > 0$, as calculated by eq II-13 from θ_c, decreases with time t because of stress relaxation. In the stress relaxation measurement at finite (large) strain, the strain dependent relaxation modulus $G(t,\gamma)$ is defined as

follows.[1,4,5]

$$G(t,\gamma) = \sigma / \gamma \qquad \text{(II-16)}$$

We measured $G(t,\gamma)$ as a function of t and γ.

II-4 Transmission Electron Microscopic (TEM) Observation

We used a transmission electron microscope (JEOL 100CX) at an acceleration voltage of 80 KV to observe directly the structure, to say, the shape of the micelles formed by CTAB with NaSal or HSal in the solutions and also higher order structure formed by the micelles.[6] Copper grids coated with formvar-carbon film were used.

II-5 Proton Nuclear Magnetic Resonance (^{1}H NMR) Measurement

The microscopic (molecular level) structure of the thread-like micelles of CTAB with NaSal or HSal was investigated by ^{1}H NMR measurement. An NMR spectrometer (JEOL FX-200) with a superconducting magnet was operated at 199.5 MHz using internal lock of D_2O in the Fourier transform (FT) mode.[7] We did not determine the absolute values of chemical shift of signals but only differences in chemical shift positions of the same nuclei on phenyl rings of NaSal or HSal, which altered the positions by varying the concentrations of the solutes. Thus, we did not add an internal standard substance such as trimethylsilane (TMS).[7] We made all the measurements

on the same instrumental conditions and at the same temperature of 25 ^{o}C.

REFERENCES

1) Ferry, J. D. Viscoelastic Properties of Polymers, 3rd Ed.; Wiley: New York, 1980.

2) Markovitz, H. J. Appl. Phys. 1952, 23, 1070.

3) Oka, S. Rheology, vol. 3; Eirich Ed., Academic Press: New York, 1960.

4) Tamura, M.; Kurata, M.; Osaki, K.; Einaga,Y.; Kimura, S. Bull. Ins. Chem. Res. Kyoto Univ. 1971, 49, 43.

5) Fukuda, M.; Osaki, K.; Kurata, M. J. Polym. Sci., Polym. Phys. Ed. 1975, 13, 1563.

6) Meek, G. A. Practical Electron Microscopy For Biologists, 2nd Ed. Wiley: New York, 1976.

7) Farrar, T. C.; Becker, E. D. Pulse and Fourier Transform NMR; Introduction to Theory and Methods; Academic Press: New York, 1971.

Chapter III

Micelles of Cetyltrimethylammonium Bromide in Aqueous Solutions

III-1 Introduction

Information about the structure of materials under investigation is indispensable to interpret their physical properties. We thus have made effort to obtain information on the structures of micelles in viscoelastic aqueous detergent solutions, employing two methods of characterization. Transmission electron microscopy (TEM) was made to directly observe the structures of the micelles and the higher order structures formed by the micelles in aqueous solutions of cetyltrimethylammonium bromide (CTAB) with some added substances. Nuclear magnetic resonance (NMR) spectroscopy measurement was carried out on deuterium oxide solutions of the same CTAB to obtain information on the molecular level structure of the micelles. In this chapter, we present the results of TEM observation and NMR measurement on the micellar systems.

III-2 Experimental

III-2-1 TEM Observation

Solutions prepared for TEM observation were of two types. One type was aqueous solution of CTAB and NaSal coded as CTAB:NaSal/W. The concentrations C_D of CTAB and C_S of NaSal were 1.0×10^{-3} mol l^{-1}. The solution showed a pronounced elastic recoil phenomenon after stirring, the fact suggesting that it was viscoelastic. Another system was a set of solutions consisting of CTAB and HSal coded as CTAB:HSal/W. The concentration C_D of CTAB was again 1.0×10^{-3} mol l^{-1} but that C_A of HSal was varied from 1.0×10^{-4} to 1.0×10^{-3} mol l^{-1}. The solutions with C_A lower than 5.0×10^{-4} mol l^{-1} were not viscoelastic as judged from visual observation.

All the specimens for the TEM observation were stained by employing a negative staining technique with uranyl acetate.[1,2] The staining solution used was an aqueous solution of uranyl acetate with 2.0 weight %. A drop of the sample solution was supplied onto a grid coated with formvar-carbon film. Then, the excess sample solution on the grid was removed with a piece of filter paper. A drop of the staining solution was supplied onto the specimen, and the specimen was dried up as soon as possible. After the specimen was dried up completely, it was set on a TEM stage.

III-2-2 NMR Measurement

For NMR measurement the chosen ranges of C_D, C_S and C_A were essentially the same as CTAB:NaSal/W and CTAB:HSal/W

systems for rheological measurements described later in Chapters IV and V. However, the range of C_A was somewhat limited compared with that of the CTAB:HSal/W systems because of the difference in the solubilities of HSal molecules in D_2O ($C_A^{sd} \cong 1.1 \times 10^{-2}$ mol l^{-1} at 25°C) and ordinary water ($C_A^{sw} \cong 1.8 \times 10^{-2}$ mol l^{-1}). We examined mainly the chemical shift of the signals from phenyl protons of salicylate ions or salicylic acid molecules.

III-3 Results and Discussion

III-3-1 Phase Behavior of CTAB:HSal/W Systems

NaSal has a very high solubility in pure water so that the CTAB:NaSal/W systems exhibit a clear one-phase diagram in all the range of concentrations of CTAB and NaSal examined. Thus, we could rather optionally vary C_D of CTAB and C_S of NaSal of the CTAB:NaSal/W systems for each experiment. On the other hand, because HSal has a limited solubility in pure water, the CTAB:HSal/W systems have a clear one-phase in only a restricted concentration range of CTAB and HSal.

We first examined the phase behavior of the CTAB:HSal/W systems at 25°C. Figure III-1 shows the results, in which the acid concentration C_A is plotted against the detergent concentration C_D. When C_A of HSal is below C_D plus C_A^{sw}, the system gave a clear one-phase solution (open circles), while for $C_A > C_D + C_A^{sw}$, needle-like crystallites of HSal precipitate from the system, yielding a two-phase solution

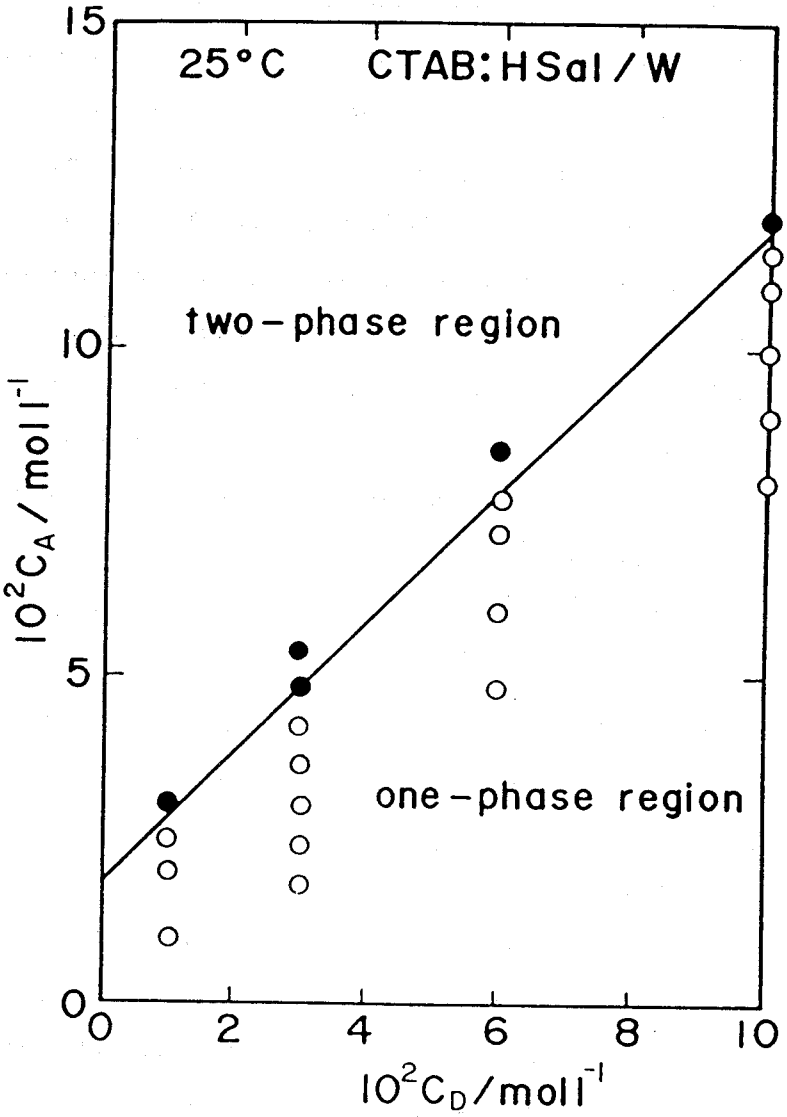

Figure III-1. Phase diagram for CTAB:HSal/W systems at 25°C. Closed circles represent two-phase solutions containing needle-like crystallites of HSal; and open circles, clear one-phase solutions.

(closed circles). In this figure, the area above the heavy solid line is the two-phase region where HSal crystallites and the micellar solution coexist, while the area below the line is the one-phase region of micellar solutions; CMC is much smaller than the C_D range studied here. The slope of the phase boundary line is approximately 1, which implies that the molar ratio of cetyltrimethylammonium ion (CTA^+) to HSal in the micelles is 1:1 in solutions on the phase boundary with concentration $C_A^s = C_D + C_A^{sw}$. The CTAB:HSal/W solutions for experiments such as TEM, NMR and rheology were belonging to the clear one-phase region in Figure III-1.

In D_2O, the solubility C_A^{sd} of HSal at 25°C is slightly lower than that C_A^{sw} in ordinary water. However, in saturated D_2O solutions with $C_A^s = C_D + C_A^{sd}$, the micelle is presumably a complex as in ordinary aqueous solutions.

III-3-2 TEM Observation

Figure III-2 shows a typical micrograph of CTAB:NaSal/W system with $C_D = C_S = 1.0 \times 10^{-3}$ mol l^{-1}. Thin thread-like objects of uniform thickness are seen in this photograph. These thread-like objects are likely to be micelles of CTAB and NaSal molecules. We thus call them thread-like micelles. They are densely entangling each other and appear to make rather a dense network structure. Terminals of the thread-like micelles were not found even in a picture of low magnification. Therefore, the length or the molecular weight of the thread-like micelles in this system should be

Figure III-2. A transmission electron micrograph for a CTAB:NaSal/W system with concentration C_D = 1.0×10^{-3} and C_S = 1.0×10^{-3} mol l^{-1}.

enormously large. The network structure seen in Figure III-2 should be responsible for the recoil phenomena.

We also made TEM observation on CTAB:HSal/W solutions with the same C_D = 1.0 x 10^{-3} mol l^{-1} and different C_A of 1.0 x 10^{-4}, 8.0 x 10^{-4}, and 1.0 x 10^{-3} mol l^{-1}. Figure III-3 shows a micrograph of the solution with C_D = 1.0 x 10^{-3} and C_A = 1.0 x 10^{-4} mol l^{-1}, which was an ordinary liquid with low viscosity. In this picture we see many spherical particles with about the same radius. These spherical particles should be micelles of CTAB and HSal molecules. It is likely that the spherical micelles seen in Figure III-3 cannot cause viscoelasticity for the solution. The solution was, in fact, not viscoelastic but only viscous.

Imae and Ikeda reported results of their light scattering studies and also the TEM observation on aqueous solutions of CTAB with sodium bromide, NaBr, as an added salt.[3,4] In the studies, they compared the dimension of the micelles observed on TEM and that determined from the light scattering data. Their TEM picture exhibited no thread-like micelles but presence of spherical micelles with radius matching the light scattering result.[4] Their result was also consistent with the viscosity measurement.[5]

The solution with C_A = 8.0 x 10^{-4} mol l^{-1} exhibited very weak viscoelasticity. Figure III-4 shows a TEM micrograph of micelles in this solution. The solution is a mixture of thread-like micelles with a uniform radius but different lengths and some spherical micelles similar to those seen in

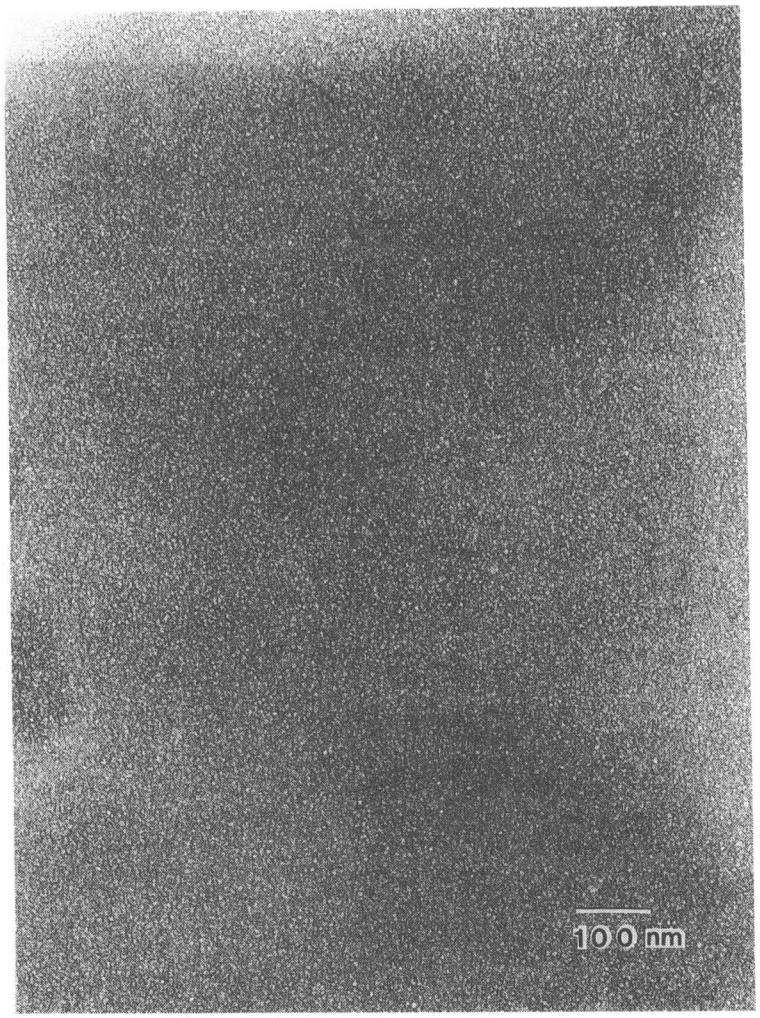

Figure III-3. A transmission electron micrograph for a solution of the CTAB:HSal/W system with C_D = 1.0×10^{-3} and C_A = 1.0×10^{-4} mol l^{-1}.

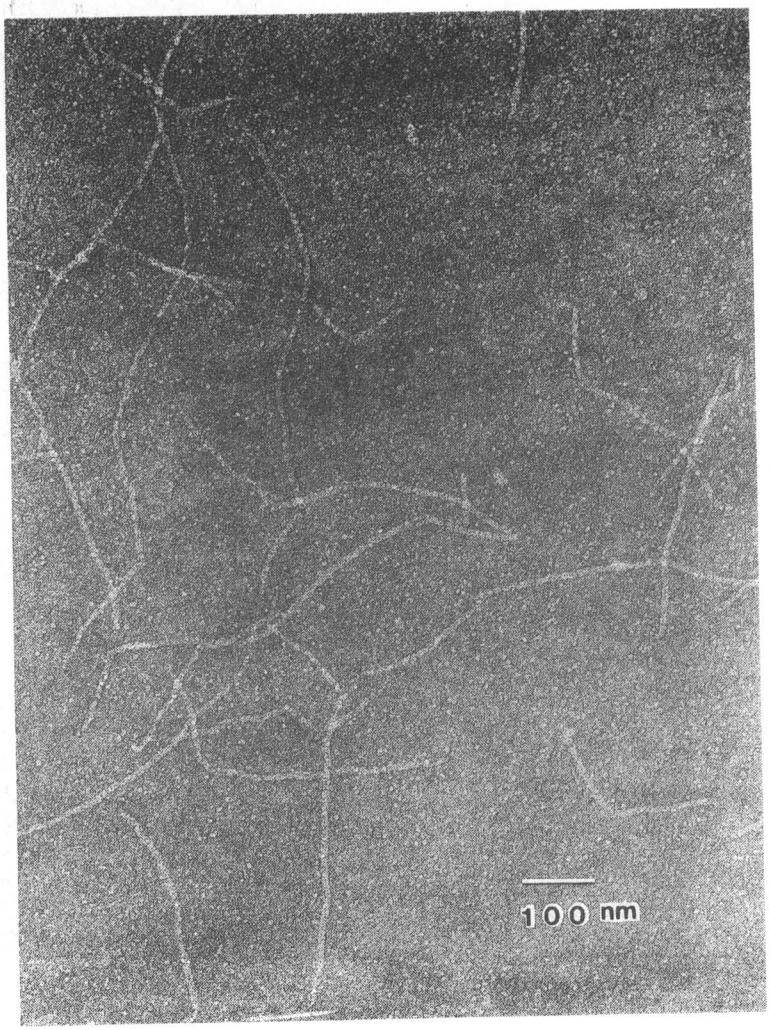

Figure III-4. A transmission electron micrograph for a solution of the CTAB:HSal/W system with C_D = 1.0×10^{-3} and C_A = 8.0×10^{-4} mol l^{-1}.

Figure III-3. Terminals of the thread-like micelles are identified in the picture in contrast to those in Figure III-2 so that the molecular weight of the thread-like micelles is finite. This figure makes one image the polymer molecules in dilute solution in which they not entangle each other.

It has been well known that the viscoelastic feature of dilute polymer solutions is successfully described in terms of the molecular theories proposed by Rouse and Zimm.[6-8] As described in the later Chapters IV and V, both of CTAB:HSal/W and CTAB:NaSal/W systems have conditions that their viscoelastic behavior are just similar to those of the Rouse-Zimm theories. Thus, the thread-like micelles seen in Figure III-5 might behave just like polymer molecules in solution without entanglements.

The microphotograph in Figure III-5 shows micelles of the solution with C_A = 1.0 x 10^{-3} mol l^{-1}. This photograph is similar to Figure III-2 of the CTAB:NaSal/W system and contains a number of long thread-like micelles. The micelles are densely entangling to form a network structure. This solution exhibited the most pronounced viscoelasticity in the three CTAB:HSal/W systems for TEM observation. The entanglement network formed by the thread-like micelles again should be responsible for the viscoelasticity.

The spectacular pictures of the entanglement network of the micellar systems in Figure III-3 and III-6 make us to expect that the micellar systems have rheological properties just similar to those of concentrated polymer systems, which

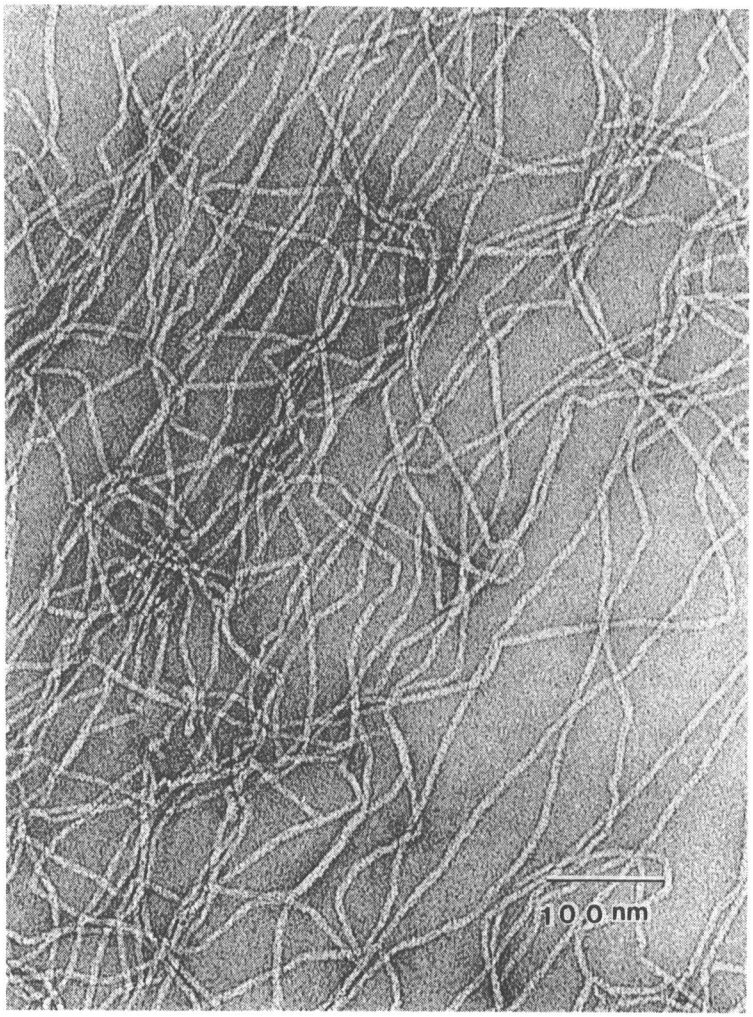

Figure III-5. A transmission electron micrograph for a solution of the CTAB:HSal/W system with C_D = 1.0×10^{-3} and C_A = 1.0×10^{-3} mol l^{-1}.

have the same concept of the entanglement.[6] However, such aqueous micellar systems have certain characteristic rheological features which have not been observed in concentrated polymer systems as described in later chapters.

The structure of the micelles changed systematically with increasing C_A as seen in Figures III-3 through III-5. This changing in the micelle structure with increasing C_A qualitatively corresponded to the change of rheological behavior. The thread-like micelles grew up and lengthened with increasing C_A. Consequently, they began to entangle each other to form a network structure and exhibited the pronounced viscoelasticity.

The results reported by Imae and Ikeda[3-5] for the aqueous CTAB solutions with NaBr are consistent with those of our studies. Their aqueous CTAB solutions with NaBr did not exhibit viscoelastic behavior but only high viscosity.[5] The thread-like micelles seen in their micrographs of the solutions with high viscosity were not so long, and the micelles looked more flexible than those in the present Figures III-3, III-5 and III-6.[4] It is likely that the thread-like micelles of CTAB alter the physical properties such as stability and flexibility with the added substances.

TEM observation is one of the most powerful method to study structures of materials directly. However, one must be careful to treat the obtained images because a lot of artificial factors occur in the preparation of specimens.[1,2] Therefore, quantitative discussion with above micrographs has

not been attempted.

III-3-3 NMR Analysis of CTAB:NaSal Micelles

The results described in the previous sections suggest that in the CTAB:NaSal/W systems some of salicylate ions (Sal^-) are immobilized in the thread-like micelles, presumably forming a certain complex with CTAB. However, other Sal^- are left free in the bulk water phase, affecting the stability of the micelles.

It is worthwhile from a colloid chemical point of view to evaluate the concentrations of immobilized and free ions from that of the total concentration C_S.[9,10] In the present study we attempted to determine the concentration C_S^* of the free Sal^- ions in the bulk water phase by NMR measurement.

We paid attention to the NMR signal of the para proton, 4H, in a Sal^- ion shown in Figure III-6. The resonance peak of the proton changes the position owing to the chemical shift, when the Sal^- ion is transferred from the bulk aqueous phase into the micelles. If the exchange rate of Sal^- between the two states is fast enough to cause a single time-averaged spectrum to appear, the position of the chemical shift ν for the 4H signal in frequency units is expressed as

$$\nu = (1 - f_{aq}) \nu_{mic} + f_{aq} \nu_{aq} \qquad \text{(III-1)}$$

where f_{aq} is the fraction of the 4H protons in the bulk aqueous (free) phase, and ν_{mic} and ν_{aq} are the chemical

shifts for the 4H protons in the micelle and bulk aqueous phase, respectively.[9-11]

If we replace the chemical shift ν expressed in the frequency unit by that δ given in ppm units, eq III-1 may be rewritten as

$$f_{aq} = (\delta - \delta_{mic}) / (\delta_{aq} - \delta_{mic}) \qquad \text{(III-2)}$$

Figure III-6 shows typical examples of the NMR signals for the CTAB:NaSal/ D_2O systems of C_D = 1.0 x 10^{-2} mol l^{-1}. The chemical shift of the 4H signal exhibits the most pronounced difference between the solution of NaSal alone (the spectrum at the top in Figure III-6) and the CTAB:NaSal/D_2O systems with C_S less than C_D (the four spectra from the top). When the concentration C_S of NaSal is low relative to C_D the 4H signal hops at once by 0.34 ppm toward the high magnetic field relative to the position of the free NaSal solution. However, it alters the position backward to the lower magnetic field with increasing C_S, and finally it approaches to the position of the free NaSal solution. Then, we assume that the chemical shift of the free NaSal solution represents δ_{aq}, while that of the system with C_S = 6.0 x 10^{-3} mol l^{-1} and $C_S C_D^{-1}$ = 0.6 represents δ_{mic}. This is because most of Sal^- in the latter system should be immobilized in the micelles, exhibiting the smallest chemical shift. Similar results were obtained for the systems with C_D = 1.0 x 10^{-1} mol l^{-1}. Thus, we estimated the fraction f_{aq} for these systems with eq III-2, using the

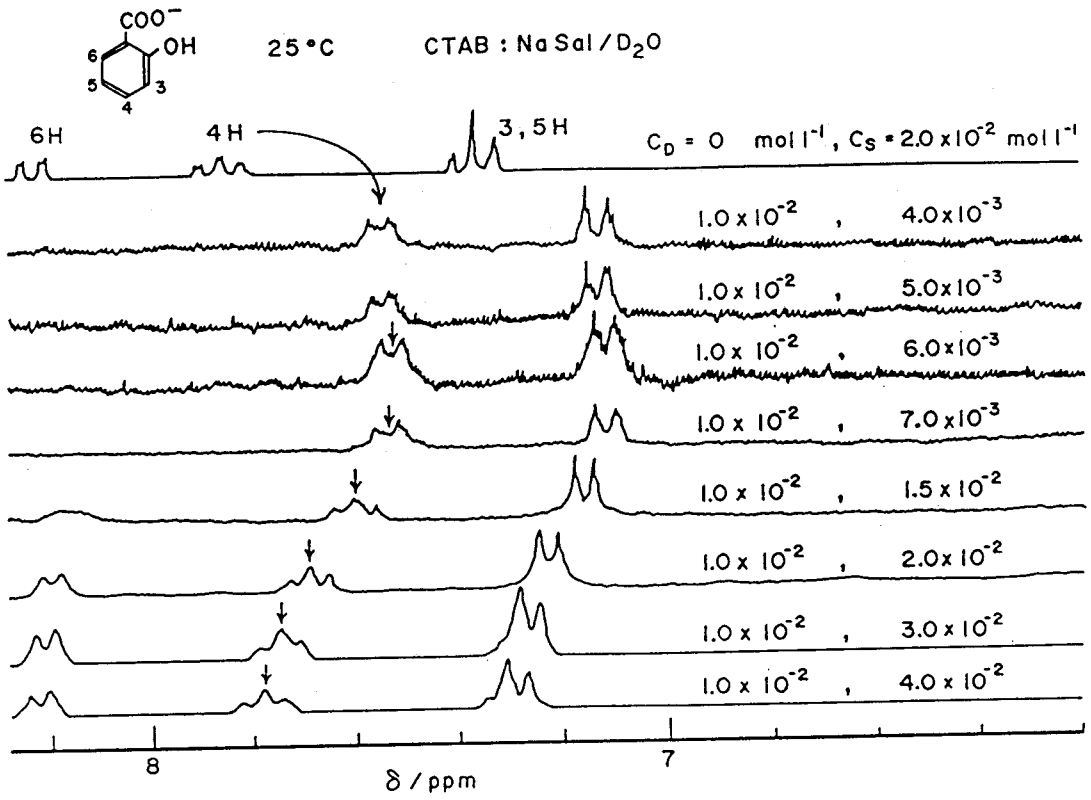

Figure III-6. ^1H NMR spectra for the aromatic region of salicylate ion of CTAB:NaSal/D_2O systems with C_D = 1.0 x 10^{-2} mol l^{-1}.

δ_{aq} and δ_{mic} values assumed as above. Obviously, the concentration C_S^* of free Sal^- in the bulk aqueous phase is $C_S^* = f_{aq} C_S$.

The value of C_S^* for the systems with $C_D = 1.0 \times 10^{-2}$ and 1.0×10^{-1} mol l^{-1} are plotted in Figure III-7 as a function of the total NaSal concentration C_S. The slope of the plot (A) for the systems with $C_D = 1.0 \times 10^{-2}$ mol l^{-1} is unity and the intercept is identical with C_D. Therefore, we conclude that in fact C_S^* represents the concentration of free Sal^- ions. For the systems with C_S sufficiently larger than C_D it can be approximated as

$$C_S^* = C_S - C_D \quad (\text{if } C_S > C_D) \qquad \text{(III-3)}$$

For the systems with $C_D = 1.0 \times 10^{-1}$ mol l^{-1} the same relation is also confirmed as seen in the plot (B) in Figure III-7. Eq III-3 is exactly followed by the systems with $C_S C_D^{-1} > 1.5$. However, the data points slightly deviate from eq III-3 in the region of C_S lower than 1.2×10^{-1} mol l^{-1} or of $C_S C_D^{-1}$ between 0.5 and 1.2.

Equation III-3 implies that the incorporation of Sal^- into the micelles appears to be most efficient in equimolar mixtures of CTAB to Sal^-. This behavior suggests that there is a special and strong interaction[12] acting between CTAB and Sal^- to form a unique and regular 1:1 complex.

On the other hand, the chemical shift of all the ring protons (see Figure III-6) provides us another information on

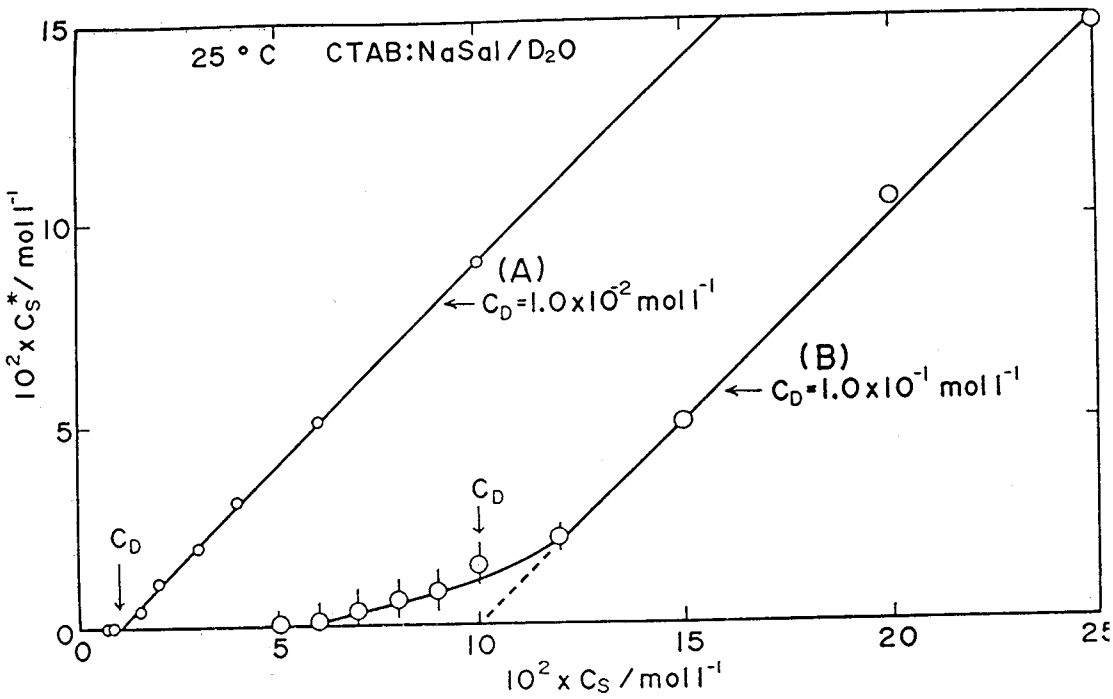

Figure III-7. Relationship between the concentration C_S^* of free Sal^- and the total one C_S for CTAB:NaSal/D_2O systems with C_D = 1.0 x 10^{-2} (A) and C_D = 1.0 x 10^{-1} mol l^{-1} (B).

the location of Sal^- in the micelles.[13,14] When compared with free Sal^-, Sal^- incorporated in the micelles exhibits the NMR signals of the 3,4 and 5H protons shifted toward the higher magnetic field, while that of the 6H proton is hardly shifted. This implies that the environment of the 3,4 and 5H protons becomes more nonpolar in the micelles, whereas that of the 6H proton has essentially the same polarity. Thus, the aromatic ring of a Sal^- ion should be located between the ammonium head groups of CTAB on the surface of the thread-like micelle and its hydroxyl and carboxyl groups should be sticking out of the micelle. Similar results of detailed NMR analyses on the location of the immobilized or solubilized molecules were published by several authors.[13,15]

III-3-4 NMR Analysis of CTAB:HSal Micelles

The phase behavior of CTAB:HSal/W systems seen in Figure III-1 suggests that the thread-like micelles are highly likely to be an equimolar complex between CTA^+ ions and HSal molecules (and/or Sal^- ions), as in the CTAB:NaSal/W systems. However, this information alone is not enough to discuss structural features of the CTA^+:HSal micelles in detail. Thus, we carried out NMR measurement on CTAB:HSal/D_2O systems to investigate the amount and the location of the immobilized HSal molecules in the micelles.

Figure III-8 shows typical NMR signals of phenyl protons of HSal in CTAB:HSal/D_2O systems with $C_D = 1.0 \times 10^{-1}$ mol l^{-1} and five different concentrations C_A with $C_A C_D^{-1}$ ranging from

0.5 to 1.10. The latter condition corresponds to the situation that the bulk D_2O phase is just saturated with HSal ($C_A^s \cong C_D + C_A^{sd}$).

In Figure III-8, we see that at $C_A = 5.0 \times 10^{-2}$ mol l^{-1} or $C_A C_D^{-1} = 0.5$, the signals of both <u>para</u> 4H and <u>ortho</u> 6H proton appear at the positions shifted by 0.34 and 0.07 ppm, respectively, from the positions for free HSal molecules in D_2O. These shifts are just the same as those found in CTAB:NaSal/D_2O systems at $C_A C_D^{-1} = 0.5$. Then, the signals gradually change their positions toward the higher magnetic field, as C_A is further increased. Similar behavior was observed for other CTAB:HSal/D_2O systems with $C_D = 3.0 \times 10^{-2}$ and 6.0×10^{-2} mol l^{-1}.

Figure III-9 shows plots of differences in the chemical shift, $\Delta\delta$, of 4H and 6H signals between those of the free and immobilized HSal molecules (or Sal^- ions) in D_2O solutions against the acid-to-detergent ratio $C_A C_D^{-1}$. We notice that the $C_A C_D^{-1}$ dependence of the chemical shift $\Delta\delta$ in the CTAB:HSal/D_2O systems are quite different from those of the CTAB:NaSal/D_2O systems seen in Figure III-6 which are reproduced here by the broken lines in the Figure III-9.

As described in the previous section, in the CTAB:NaSal/D_2O systems, when $C_S C_D^{-1}$ was low (<1) and all Sal^- ions were immobilized in the micelles, the 4H and 6H signals shifted by 0.34 and 0.07 ppm, respectively, to the high magnetic field from the positions for the free Sal^-. They remained essentially unchanged until the $C_S C_D^{-1}$ ratio reached

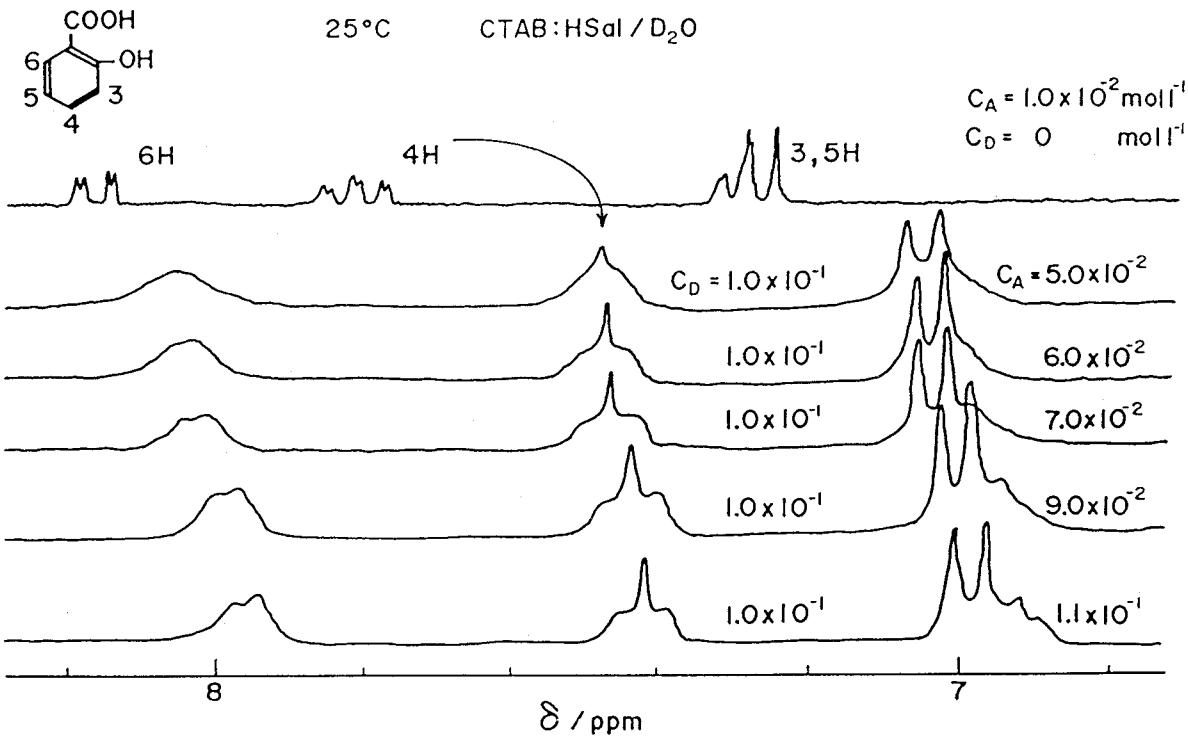

Figure III-8. ^1H NMR signals at 25°C of phenyl protons for HSal in D_2O solution and in the CTAB:HSal/D_2O systems with C_D = 1.0 x 10^{-1} mol l^{-1} and varying C_A.

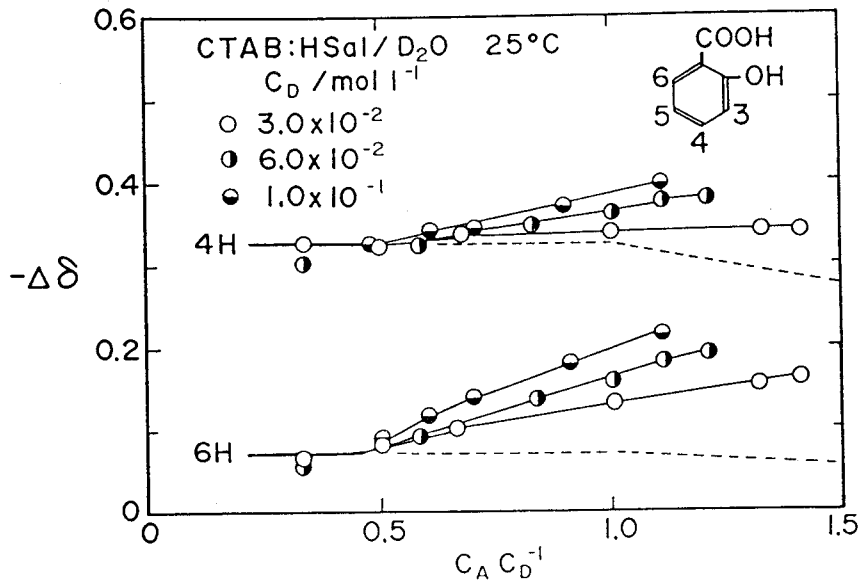

Figure III-9. Dependence on the acid-to-detergent $C_A C_D^{-1}$ ratios of the differences $\Delta\delta$ in NMR chemical shifts of <u>para</u> 4H and <u>ortho</u> 6H protons for CTAB:HSal/D_2O systems. The broken lines represent the similar data for CTAB:NaSal/D_2O systems.

approximately 1. However, with increasing $C_S C_D^{-1}$ beyond 1, the signals shifted backward to the lower magnetic field side, as shown in Figure III-9 by the broken lines. Moreover, the magnitudes of the shifts $\Delta \delta$ were essentially independent of C_D. Thus, we postulated that the Sal^- ions may assume two states: a free ion state in the bulk aqueous phase and an immobilized state in the micelles.

However, we see in Figure III-8 and III-9 that the present CTAB:HSal/D_2O systems behave quite differently from the CTAB:NaSal/D_2O systems: With increasing $C_A C_D^{-1}$ the signals shift to the higher magnetic field side further away from those of the free ions or HSal molecules; and the shifts $\Delta \delta$ are dependent on C_D as well.

To interpret these results, we postulate that HSal molecules may assume three different states: A free molecular (or ion) state in the bulk aqueous phase and two immobilized states in the micelles, which we call the free (a) state, and the immobilized (b) and (c) states, respectively. We further assume that the free (a) state is the same as defined already for the CTAB:NaSal/D_2O systems, and the other two (b) and (c) states correspond to the ones under the low and high magnetic field, respectively. Then, the observed chemical shift δ of the protons distributed over these three states with the chemical shift δ_i in the molar ratio $C_i C_A^{-1}$ (i = a, b, or c) may be expressed as,[13]

$$\delta = (C_a \delta_a + C_b \delta_b + C_c \delta_c) / C_A \qquad \text{(III-4)}$$

Employing the difference $\Delta\delta$ in the chemical shift from that δ_a of the free (a) state as a measure, we can rewrite eq III-4 as

$$\Delta\delta = \delta - \delta_a = (C_b\Delta\delta_b + C_c\Delta\delta_c) / C_A \qquad \text{(III-5)}$$

where $\Delta\delta_b = \delta_b - \delta_a$ and $\Delta\delta_c = \delta_c - \delta_a$ by definition.

In Figure III-9, we see that for both 4H and 6H protons the differences $\Delta\delta$ in the chemical shift for the CTAB:HSal/D_2O systems with the same $C_AC_D^{-1} = 0.5$ but with different C_D are the same with one another and also with that of the immobilized state of Sal^- ions in the CTAB:NaSal/D_2O systems at $C_SC_D^{-1} = 0.5$. This result implies that the (b) state at the low field is in much the same environment as that of the immobilized state in the CTAB:NaSal/D_2O systems. In other words, in the CTAB:HSal/D_2O systems with $C_AC_D^{-1} \leqq 0.5$, all the HSal molecules are presumably complexed with CTAB and immobilized at the sites in the (b) state, as in the CTAB:NaSal/D_2O systems. Thus, we assume that $C_A = C_b$ when $C_A \leqq 0.5C_D$, and $C_b = 0.5C_D$ when $C_A \geqq 0.5C_D$. Then, from the data for the systems with $C_AC_D^{-1} = 0.5$, we may assign for 4H protons $\Delta\delta_b^{4H} = -0.34$ ppm, and for 6H protons $\Delta\delta_b^{6H} = -0.07$ ppm.

As C_A is further increased beyond $0.5C_D$, some HSal molecules (or ions protonated to HSal) may presumably be pushed deeper into the micelles and begin to occupy the (c)

state sites, but some others might remain in the bulk aqueous phase, thereby, on the average, the proton signals shifting to the high field side.

Finally, when the concentration C_A of HSal reached the saturation C_A^s ($\cong C_D + C_A^{sd}$), the (c) state sites should now be fully occupied and $C_c = 0.5C_D$, because the molar ratio of CTA^+ to HSal in the micelles is 1:1 at the saturation C_A^s. We can write $C_a = C_A^{sd}$ (= 1.1×10^{-2} mol l^{-1}) and $C_b = C_c = 0.5C_D$ for the CTAB:HSal/D_2O systems at $C_A = C_A^s$. Then, from eq III-5, the difference $\Delta\delta^s$ in the chemical shift at $C_A = C_A^s$ may be given as,

$$\Delta\delta^s = 0.5C_D(\Delta\delta_b + \Delta\delta_c) / C_A^s \qquad \text{(III-6)}$$

Using the observed values of $\Delta\delta^s$ and the assigned value of $\Delta\delta_b$, we can determine from eq III-6 the difference $\Delta\delta_c$ as shown in the Table III-1. The values of $\Delta\delta_c^{4H}$ and $\Delta\delta_c^{6H}$ thus determined for the systems with three different C_D are nearly independent of C_D, as we have anticipated from the three-state model employed here.

The above analysis suggests that HSal molecules may assume two different types of immobilized sites in the thread-like micelles of the CTA^+:HSal complex. Both of the $\Delta\delta_c^{4H}$ and $\Delta\delta_c^{6H}$ values of the (c) state are significantly smaller than those of the (b) state as seen in Table III-1. In particular, the large difference between $\Delta\delta_c^{6H}$ and $\Delta\delta_b^{6H}$ than that between $\Delta\delta_c^{4H}$ and $\Delta\delta_b^{4H}$ suggests that the location of the

Table III-1. Chemical shift difference $\Delta \delta_c^{4H}$ and $\Delta \delta_c^{6H}$ of para and ortho protons, respectively, in the phenyl ring of HSal for the Immobilized state (c) in the thread-like micelles for CTAB:HSal/D_2O systems with several CTAB concentration C_D.*

C_D / mol $^{-1}$	3.0×10^{-2}	6.0×10^{-2}	1.0×10^{-1}
$\Delta \delta_c^{4H}$ / ppm	-0.59	-0.54	-0.54
$\Delta \delta_c^{6H}$ / ppm	-0.34	-0.37	-0.34

*Determined by eq III-6 with $\Delta \delta_b^{4H}$ = -0.34 ppm and $\Delta \delta_b^{6H}$ = -0.07 ppm.

(c) state sites should be in a much deeper position in the thread-like micelles relative to the location of the (b) state sites. On the other hand, the location of the (b) state sites should be equivalent to the location of salicylate Sal^- ions in CTAB:NaSal complex, in which sal^- ions should be arranged side by side of the cationic ammonium head groups on the micelle surface.[14-16]

Now, using eq III-5 with the assigned $\Delta\delta_i$ (i = b and c) values (and assuming $C_b = 0.5C_D$), we can estimate the concentration C_c of HSal occupying the (c) state sites. Accordingly, we can evaluate C_A^* (= C_a) of the free HSal in the bulk aqueous phase from observed $\Delta\delta$ data for the systems with $C_A \geqq 0.5C_D$ as follows,

$$C_A^* = C_A - 0.5C_D - (C_A\Delta\delta - 0.5C_D\Delta\delta_b) / \Delta\delta_c \qquad \text{(III-7)}$$

Figure III-10 shows plots of C_A^* vs C_A thus obtained by eq III-7 from the data shown in Figure III-9. The C_A^* values estimated from 4H and 6H proton signals show a fairly good agreement, again as anticipated from the model.

Because the solubility of HSal in D_2O at 25°C is somewhat lower than that in ordinary water, we could not determine C_A^* in all the C_A region covered by the viscoelastic measurements on the CTAB:HSal/W systems described in Chapter V. However, since the molar ratio in the micelles should reach 1:1 at the saturation, C_A^* should also approach the relation expressed by eq III-8 with increasing C_A beyond C_A^S in the D_2O solutions.

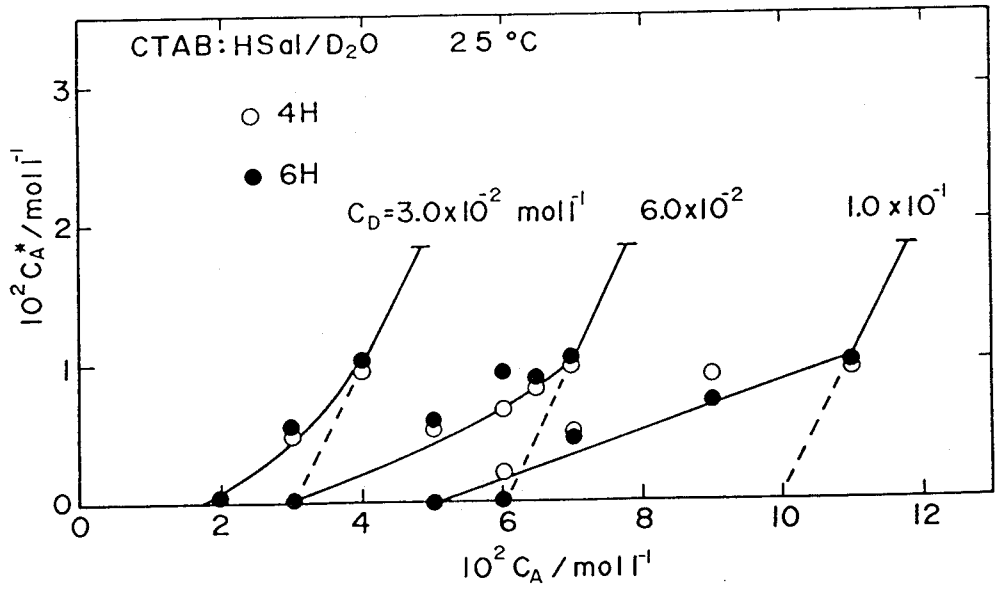

Figure III-10. Relationship between the concentration C_A^* of free HSal in the bulk aqueous phase and the added acid concentration C_A for CTAB:HSal/D_2O systems at 25°C determined by using eqs III-7 and III-8.

$$C_A^* = C_A - C_D \qquad \text{(III-8)}$$

Therefore, we assumed C_A^* to change as shown in Figure III-10 with the solid lines, and eq III-8 is valid when $C_D + C_A^{sw} > C_A > C_D + C_A^{sd}$.

III-3-5 Structural Features of the Micelles

The shapes of the thread-like micelles of the CTAB:NaSal/W and CTAB:HSal/W systems are quite similar to each other as seen in Figures III-2 and III-5. The micelles of both systems are enormously long and have uniform thin radii of nearly the same dimension. However, we could find out distinct points in the micelle structures of these systems through the NMR measurements.

The thread-like micelle of the CTAB:NaSal/W systems is a 1:1 intermolecular complex between CTA^+ cations and Sal^- anions, and Sal^- ions have only one immobilized site (state) in the micelle, which may would be the side of the ammonium head groups on the micelle surface.[14-16] On the other hand, the thread-like micelle of the CTAB:HSal/W systems is a 1:1 complex between CTA^+ cations and HSal molecules, and HSal molecules have two distinct immobilized states. One has the location equivalent to that of Sal^- ions in the micelles of CTAB:NaSal/W systems. Another has the location of much deeper position in the micelles relative to that of the former.

The HSal molecules in the different two states in the

micelles would contribute to relaxation of topological and dynamical interactions among the micelles in the systems presumably in somewhat different manners.

Since the thread-like micelle of CTAB:NaSal/W systems is a 1:1 complex between CTA^+ and Sal^-, the surface of the micelles should be electrostatically neutral, and an electrostatic interaction among the micelles should be weak. On the other hand, the surface of the thread-like micelles of the CTAB:HSal/W systems would be positively charged because the micelle is a complex between CTA^+ and HSal. An electrostatic interaction among the micelles of the CTAB:HSal/W systems should be much stronger than that of the CTAB:NaSal/W systems, and the electrostatic interaction would significantly affect dynamical features of the systems.

REFERENCES

1) Brenner, S.; Horne, R. W. Biochem. Biophys. Acta 1959,34, 103.

2) Hayat, M. A. Fixation for Electron Microscopy; Academic Press: New York, 1981.

3) Imae, T.; Kamiya, R.; Ikeda, S. J. Colloid Interface Sci. 1984, 99, 300.

4) Imae, T.; Kamiya, R.; Ikeda, S. J. Colloid Interface Sci. 1985, 108, 215.

5) Imae, T.; Ikeda, S. J. Phys. Chem. 1988, 92, 1548.

6) Ferry, J. D. Viscoelastic Properties of Polymers; 3rd ed., John Wiley: New York, 1980.

7) Rouse Jr., P. E. J. Chem. Phys. 1953, 21, 1272.

8) Zimm, B. H. J. Chem. Phys. 1956, 24, 269.

9) Nakagawa, T.; Tori, K. Kolloid Z. Z. Polym. 1964, 194, 143.

10) Muller, N.; Birkhahn, R. H. J. Phys. Chem. 1967, 71, 957.

11) Pople, J. A.; Schneider, W. G.; Bernstein, H. J. High Resolution Nuclear Magnetic Resonance; McGraw-Hill: New York, 1959.

12) Elowrthy, P. H.; Florence, A. T.; Macfarlane,C. B. Solubilization by Surface Active Agents and its Application in Chemistry and the Biological Sciences; Chapman Hall: London, 1968.

13) Eriksson, J. C.; Gillberg, G. Acta Chem. Scand. 1966, 20, 2019.

14) Donbrow, M.; Rhodes, C. T. J. Pharm. Pharmacal. 1966, 18, 424.

15) Bunton, C. A.; Minch, M.; Hidalgo, J.; Sepulveda, L. J. Amer. Chem. Soc. 1973, 95, 3262.

16) Bunton, C. A. Reaction Kinetics in Micelles; Plenum: New York, 1973.

Chapter IV

Dynamic Viscoelastic Behavior of Aqueous Solutions of Cetyltrimethylammonium Bromide with Sodium Salicylate

IV-1 Introduction

Aqueous solutions of cetyltrimethylammonium bromide (CTAB) containing sodium salicylate (NaSal), which are coded as CTAB:NaSal/W systems, exhibit pronounced viscoelastic behavior. Thread-like micelles in the systems are entangling or topologically interacting with each other as seen in the previous chapter and therefore exhibit the pronounced viscoelasticity similar to that of concentrated polymer solutions.

In this chapter, we deal with dynamic viscoelastic behavior of CTAB:NaSal/W systems, hoping to establish a relationship between the micelle structure and viscoelastic properties. We fully discuss dependence of their viscoelasticity on concentration C_D of CTAB and C_S of NaSal in comparison with those of flexible polymer solutions to understand the effect and the nature of topological interactions prevailing among the thread-like micelles in the CTAB:NaSal/W systems.

IV-2 Experimental

For rheological measurements on CTAB:NaSal/W solutions, the concentration C_D of CTAB was 6.0×10^{-3}, 1.0×10^{-2}, 2.0×10^{-2}, 3.0×10^{-2}, 6.0×10^{-2}, and 1.0×10^{-1} mol l^{-1}. On the other hand, the concentration C_S of NaSal was adjusted to the value from 1.8×10^{-3} to 6.0 mol l^{-1} for each solutions with given C_D. All the solutions were kept standing at 25°C before the measurements for at least two days for equilibration.

For the dynamic measurement the amplitude of oscillatory strain was 0.67 so that we could observe the linear viscoelastic response of the system. The angular frequency ω was varied in the range between 6.28×10^{-3} and 6.28 radian s^{-1}. All the measurements were carried out at 25 °C. The storage G' and loss G" moduli were determined by the Markovitz equation[1], and relaxation spectra H were determined from the G' and G" curves by using Tschoegl's second order approximation.[2]

IV-3 Results

IV-3-1 Storage and Loss Moduli

Figure IV-1 shows the frequency ω dependence of G' and G" for CTAB:NaSal/W systems of $C_D = 1.0 \times 10^{-1}$ mol l^{-1} with different molar ratio $C_S C_D^{-1}$. Significant changes in the rheological behavior by changing $C_S C_D^{-1}$ are found.

In the region of low $C_S C_D^{-1}$ between 0.25 and 0.275 shown

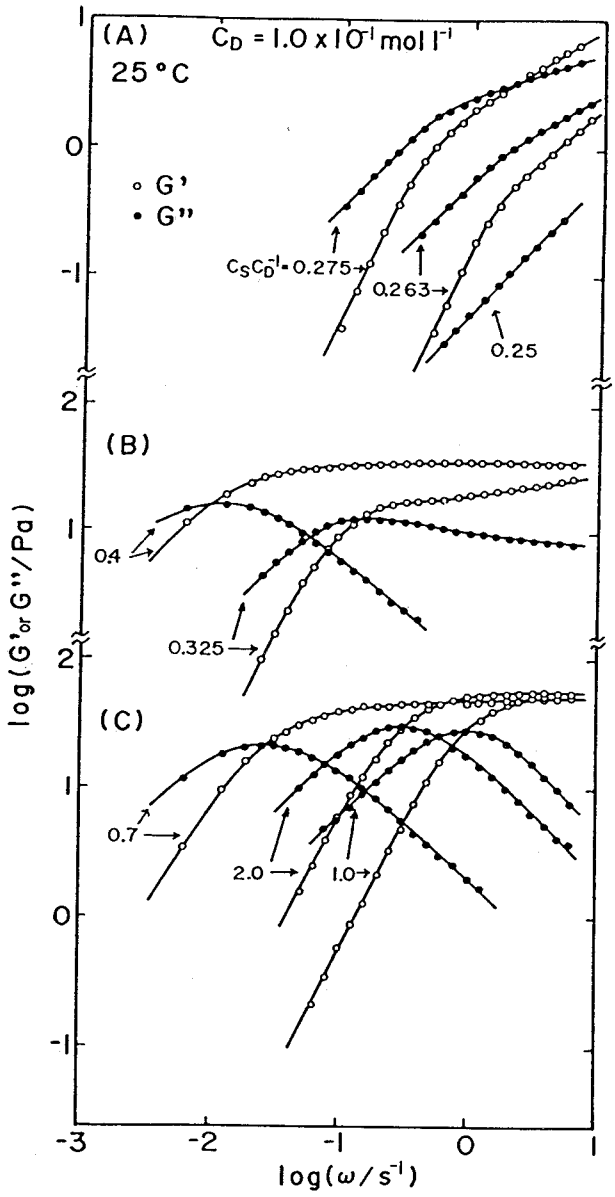

Figure IV-1. Dependence of the storage G' and loss G" moduli on frequency ω for CTAB:NaSal/W systems with $C_D = 1.0 \times 10^{-1}$ mol l^{-1} and varying $C_S C_D^{-1}$.

in Figure IV-1A, the G' and G" are proportional, respectively, to ω^2 and ω at the low frequencies but become proportional to $\omega^{0.5}$ in the range of intermediate to high frequencies. In addition, the two curves for the solution with $C_S C_D^{-1}$ = 0.263 do not cross each other in the measured frequencies.

As $C_S C_D^{-1}$ is increased to 0.3 to 0.5, the low frequency ends of the G' and G" curves shift to the lower frequency side. The G' curve moves more rapidly than the G" curve, thereby the two curves began to cross each other. Moreover, around the low frequency ends a plateau appears in the G' curve and a maximum in the G" curve as seen in Figure IV-1B.

Finally, as seen in Figure IV-1C, when $C_S C_D^{-1}$ exceeds 0.6, the height of the plateau of the G' curves approaches a constant level G_N^0 which is dependent on C_D but independent of $C_S C_D^{-1}$. The G" curve is proportional to ω in the low frequency side but to ω^{-1} in the high frequency side of the peak at ω_m. The modulus G_N^0 may be called the plateau modulus and its reciprocal, J_N^0 (= $1/G_N^0$), the plateau compliance.

These G' and G" data give beautiful semicircular Cole-Cole plots[3,4]. Figure IV-2 shows typical examples of the Cole-Cole plots for CTAB:NaSal/W systems with rather high $C_S C_D^{-1}$. Such a perfect semicircular Cole-Cole plot is typical of a Maxwell model[2] characterized by a single relaxation time τ_m (= $1/\omega_m$) and the modulus G_N^0.[3] Then, the frequency dependence of the G' and G" curves may be given as:

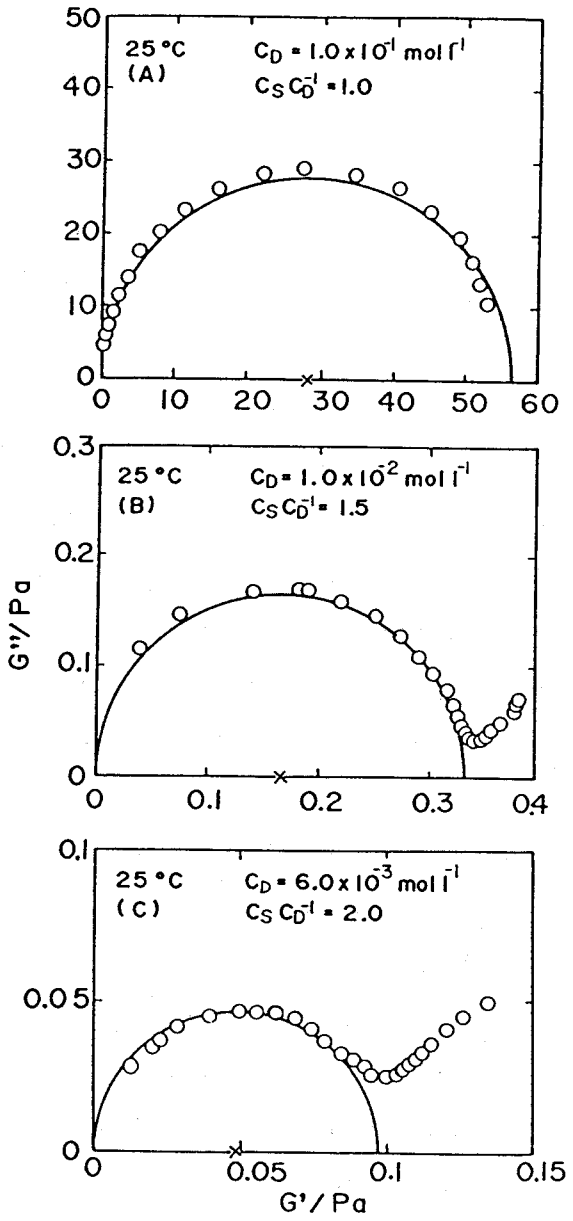

Figure IV-2. Cole-Cole plots of the G' and G" data for CTAB:NaSal/W systems with C_D and $C_S C_D^{-1}$ of (A) 1.0×10^{-1} mol l^{-1} and 1.0 , (B) 1.0×10^{-2} mol l^{-1} and 1.5, and (C) 6.0×10^{-3} mol l^{-1} and 2.0.

$$G'(\omega) = G_N^0 \omega^2 \tau_m^2 / (1 + \omega^2 \tau_m^2) \qquad \text{(IV-1)}$$

$$G''(\omega) - \eta_s \omega = G_N^0 \omega \tau_m / (1 + \omega^2 \tau_m^2) \qquad \text{(IV-2)}$$

where η_s is the solvent viscosity. The peak relaxation time τ_m of the Maxwell model coincides with the terminal relaxation time τ_w defined later by eq IV-5.

For all the tested solutions with C_D from 6.0×10^{-3} to 1.0×10^{-1} mol l^{-1}, we observed more or less similar changes in the G' and G" curves depending upon $C_S C_D^{-1}$ to those illustrated in Figures IV-1 and IV-2. As shown in Figure IV-1A, in the low $C_S C_D^{-1}$ range the viscoelastic behavior is similar to that often observed for unentangled flexible chain polymer systems such as dilute solutions of high molecular weight polymers or concentrated solutions of low molecular weight polymers.[5] The behavior of such polymer solutions may be well described by the Rouse[6] and Zimm[7] theories. In the intermediate $C_S C_D^{-1}$ range the viscoelastic behavior is more like that of concentrated high molecular weight polymer solutions or the bulk state, in which the polymer chains are entangling.[5] Finally, the systems with high $C_S C_D^{-1}$ exhibit the Maxwell model-type behavior, as seen in Figure IV-1C and IV-2. This behavior has never been seen in the flexible polymer solutions.

IV-3-2 Relaxation Spectra

Figure IV-3 shows relaxation spectra H for the systems with C_D = 6.0 x 10^{-3}, 2.0 x 10^{-2}, and 1.0 x 10^{-1} mol l^{-1} and various $C_S C_D^{-1}$ ratios. The features observed above for the G' and G" curves are also recognized in these spectra.

For example, as seen in Figure IV-3A for the system with C_D = 1.0 x 10^{-1} mol l^{-1} and $C_S C_D^{-1}$ = 0.263, the relaxation spectrum H is of wedge type often observed for unentangled flexible polymer systems.[5] As $C_S C_D^{-1}$ is increased to 0.275, a shoulder appears at the long time end of H. As $C_S C_D^{-1}$ exceeds 0.325, the shoulder develops to a box-type spectrum with the plateau height G_N^0. This kind of transition in the relaxation spectra H is often observed for polymer solutions when the polymer concentration or the molecular weight exceeds beyond a certain critical value.[5]

When $C_S C_D^{-1}$ is increased beyond this level (> 0.35), the intensity of the fast modes diminished, while a strong peak with the height same to G_N^0 appears at the time scale of τ_m corresponding to the Maxwell model-type behavior.

A peculiar feature observed is that as $C_S C_D^{-1}$ is increased from 0.35 to 1.0, the peak of the spectrum representing the relaxation time τ_m first shifts to the longer time side and then shifts back to the shorter time side with keeping the height practically constant. This implies that the plateau modulus G_N^0 is practically constant but the relaxation time τ_m varies with $C_S C_D^{-1}$.

As seen in Figures IV-3B and C, similar features are

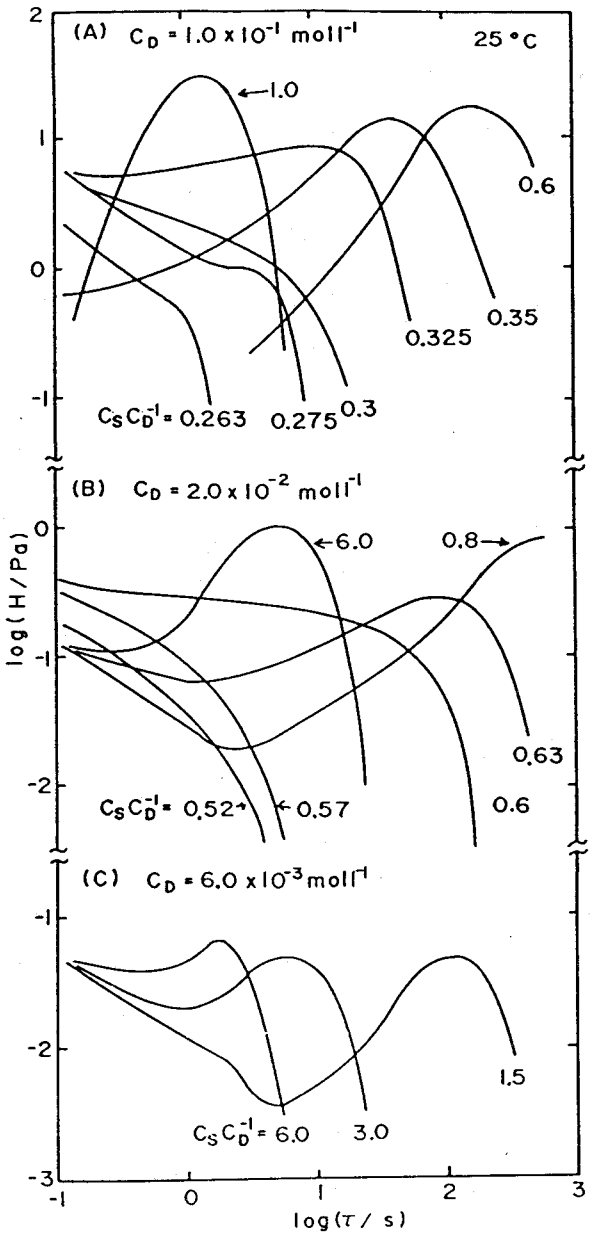

Figure IV-3. Relaxation spectra H for CTAB:NaSal/W systems of C_D = (A) 1.0 x 10^{-1} , (B) 2.0 x 10^{-2}, and (C) 6.0 x 10^{-3} mol l^{-1} and varying $C_S C_D^{-1}$ as indicated.

observed in the solutions with much lower C_D, although the changes in the spectral shape occur at somewhat different $C_SC_D^{-1}$. Again, the peak first shifts to the longer time side and then shifts back to the shorter time side as $C_SC_D^{-1}$ is increased from 0.6 to 6.0.

These dilute solutions with C_D = 1.0 x 10^{-2} mol l^{-1} have an additional feature which was not observed in the concentrated solution with C_D = 1.0 x 10^{-1} and 6.0 x 10^{-2} mol l^{-1}. As seen in Figure IV-3B and 3C for the solutions with low C_D but high $C_SC_D^{-1}$, the spectra appear to split into two regions: The one is the Maxwell model-type peak at the long time end with approximately the same height but found at different locations depending on $C_SC_D^{-1}$; and the other is the Rouse-wedge type portion appearing independently of $C_SC_D^{-1}$ in the shorter time side. The latter appears to become more pronounced with decreasing C_D. The Cole-Cole plots for these dilute solutions also exhibit corresponding extra tails in the high frequency side as seen in Figures IV-2B and 2C.

IV-3-3 Compliance and Relaxation Time

From the slopes of the G' and G" curves at the low frequency ends one can determine some viscoelastic material parameters such as the steady-state compliance J_e^0, the zero shear viscosity η_0, and the (weight average) terminal relaxation time τ_w as follows:[5]

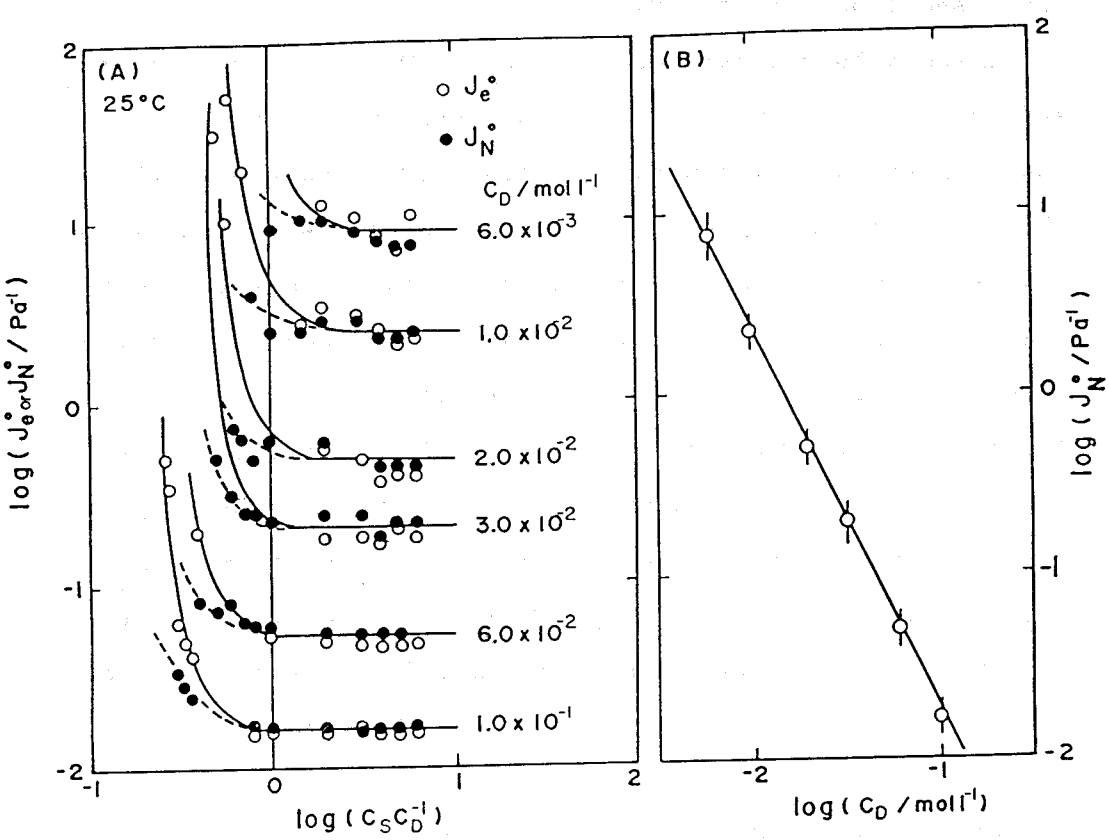

Figure IV-4. Dependence of (A) the steady state compliance J_e^0 and the plateau compliance J_N^0 on $C_S C_D^{-1}$ and of (B) J_N^0 on C_D.

$$G' = J_e^0 \eta_0^2 \omega^2 \qquad (\omega \rightarrow 0) \qquad \text{(IV-3)}$$

$$G'' = \eta_0 \omega \qquad (\omega \rightarrow 0) \qquad \text{(IV-4)}$$

$$\tau_w = J_e^0 \eta_0 \qquad \text{(IV-5)}$$

Once a plateau appears in the G' curve, one can determine the plateau modulus G_N^0 or compliance J_N^0 ($= 1/G_N^0$) from the plateau height and the relaxation time τ_m ($= 1/\omega_m$) from the peak frequency ω_m of the corresponding G" curve.[5]

Figure IV-4A shows dependence of J_e^0 and J_N^0 on $C_S C_D^{-1}$. For all the solutions examined here, J_e^0 is larger than J_N^0 at low $C_S C_D^{-1}$, but both compliances decrease rapidly with increasing $C_S C_D^{-1}$ and level off to a common value independent of $C_S C_D^{-1}$ after $C_S C_D^{-1}$ exceeds about 1. This result implies that distribution of the relaxation times is sharp, as anticipated for the Maxwell model.

As seen in Figure IV-4A, this tendency appears to be true for all the solutions. Then, the constant J_N^0 are double-logarithmically plotted against C_D in Figure IV-4B. The slope is -2.0 to -2.2. The same dependence was also found for ordinary chain-polymer solutions.[5]

We also estimated the terminal relaxation time τ_w from the low frequency ends of the G' and G" curves using eqs IV-3 to IV-5 or the relaxation time τ_m from the peak frequency ω_m of the G" curve or the Cole-Cole plot using eqs IV-1 and IV-2. Figure IV-5 shows the results plotted against $C_S C_D^{-1}$. The

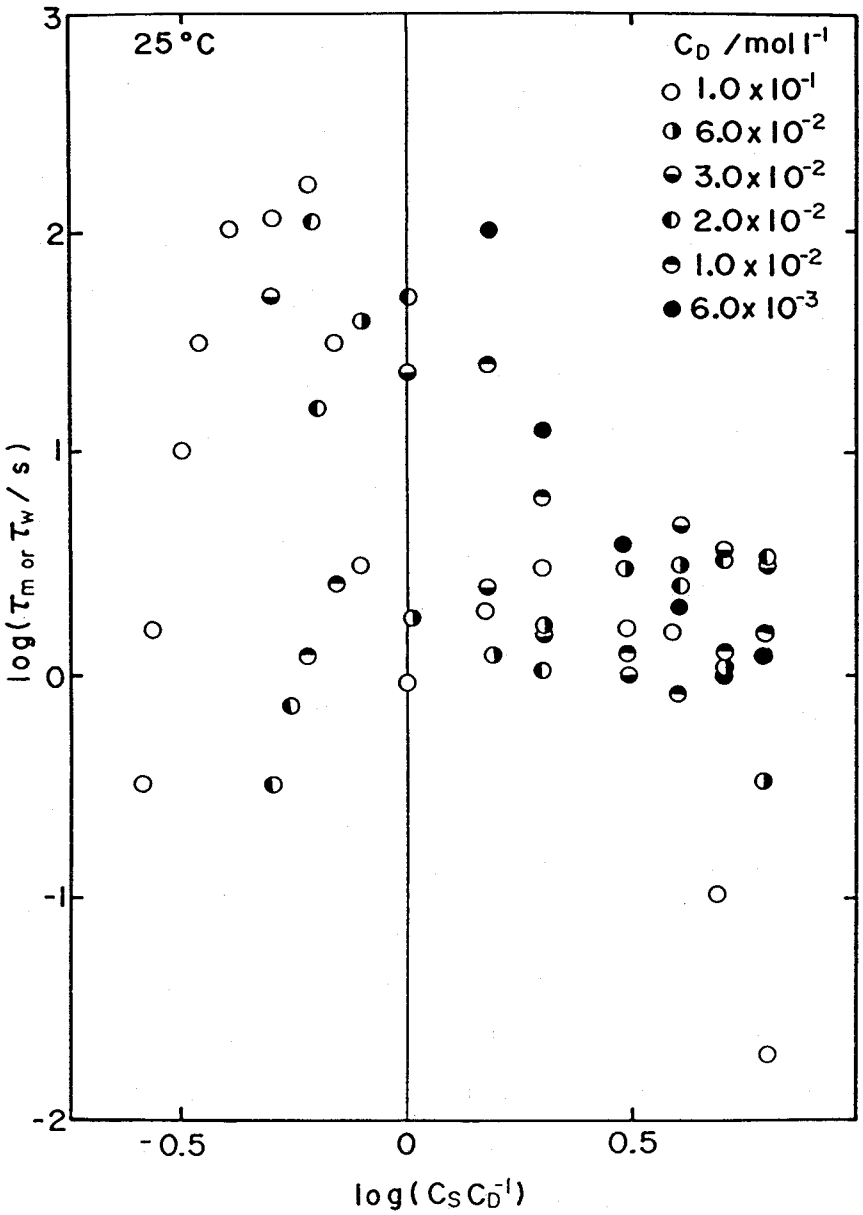

Figure IV-5. Plots of the longest relaxation times τ_m and τ_w on $C_S C_D^{-1}$ for CTAB:NaSal/W systems with different C_D.

plotted data points scatter in a complicated manner. Therefore, $C_S C_D^{-1}$ is not an essential factor governing the relaxation mechanisms in the present CTAB:NaSal/W system.

Although the data points scatter in a very complicated manner, we can trace the data points for a given C_D to obtain a series of τ_m versus $C_S C_D^{-1}$ curves. The resulting curves appear to have a common feature.

In each curve the time τ_w first increases monotonously until $C_S C_D^{-1}$ reaches to a certain value (dependent on C_D), where τ_w becomes identical to τ_m (and J_e^0 to J_N^0 independent of $C_S C_D^{-1}$). As $C_S C_D^{-1}$ is further increased above the critical value, the τ_m (or τ_w) decreases to reach a minimum, then increases again to pass through a small maximum, and finally the τ_m decreases again rapidly. Interestingly, after the critical $C_S C_D^{-1}$ the J_N^0 remains the same independent of $C_S C_D^{-1}$.

According to Bunton,[8] the viscosity of aqueous CTAB solutions containing sodium tosylate as an added salt increased with increasing concentration C_S of tosylate ions until C_S reaching C_D, and then decreased. These results also suggest that CTAB molecules form equimolar complexes with tosylate ions in the micelles. When tosylate ions were in excess, the thread-like micelles broke up.[8]

IV-4 Discussion

IV-4-1 Classification of Viscoelastic Behavior

As we have seen in Figure IV-1 through IV-5, the change in

$C_S C_D^{-1}$ for these CTAB:NaSal/W systems of a given C_D induces transitions in their viscoelastic behavior. These transitions may be classified into three types. We call the behavior appearing in the low to intermediate value of $C_S C_D^{-1}$ the type I and II, respectively, and that appearing in the high values of $C_S C_D^{-1}$ and resembling to that of the Maxwell model the type III behavior. Recently, Hoffmann and coworkers[9,10] examined the viscoelastic behavior of aqueous solutions consisting of cetylpyridinium salicylate and sodium salicylate, and they found that the zero-shear viscosity changed dramatically depending on the concentration of sodium salicylate and they also classified the behavior into some types.

In case of ordinary polymer solutions and those of rigid polymers as well, the relaxation times may be represented as $\zeta_0 F(c,M)$, where ζ_0 is the monomeric friction factor. The function $F(c,M)$, which depends on polymer concentration c and molecular weight M, is the structural factor reflecting the characteristics of the molecular dynamics of the individual chains and the nature of the topological interactions due to entanglement. Transitions of the rheological behavior may occur when the polymer concentration c and/or molecular weight M are increased beyond certain limits so that the polymer molecules begin to entangle. The M and c dependences of η_0, J_e^0 and τ_m of flexible-chain polymer solutions may be summarized in the following power-law forms:[5]

$$\eta_0 \propto \zeta_0 cM \; ; \quad J_e^0 \propto M/c \; ; \quad \tau_w \propto \zeta_0 M^2 \qquad \text{(IV-6)}$$

for unentangled systems with $cM < M_c^0$ or $M_c'^0$, and

$$\eta_0 \propto \zeta_0 (cM)^{3.5} \; ; \; J_e^0 \propto M^0/c^2 \; ; \; \tau_w \propto \zeta_0 c^{1.5} M^{3.5} \qquad \text{(IV-7)}$$

for fully entangled systems with $cM > M_c^0$ or $M_c'^0$. Here, M_c^0 and $M_c'^0$ are the critical molecular weight for η_0 and J_e^0 (and τ_w) for the bulk polymers, respectively.[5] Rigid polymer systems give much stronger dependences of these quantities on c and M.[5,11]

Although the exact correspondence between the present micellar solutions (CTAB:NaSal/W) and flexible-chain polymer solutions is not clear, we notice qualitative resemblances between their rheological behavior at least in the region of low $C_S C_D^{-1}$. The features of the type I behavior are similar to the one observed for unentangled flexible-chain polymer systems.[5] On the other hand, the type II behavior resembles that of semidilute to concentrated solutions of flexible-chain polymers, in which the effect of entanglement emerges and entanglement network develops to the full extent. However, the type III behavior represented by the Maxwell model is unique to the present CTAB:NaSal/W micellar systems.

An elongated rigid rod model[5,11] might be applied to the present systems, since an electron micrographs of the thread-like micelles previously shown in Chapter III suggest that the micelles might be rather rigid. However, the detailed features of the rheological behavior such the shape of the G' and G" curves and the relaxation spectra of the present

systems do not match those of the rigid rod model.[5]

The relaxation mechanisms in detergent solutions must also be governed by the dynamics and the topological interactions between the thread-like micelles. Thus, their behavior must depend on C_D and C_S, and reflecting the state of aggregation of the detergent and salt molecules and also the nature of entanglement among the thread-like micelles.

IV-4-2 A Factor Controlling The Maximum Relaxation Time

As pointed out previously, the ratio of $C_S C_D^{-1}$ is not a factor controlling the maximum relaxation time τ_m of the CTAB:NaSal/W systems. It is very important to elucidate the factor which essentially controls the τ_m for understanding a relaxation mechanism.

In Chapter III, we discussed a molecular level structure of the thread-like micelles and estimated the free salicylate Sal^- ion concentration C_S^* for all the systems with $C_S C_D^{-1} \geqq 1.5$ using eq III-3 simply as the excess C_S over C_D. For the systems of $C_D = 1.0 \times 10^{-1}$ mol l^{-1} with $0.5 < C_S C_D^{-1} < 1.5$, we estimated C_S^* by using plots in Figure III-8(B). The difference between the stabilities of the micelles in ordinary and deuterated water should be negligible.

In the CTAB:NaSal/W systems, a characteristic viscoelastic behavior, which is called type III behavior, starts nearly at the condition with $C_S = C_D$. Therefore, we chose the concentration C_S^* of free Sal^- as the variable to describe the maximum relaxation time τ_m in the type III systems of the

CTAB:NaSal/W with $C_S C_D^{-1} > 1$.

Figure IV-6 shows plots of τ_m versus C_S^*. The data points of the $C_D = 1.0 \times 10^{-1}$ mol l^{-1} systems with $0.5 < C_S C_D^{-1} < 1.5$ are represented by the symbols with pips. Interestingly, all the τ_m data points fall on the solid curve which is subject only to C_S^* and is independent of C_D. Therefore, we conclude that the main factor controlling the relaxation mechanism is C_S^*.

It is interesting to note that the τ_m for the type III systems never depend on C_D. It is well known that, for fully entangling concentrated polymer systems, the maximum relaxation times τ_m are strongly dependent both on the molecular weight and the concentration of the polymer.[5] This feature of the entangled polymer systems implies that the relaxation of entanglement is controlled by the diffusional processes (often called reptation) of the polymer molecules.[5,12-17] The motion or diffusion of the thread-like micelles in the present micellar systems should be highly restricted with increasing C_D. Therefore, the negligible effect of C_D on τ_m for these micellar systems strongly suggest that the diffusional process of the thread-like micelles bears no influence on the relaxation mechanisms in the type III behavior.

IV-4-3 Type III Behavior

After the type II behavior, emerges the peculiar type III (Maxwell model-type) behavior never seen in ordinary polymer

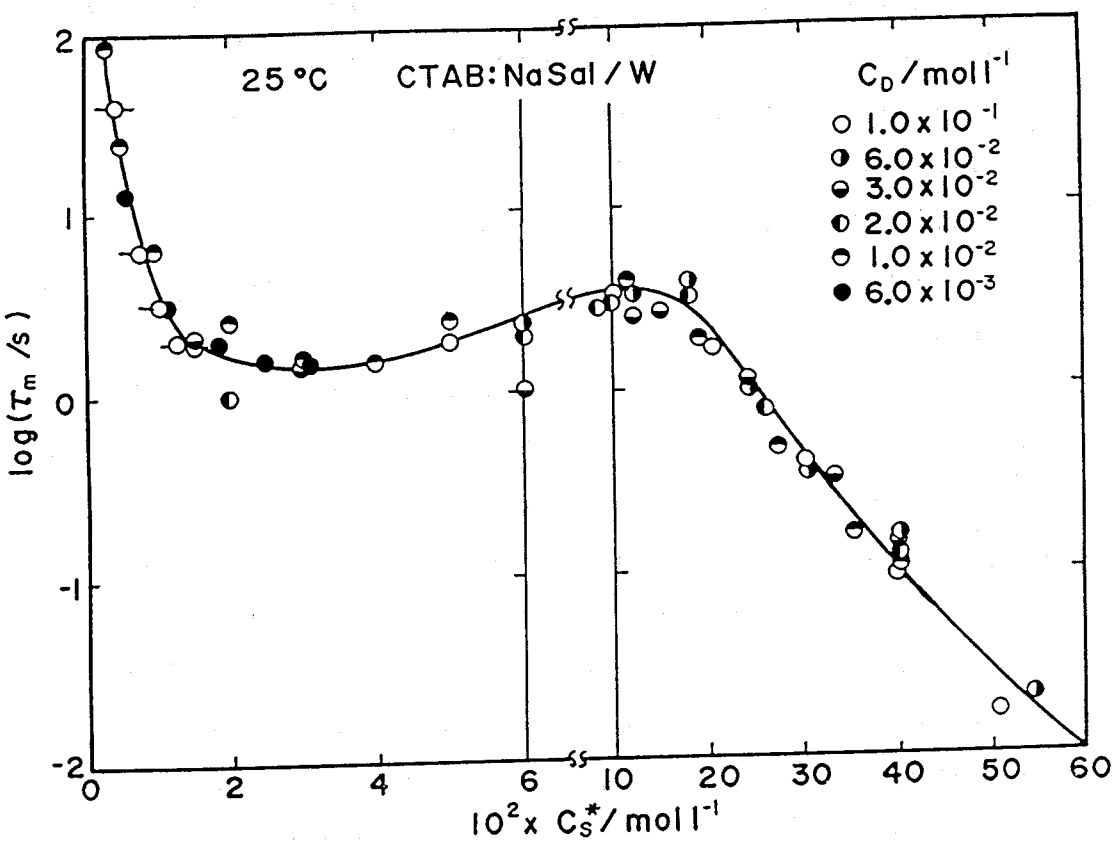

Figure IV-6. Dependence of the maximum relaxation time τ_m for the type III behavior on the concentration C_S^* of free Sal^-.

solutions. The $C_D^{-2.2}$ dependence of J_N^0 suggests that the fully entangled network of the thread-like micelles still exists in the type III region.

However, for the polymer solutions, the terminal relaxation times τ_w increases very rapidly with increasing c and M, as shown by eq IV-7, which implies that the entanglement network may be disentangled by diffusion of the chain molecules under the topological constraints imposed by the surrounding chains. In terms of the tube theory for relaxation in entangled polymer systems developed by Edwards,[12] de Gennes[13] and Doi and Edwards[14-17] this diffusional motion is called reptation.

On the other hand, the dependence of τ_m on C_D and $C_S C_D^{-1}$ for the present micellar solutions is entirely different from the picture expected from the ordinary polymer solutions. The decrease in τ_m with increasing $C_S C_D^{-1}$ beyond the critical value might suggest a decrease in the length of the micelles. However, this is unlikely because J_N^0 and hence the entanglement density remains the same even after τ_m has become shorter than that of the low $C_S C_D^{-1}$ solutions observed in the type I and II regions.

According to classical theories of entanglement relaxation employing a quasi-network model with transient junctions which temporarily break and reform,[5,18,19] the relaxation time may be determined by the life time of the junctions and/or the effective network chains. This leads to a conclusion that there are two (or more) competing mechanisms responsible for

the relaxation of the micellar solutions: The one may be controlled by a chemorheological process[5,21] involving actual breaking-down and reformation of the entanglement network presumably by scission and reformation of the thread-like micelles themselves; and the other by disentanglement due to diffusion of the network chains but without accompanying their break-down.

The important feature of the type III behavior is that the mechanism is a single relaxation time process. This suggests that this relaxation mechanism is a chemorheological process which involves actual breaking-down and reformation of the entanglement network, independent of the length (molecular weight)of the thread-like micelles. If a diffusional process were prevailing, the τ_m should be highly dependent on the thread length and concentration. This is obviously not the case.

As early as in 1950s Yamamoto[18] and Lodge[19,20] independently developed theories of entanglement relaxation employing a quasi-network model with transient junctions which temporarily break and reform.[5,18-20] According to their theories, the relaxation time may be determined by the life time of the junctions or of the effective network chains. The stress tensor σ (t) at time t is expressed in the Lodge's form as follows

$$\sigma(t) = f \int_{-\infty}^{t} \mu(t-t')\, B(t')\, dt' \qquad \text{(IV-8)}$$

where $\mu(t-t')dt'$ is the number density of the junctions which have been generated in the past time between t' and t' + dt' and still existing at t; B(t') is Finger tensor at t'; and f is the proportionality constant between stress and the number density of the junctions.[20] All the viscoelastic functions such as G', G", and the stress relaxation modulus are derived from eq IV-8.[20]

Hence, we apply the quasi-network theory to the type III behavior. First, we must consider the function $\mu(t-t')$. Supposing that the thread-like micelles are composed of subunits M, and that the entanglement junction E of the micelles is formed as a result of a certain chemical reaction between the two subunits (see Figure IV-7), we can write the process of entanglement formation-scission by

$$2\,M \underset{k_2}{\overset{k_1}{\rightleftharpoons}} E \qquad \text{(IV-9)}$$

where k_1 and k_2 are the rate constants of the entanglement formation and scission, respectively. Then, the rate equation for the number density $\mu(t-t')$ of E should be as

$$d\mu(t-t') / dt = (1 / 2)k_1[M]^2\delta(t-t') - k_2\mu(t-t') \quad \text{(IV-10)}$$

where [M] is the number density of M and $\delta(t-t')$ is Dirac's delta function. Equation IV-10 can be easily integrated, leading to

$$\mu(t-t') = (1 / 2)k_1[M]^2\exp\{-k_2(t - t')\} \quad \text{(IV-11)}$$

With an equilibrium constant K ($= k_1 / k_2$) and the relaxation time τ ($= 1 / k_2$) for eq IV-19, eq IV-11 can be rewritten as follows.

$$\mu(t-t') = \{K / (2\tau)\}[M]^2\exp\{-(t - t') / \tau\} \quad \text{(IV-12)}$$

Substituting eq IV-12 to eq IV-9, we obtain the frequency ω dependence of G' and G" as follows.

$$G'(\omega) = (fK / 2)[M]^2\omega^2\tau^2 / (1 + \omega^2\tau^2) \quad \text{(IV-13)}$$

$$G"(\omega) = (fK / 2)[M]^2\omega\tau / (1 + \omega^2\tau^2) \quad \text{(IV-14)}$$

Equations IV-13 and IV-14 are identical to those derived for a Maxwell model with the relaxation time τ and the plateau modulus $G_N^0 = (f K / 2)[M]^2$. Because [M] is proportional to C_D, the plateau modulus G_N^0 is proportional to the square of C_D, conforming to the present experimental results of the type III behavior as shown previously in

Chapter IV. Moreover, since the rate constant k_2 is independent of C_D, the eqs IV-13 and IV-14 well explain the features of the type III behavior. Therefore, we can conclude that the viscoelastic properties of the present type III systems could be well described by the quasi-network model.

IV-4-4 The Relaxation Mechanism

For the stresses of the entanglement network to relax, some portions of the thread-like micelles must be broken down, if the diffusion of the network chains is not a main mechanism. According to the chemorheological consideration introduced above, there are two possibilities where the micelles break.[21] One is that the micelles may break down at only entanglement junctions. The other is that the micelles may break down anywhere along the chains between entanglement junctions.[21,22]

In the electron micrographs of the viscoelastic aqueous detergent systems, we could not find any terminals of the thread-like micelles as seen in Figure III-3. If the micelles are cut down to relax, we might be able to see the ends of the micelles, although the view of the micrographs is still too narrow to see broken micelles. This means that breaking down of the micelles is likely to be occurring without actually breaking the micelles. Presumably, the micelles could pass through each other with the rate constant k_2 at the entanglement junctions just like a ghost. Figure IV-7 schematically illustrates the situation.

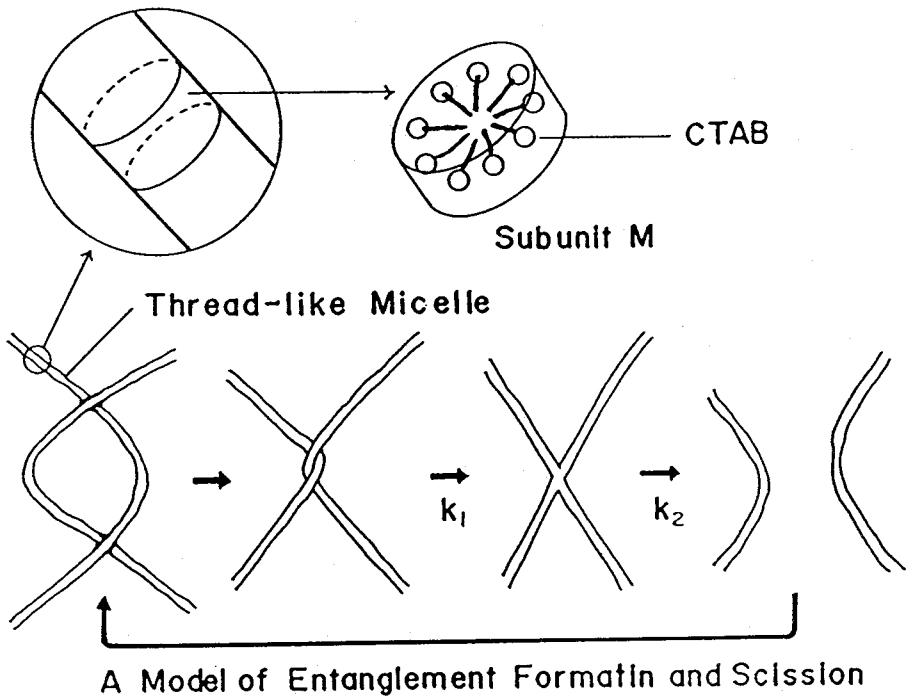

Figure IV-7. Schematic diagrams representing structure of the thread-like CTAB micelles and chemical reactional process of entanglement formation and scission between the two thread-like micelles.

Recently, Kato and coworkers[23] and Nilsson and coworkers[24] measured self-diffusion coefficients of nonionic surfactant molecules in aqueous solution in which thread-like micelles formed by the nonionic surfactants were entangling (semidilute condition) by using pulsed-gradient NMR technique. They found that the self-diffusion coefficient first decreased with increasing surfactant concentration until a certain value, and then increased gradually. Nilsson et al. have noted that this increase comes from intermicellar exchange of surfactant molecules resulting from the micelles encounters.[24] This may support our idea for mechanism of the entanglement relaxation.

Free Sal^- ions play an important and essential role in the entanglement relaxation as described previously. A further implication of their possible role is that the free Sal^- concentration C_S^* rather than C_D controls the relaxation time τ_m. Thus, free Sal^- ions appear to act as a catalyst for the chemorheological reaction, in which the free Sal^- ions control only the rate constant (the relaxation time τ_m) but not the equilibrium constant (the modulus G_N^0 or the entanglement density).

We replotted the data points in Figure IV-6 in the double-logarithmic plot in Figure IV-8. In this figure, two straight lines with the slope of -2.0 and -5.0 are found in the low and high C_S^* regions, respectively.

If we assume n free Sal^- ions catalyze scission of an entanglement junction, we can rewrite the process as

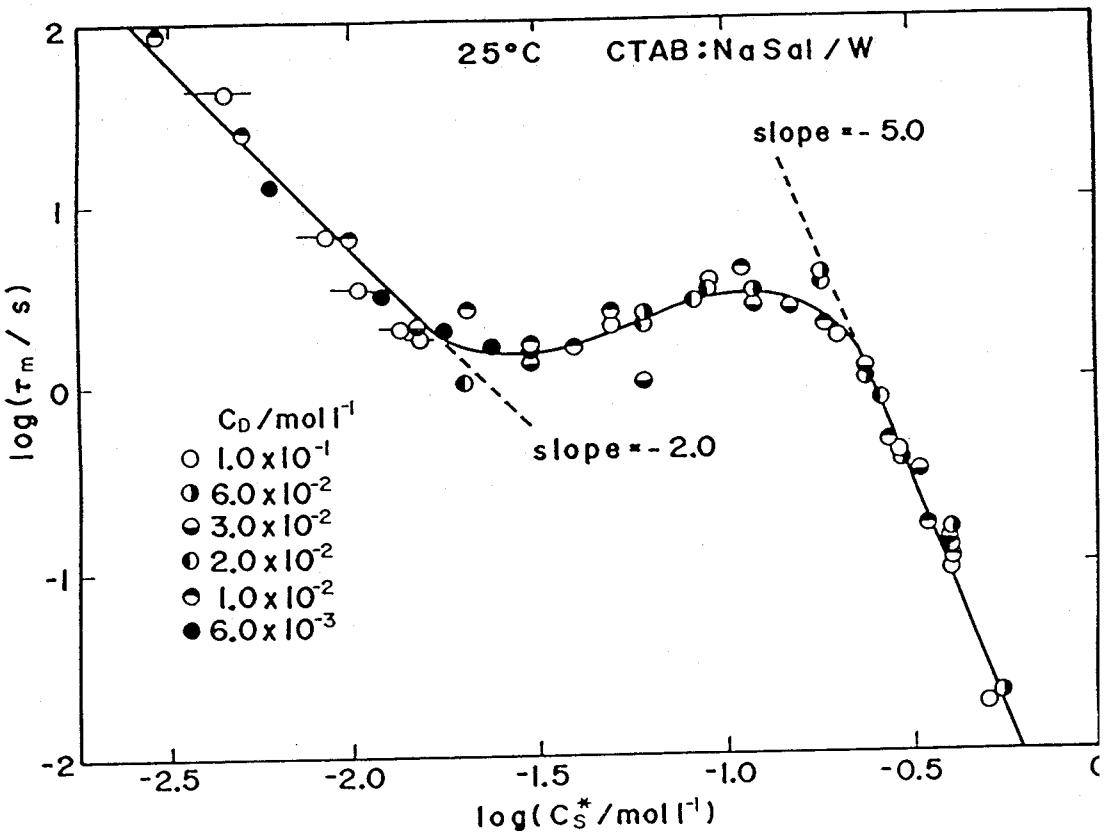

Figure IV-8. Double-logarithmic plots of the maximum relaxation time τ_m on C_S^*.

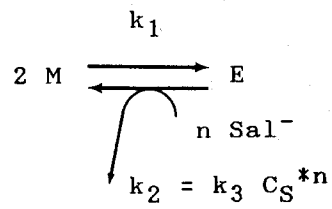

(IV-15)

with a new rate constant k_3 independent of C_S^*. Then, the τ_m is written from eqs IV-11, IV-12 and IV-15 as

$$\tau_m = k_3^{-1} C_S^{*-n} \qquad \text{(IV-16)}$$

Then we can estimate the necessary number n of the free Sal^- and k_3 from the slope and intercept of the double-logarithmic plot between τ_m and C_S^*. However, Figure IV-18 exhibits a curve with two straight regions with slopes of -2.0 and -5.0. It is likely that the mechanism of the entanglement scission is not necessarily so simple as expressed in eqs IV-15 and IV-16.

The implication is that the entanglement junction would be cleaved and the entangling two thread-like micelles could pass through each other assisted by free Sal^- ions. All the portions along the thread-like micelles are equally likely to be attacked by free Sal^- ions at the same time. However, only strained positions (the entanglement junctions) can be cleaved by such an attack.

An elementary process of the scission of entanglement would be an exchange process of the individual Sal^- molecules between the micelle and bulk aqueous phase. Thus, the

relaxation time τ_m in the type III systems must be related to a rate constant of the elementary exchange process of Sal^- which should be estimated by other experimental techniques.

REFERENCES

1) Markovitz, H. J. Apply. Phys. 1952, 23, 1070.

2) Tschoegl, N. W. Rheol. Acta 1971, 10, 582.

3) Cole, K. S.; Cole, R. H. J. Chem. Phys. 1941, 9, 341.

4) Noll, A. W. J. Polym. Sci. 1950, 5, 1.

5) Ferry, J. D. Viscoelestic Properties of Polymers; 3rd ed., John Wiley: New York, 1980.

6) Rouse Jr., P. E. J. Chem. Phys. 1953, 21, 1272.

7) Zimm, B. H. J. Chem. Phys. 1956, 24, 269.

8) Bunton, C. A. Reaction Kinetics in Micelles; Plenum: New York, 1973.

9) Hoffmann, H.; Lobl, H.; Wunderlich, Bayreuth, I. Tenside Detergents 1985, 22, 290.

10) Rehage, H.; Hoffmann, H., J. Phys. Chem. 1988, 92, 4712.

11) Tschoegl, N. W.; Ferry, D. J. J. Phys. Chem. 1964, 86, 1474.

12) Edwards, S. F. Proc. Phys. Soc. 1967, 92, 9.

13) de Gennes, P. G. J. Chem. Phys. 1971, 55, 572.

14) Doi, M.; Edwards, S. F. J. Chem. Soc., Farady Trans. II 1978, 74, 1789.

15) Doi, M.; Edwards, S. F. J. Chem. Soc., Farady Trans. II 1978, 74, 1802.

16) Doi, M.; Edwards, S. F. J. Chem. Soc., Farady Trans. II 1978, 74, 1818.

17) Doi, M.; Edwards, S. F. The Theory of Polymer Dynamics; Oxford University Press: Oxford, 1986.

18) Yamamoto, M. J. Phys. Soc., Japan 1956, 11, 413.

19) Lodge, A. S. Trans. Farady Soc. 1956, 52, 120.

20) Lodge, A. S. Elastic Liquids; Academic Press: London, 1964.

21) Tobolsky, A. V.; Prettyman, I. B.; Dillon, J. H. J. Appl. Phys. 1944, 15, 380.

22) Bueche, A. M. J. Chem Phys. 1953, 21, 614.

23) Nilsson, P. G.; Wennerström, H.; Lindman, B. J. Phys. Chem. 1983, 87, 1377.

24) Kato, T.; Anzai, S.; Seimiya, T. J. Phys. Chem. 1987, 91, 4655.

Chapter V

Dynamic Viscoelastic Properties of Aqueous Solutions of Cetyltrimethylammonium Bromide with Salicylic Acid

V-1 Introduction

Aqueous solutions of cetyltrimethylammonium bromide (CTAB) with salicylic acid (HSal), coded as CTAB:HSal/W, produce thread-like micelles of the appearance similar to those of CTAB:NaSal/W systems as previously described in the Chapter III. HSal, however, has a limited solubility and a small pK_a value in aqueous media, as opposed to NaSal. We anticipate that these differences should lead to differences in the micellar structure and life time of the entanglement network between the CTAB:NaSal/W and CTAB:HSal/W systems. We thus compare viscoelastic properties of these two systems. The small value of pK_a of HSal should result in formation of positively charged micelles composed of CTA^+:HSal complex, being subject to strong electrostatic repulsion. We also compare the effects on the viscoelastic properties of adding a simple electrolyte such as NaBr to CTAB:HSal/W and CTAB:NaSal/W solutions.

V-2 Experimental

V-2-1 Sample Solutions

For the rheological measurement, the concentration C_D of CTAB of the CTAB:HSal/W systems was varied from 1.0×10^{-2} to 1.0×10^{-1} mol l^{-1}, while the concentration C_A of HSal was varied in the range of the acid-to-detergent ratio $C_A C_D^{-1}$ from 0.3 to $C_A^s \cong C_D + C_A^{sw}$, where the system became saturated with HSal. The C_A^{sw} (= 1.8×10^{-2} mol l^{-1} at 25°C) is the concentration of HSal at the saturation in pure water.

The solutions on which the influence of addition of NaBr on the viscoelastic properties was examined were coded as CTAB:HSal:NaBr/W or CTAB:NaSal:NaBr/W systems. The concentration C_{AS} of NaBr of their systems was varied from 0 to the concentration C_D of CTAB.

All the samples solutions were kept standing at 25°C for equilibration more than 2 days before the measurements.

V-2-2 Rheological Measurement

For the dynamic measurements the amplitude of oscillatory strain was 0.33. The angular frequency ω covered the range between 6.28×10^{-3} and 6.28 rad s^{-1}.

For the shear stress relaxation experiments the same rheometer was used. The CTAB:HSal/W systems were subjected to a small step strain γ, and subsequent stress relaxation was followed for a few ten minutes. The magnitude of γ was 0.1 to 0.2, under which the stress relaxation moduli G(t) were independent of γ.

V-3 Results and Discussion

V-3-1 Dynamic Behavior

In Chapter IV on CTAB:NaSal/W systems, we classified their viscoelastic behavior into three types, which changed with increasing salt concentration C_S when the detergent concentration C_D was kept constant as described in the previous Chapter IV. Here, we first examine CTAB:HSal/W systems to see whether their viscoelastic behavior also follow a similar pattern to that of the CTAB:NaSal/W systems upon changing C_A relative to C_D.

Figure V-1 shows dynamic G' and loss G" moduli vs angular frequency ω curves (in a double-logarithmic scale) for three CTAB:HSal/W systems with C_D = 6.0 x 10^{-2} mol l^{-1} and C_A from $C_AC_D^{-1}$ of 0.4 to 0.8. When C_A = 2.4 x 10^{-1} mol l^{-1} (or $C_AC_D^{-1}$ = 0.4), the slope of the G' and G" curves approach 2 and 1, respectively, at their low frequency ends. They merge in the high frequency region to a curve with the slope of 1/2. This behavior resembles that of dilute polymer solutions of high molecular weight or of concentrated solutions of low molecular weight, in either of which polymer chains are not entangling with one another.[1] This behavior correspond to the type I behavior of the previous CTAB:NaSal/W systems, and is well described by Rouse and Zimm theories.[2,3]

When the C_A is increased to 3.0 x 10^{-2} mol l^{-1} (or $C_AC_D^{-1}$= 0.5), the longest relaxation time is increased about 100 fold, and the G" curve shows a broad maximum with a very long tail extending to the high frequency side. Obviously, the system

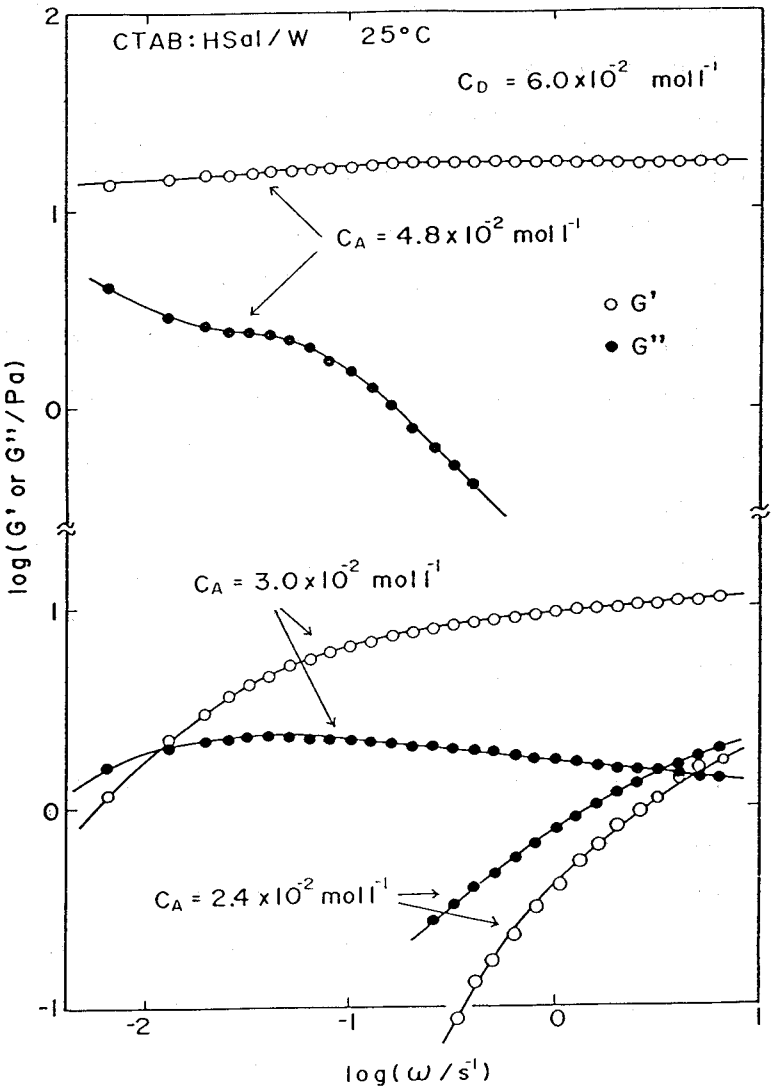

Figure V-1. Frequency ω dependence of G' and G" for CTAB:HSal/W systems at 25°C with the detergent concentration C_D = 6.0 x 10^{-2} mol l^{-1} and three different acid concentrations C_A*.

now has a very broad distribution of relaxation times similar to concentrated polymer solutions of high molecular weight, in which entanglement effects become dominant.[1,4] The thread-like micelles of the CTAB:HSal/W systems appear to have become longer with increasing $C_A C_D^{-1}$ from 0.4 to 0.5 so that the thread-like micelles begin to entangle among one another. Thus we may say that the CTAB:HSal/W systems with low to intermediate $C_A C_D^{-1}$ ratio exhibit the typical polymer solution behavior similar to the corresponding (type II) behavior of the CTAB:NaSal/W systems.

When C_A is further increased to 4.8×10^{-2} mol l^{-1} (or $C_A C_D^{-1} = 0.8$), the G' curve becomes a plateau with the height nearly independent of ω, and the G" curve rapidly decreases in the high frequency side. The low frequency ends of the curves are no longer observable in the frequency range accessible to our rheometer of the limited capacity. These features of the dynamic and loss moduli suggest that the relaxation modes in the high frequency range have disappeared. The systems becomes like an elastic gel. This behavior also is similar to the type III behavior found in the CTAB:NaSal/W systems with the $C_S C_D^{-1}$ ratio of the same level.

However, we observe a significant difference between behavior of these two systems. Namely, for the CTAB:HSal/W system with $C_A C_D^{-1} = 0.8$, we see a small bump in a nearly flat plateau in the G' curve, and a shoulder at around 0.1 rad s^{-1} in a rapidly decreasing tail of the high frequency side of the G" peak (although the peak itself cannot be seen in the

frequency range examined here). These features imply that the CTAB:HSal/W system possesses at least two relaxation modes: A slow mode below ω = 0.01 s^{-1} and an additional fast mode at around ω = 0.1 s^{-1}. For other CTAB:HSal/W systems with C_D = 1.0 x 10^{-2}, 3.0 x 10^{-2} and 1.0 x 10^{-1} mol l^{-1}, we observed similar systematic changes in the viscoelastic behavior with increasing C_A or $C_A C_D^{-1}$.

Figures V-2A and V-2B are typical examples of the double-logarithmic plots of the G' and G" vs frequency (ω) curves for the systems with C_D = 6.0 x 10^{-2} and 3.0 x 10^{-2} mol l^{-1}, respectively, and varying C_A from $0.8C_D$ up to the saturation C_A^s. Those systems with $C_A C_D^{-1}$ = 0.8 to 1.0 exhibit, at least, two modes with the relaxation time τ_1 and τ_2 from the low frequency side. The longer relaxation time τ_1 at the lower frequency side seems to shift faster with increasing C_A than the other one, τ_2, to the high frequency side. Thus the two modes merge to a single mode, as C_A is increased to C_A^s. The single mode behavior of the CTAB:HSal/W systems at high $C_A C_D^{-1}$ resembles the Maxwell-model behavior of the CTAB:NaSal/W systems with the $C_S C_D^{-1}$ ratio of the same level as described in the previous Chapter IV.

Then we attempt to separate the dynamic moduli into two separate relaxation modes by employing a four-element mechanical model[2] composed of two Maxwell elements with the relaxation strengths G_i and times τ_i (i = 1 and 2), connected in parallel. The G' and G" moduli of this model can be expressed as follows

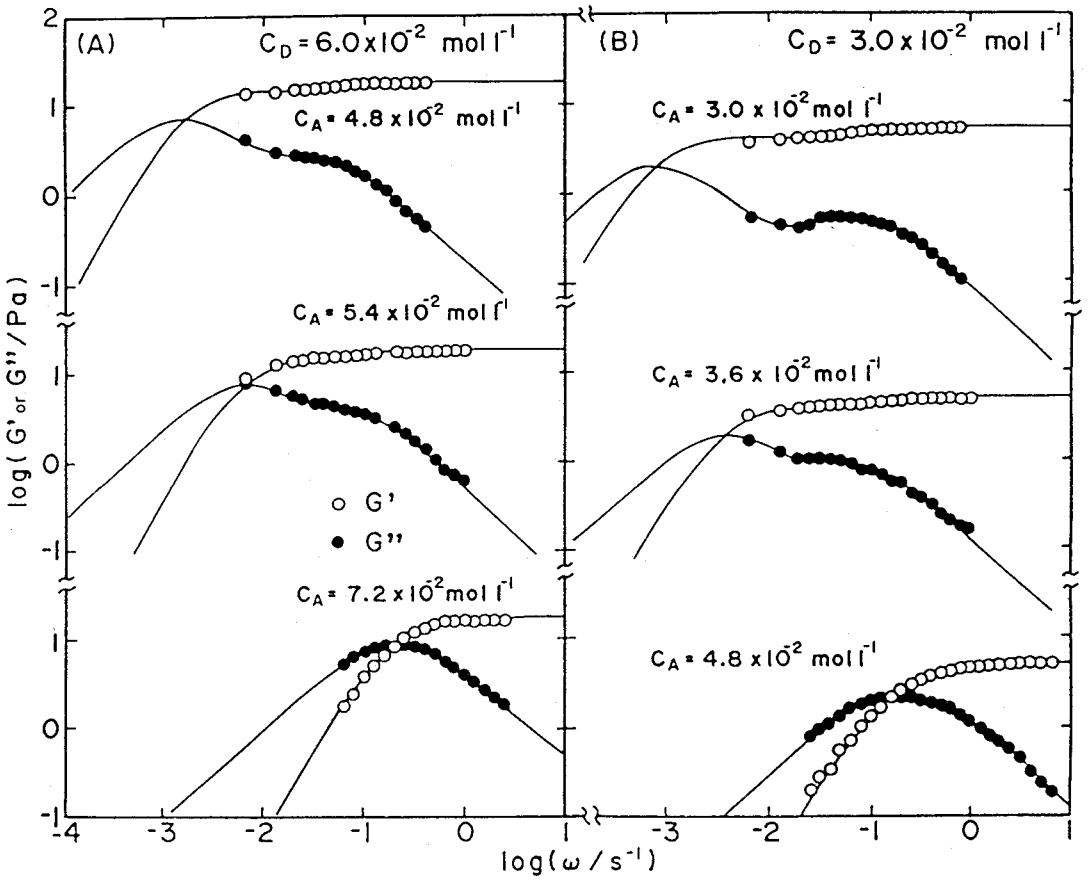

Figure V-2. Frequency ω dependence of G' and G" for CTAB:HSal/W systems at 25°C with the detergent concentration C_D = (A) 6.0 x 10^{-2} and (B) 3.0 x 10^{-2} mol l^{-1} and different acid concentrations C_A, both exhibiting typical type III behavior. Solid lines represent the calculated G' and G" curves obtained by using a simple mechanical model consisting of two Maxwell elements with the modulus G_i and the relaxation time τ_i (i = 1 and 2) connected in parallel.

Table V-1. Relaxation strength G_i and time τ_i (i = 1 and 2) for the slow and fast relaxation modes of CTAB:HSal/W systems at 25°C.

$10^2 C_D$/ mol l^{-1}		$10^2 C_A$/mol l^{-1}					
	10.0	7.0	8.0				
$\log(\tau_1/s)$		1.9	1.6				
$\log(G_1/Pa)$		1.5	1.45				
$\log(\tau_2/s)$		0.8	0.5				
$\log(G_2/Pa)$		1.25	1.25				
	6.0	3.6	4.8		5.4	6.0	7.2
$\log(\tau_1/s)$		3.1	2.8	2.78*	2.2	1.7	0.8
$\log(G_1/Pa)$		1.07	1.15	1.15*	1.15	1.12	1.12
$\log(\tau_2/s)$		1.5	1.4	1.44*	1.1	0.8	0.3
$\log(G_2/Pa)$		0.6	0.6	0.57*	0.7	0.7	0.7
	3.0	2.4	3.0	3.6	3.9	4.8	
$\log(\tau_1/s)$		3.2	3.1	2.24	1.75	0.98	
$\log(G_1/Pa)$		0.63	0.6	0.57	0.5	0.5	
$\log(\tau_2/s)$		1.25	1.2	1.1	0.65	0.25	
$\log(G_2/Pa)$		0.25	0.0	0.13	0.2	0.2	
	1.0	1.5	2.0	2.5			
$\log(\tau_1/s)$		3.2	2.5	1.5			
$\log(G_1/Pa)$		-0.45	-0.52	-0.68			
$\log(\tau_2/s)$		1.2	0.85	0.4			
$\log(G_2/Pa)$		-1.3	-1.25	-1.25			

*Detected from shear stress relaxation measurement.

$$G'(\omega) = G_1\tau_1^2\omega^2/(1+\tau_1^2\omega^2)+G_2\tau_2^2\omega^2/(1+\tau_2^2\omega^2) \qquad (V\text{-}1)$$

$$G''(\omega) = G_1\tau_1\omega/(1+\tau_1^2\omega^2)+G_2\tau_2\omega/(1+\tau_2^2\omega^2) \qquad (V\text{-}2)$$

Since the G' and G" data have been obtained only in the limited range of frequency, we determined the model parameters in eqs V-1 and V-2 employing a nonlinear least-square fitting technique on a microcomputer repeating the calculation until the calculated curves were fitted to the observed curves. The results are summarized in Table V-1. The solid curves in Figures V-2A and V-2B represent the values of G' and G" calculated with these parameters. We see that the agreement between the experimental and calculated curves is fairly good.

V-3-2 Shear Stress Relaxation

The above analysis of the G' and G" curves based on the four-element model may appear too ambiguous and the tabulated values of $\log(G_1)$ and $\log(\tau_1)$ could be a mere artifact of the least-square fitting technique employed here, because the rheometer we used cannot effectively cover the frequency range below $\log\omega = -2.2$ where the G" peak of the slow relaxation mode, if it exists, should appear. To confirm the validity of the above procedure we carried out shear stress relaxation measurement on these systems. Figure V-3A shows a typical example of a semi-logarithmic plot of the relaxation modulus G(t) vs time for CTAB:HSal/W system with $C_D = 6.0 \times 10^{-2}$ and $C_A = 4.8 \times 10^{-2}$ mol l^{-1}. As seen in Figure V-3A, we

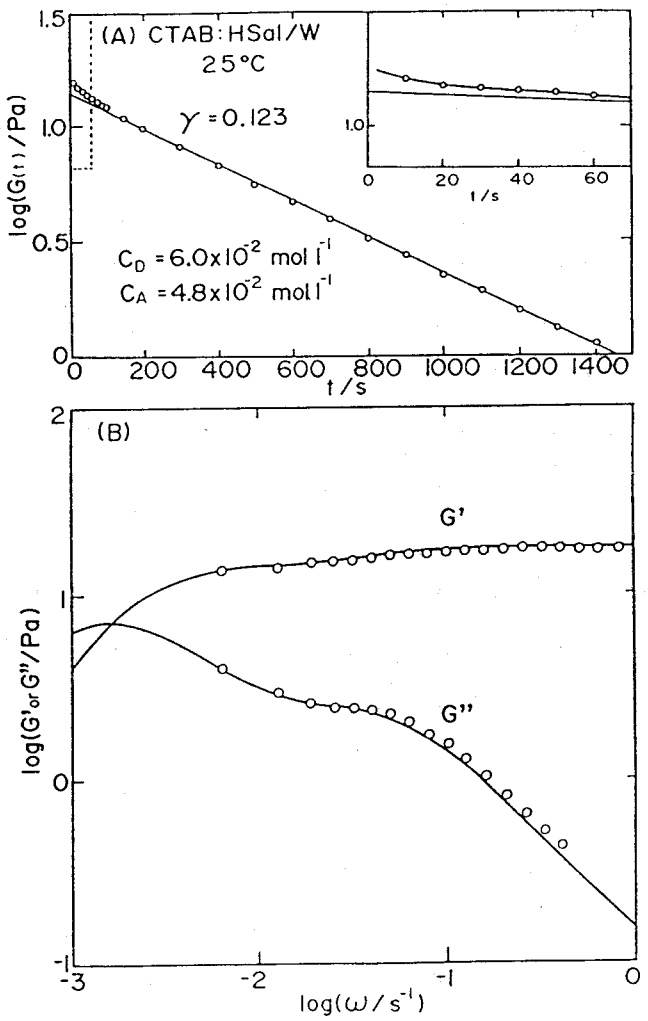

Figure V-3. A: A semi-logarithmic plot between a stress relaxation function G(t) and time t for the system with C_D = 6.0 x 10^{-2} and C_A = 4.8 x 10^{-2} mol l^{-1}. B: Comparison between G' and G" curves (solid lines) estimated from the stress relaxation data shown in the above figure with eqs III-1 and III-2 and G' and G" data (circles) obtained from the dynamic measurements.

determined the longest relaxation time τ_1 and its strength G_1, respectively, from the slope and the intercept of the straight line portion of the curve at the long time end. Then, subtracting the contribution of this longest relaxation time mode from the G(t) curve, we again obtained a straight line in the semi-logarithmic scale, from which we determined the contribution of the second-longest relaxation mode, and so on. This procedure developed earlier by Tobolsky and Murakami[6] was called "procedure X". The relaxation modulus of the present system was split practically into two modes as,

$$G(t) = G_1 \exp(-t/\tau_1) + G_2 \exp(-t/\tau_2) \qquad \text{(V-3)}$$

The G_i and τ_i values thus determined are also listed in Table V-1 with asterisk. The agreement between the values determined through the curve fitting and the procedure X is excellent.

According to the theory of linear viscoelasticity,[1,8] the G' and G" moduli are obtainable from G(t) by the Fourier transforms,

$$G' = \omega \int_0^\infty G(t) \sin(\omega t) dt \qquad \text{(V-4)}$$

$$G'' = \omega \int_0^\infty G(t) \cos(\omega t)dt \qquad (V\text{-}5)$$

substituting observed G(t) data into eqs V-4 and V-5, we obtain $G'(\omega)$ (eq V-1) and $G''(\omega)$ (eq V-2), respectively, in the frequency range where the dynamic experiments could not cover. The G' and G" curves thus determined are shown in Figure V-3B together with the directly determined data points. Again the agreement is excellent.

Thus above results indicate that the two-mode model reasonably explains the behavior of CTAB:HSal/W systems with C_A in the range of $0.8C_D < C_A < C_A^s$.

V-3-3 Relaxation Strengths

Now we turn our attention to examine the rheological data of the CTAB:HSal/W systems on the two-mode model with G_1 and τ_1 and G_2 and τ_2 for slow and fast modes, respectively. Figure V-4A and V-4B show dependence of the relaxation strengths G_1, G_2 and the sum $(G_1 + G_2)$ on $C_A C_D^{-1}$ and C_D, respectively. The magnitude of G_2 is about 1/3 of G_1. We see that both G_1 and G_2 are independent of $C_A C_D^{-1}$ but are proportional to $C_D^{2.2}$ when $C_A C_D^{-1} > 0.8$. This power law index of 2.2 is identical to that for the plateau modulus G_N^0 vs C_D for CTAB:NaSal/W systems shown in the same figure and also to that usually found for concentrated, high molecular-weight polymer solutions.[1,4] The sum $(G_1 + G_2)$ is equal to

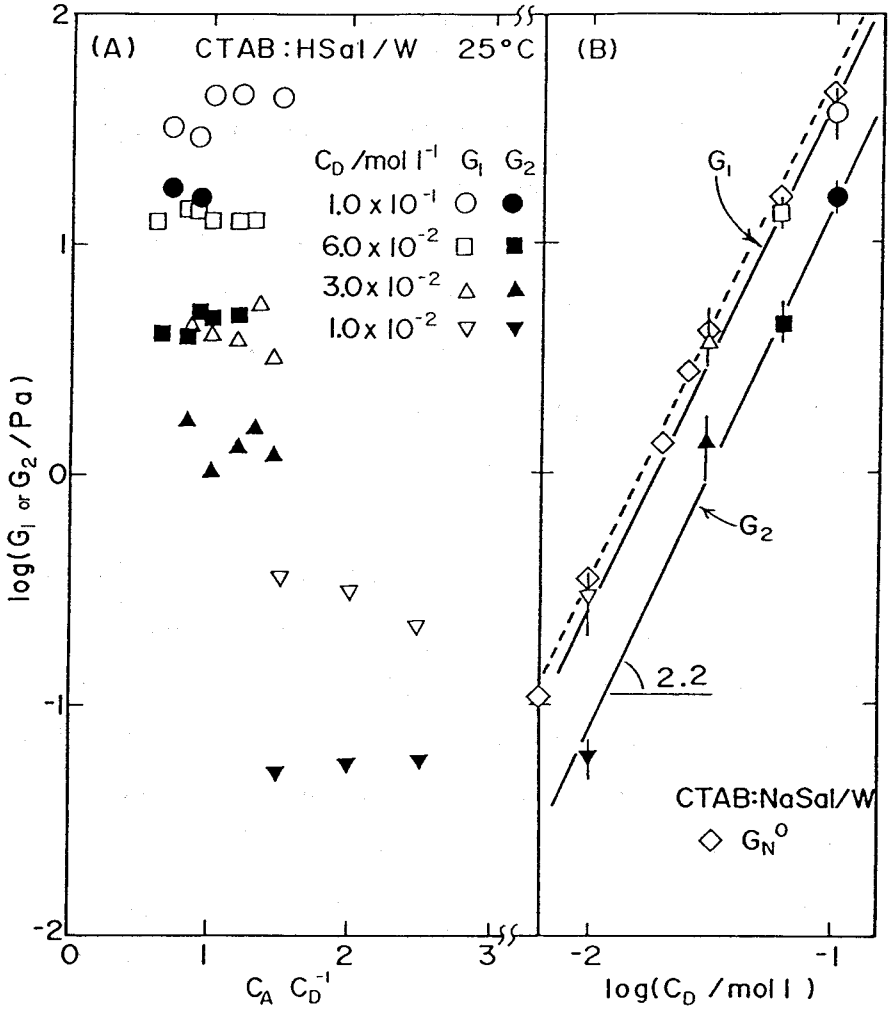

Figure V-4. The dependence of the relaxation strengths G_1 and G_2 (A) on the acid-to-detergent $C_A C_D^{-1}$ ratio and (B) on the detergent concentration C_D for CTAB:HSal/W systems at 25°C. Dashed line represents $G_1 + G_2$.

G_N^0 of the CTAB:NaSal/W systems not only in their C_D dependence but also in the absolute magnitude, as seen in Figure V-4B. The origin of the elasticity of the present CTAB:HSal/W systems is undoubtedly due to the entanglement network among the thread-like micelles existing in the systems. The observation of the CTAB:HSal/W systems made on a transmission electron microscope (TEM) confirmed that the thread-like micelles were densely entangling among one another as described in the previous Chapter III.

V-3-4 Relaxation Times

In the studies on CTAB:NaSal/W systems in Chapter IV, we found that the relaxation time τ_m was independent of C_D but a function of the concentration C_S^* of free Sal^- ions in the bulk aqueous phase. We anticipated that this could also be the case for the the present CTAB:HSal/W systems. We thus examined the dependence of τ_1 and τ_2 on C_A^* of free HSal in the bulk aqueous phase, which had been estimated in the previous Chapter III. Figure V-5 shows the results. We see that the relaxation time τ_1 for the slow mode strongly depends on both C_A^* and C_D, while the τ_2 of the fast mode is independent of C_D but depends on C_A^*. Interestingly, the behavior of the fast mode is identical to that of τ_m of CTAB:NaSal/W systems indicated by the dashed line in the figure. Figure V-6 shows double-logarithmic plots of τ_2 vs C_A^* for the CTAB:HSal/W systems with different C_D.

Another interesting feature is that the τ_1 of the slow

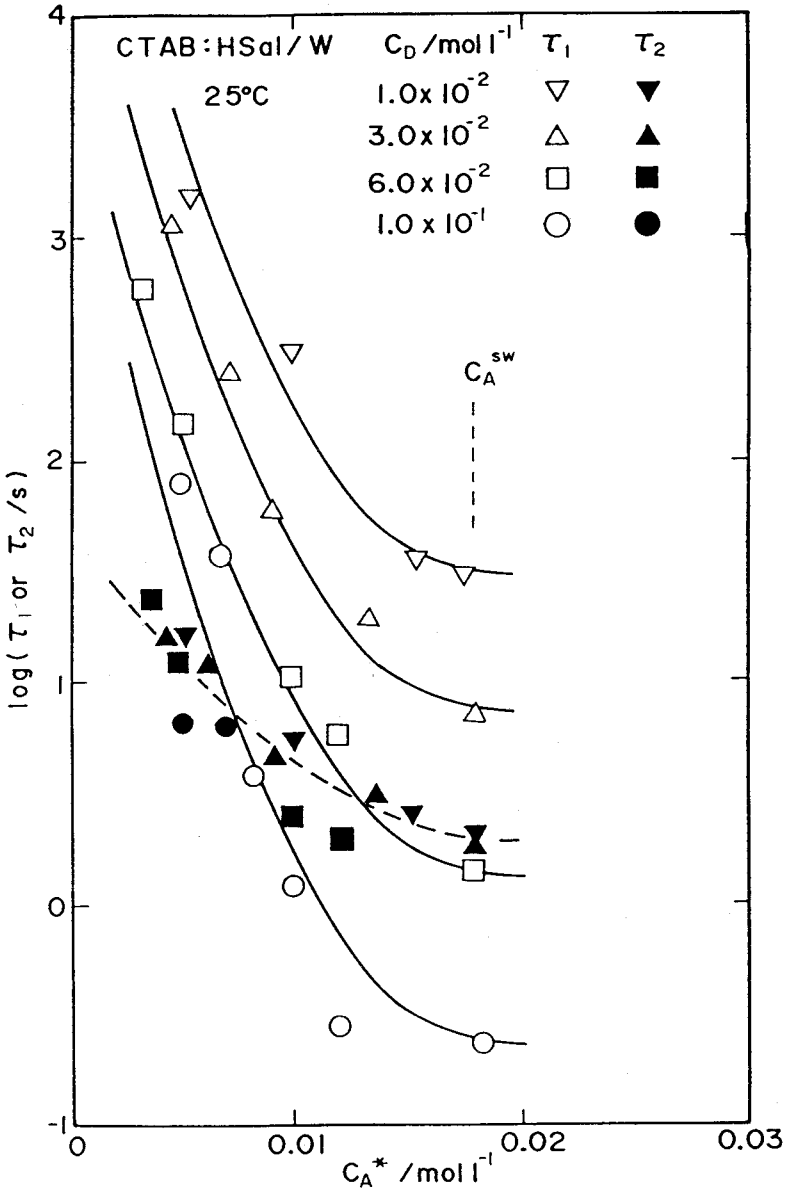

Figure V-5. Dependences of the relaxation times τ_1 and τ_2 of the slow and fast relaxation modes on the concentration C_A^* for CTAB:HSal/W systems at 25°C.

mode decreases with increasing C_D and decreases much faster than the τ_2 with increasing C_A^*. Therefore, the slow mode merges into the fast mode as C_A is increased relative to C_D. Although τ_1 is strongly dependent on C_D, the dependence of τ_1 on C_A^* is quite similar among all the systems examined here. We therefore shifted the $\log(\tau_1)$ vs C_A^* curves vertically by an amount $\log(a_c)$ relative to that of the system with $C_D = 1.0 \times 10^{-2}$ mol l^{-1} chosen arbitrarily as the reference. Figure V-6 shows the obtained composite curve of $\log(\tau_1 a_c)$ vs $\log(C_A^*)$. The insert in Figure V-6 indicates the plot of $\log(a_c)$ vs $\log(C_D)$, which has the slope of 2. Figure V-6 also shows double-logarithmic plot of τ_2 vs C_A^* for the CTAB:HSal/W systems with different C_D. The τ_2 are independent of C_D but dependent on C_A^* as $\tau_2 \propto C_A^{*-2}$.

Thus, we can summarize the τ_1 and τ_2 data (for the systems with $C_D + C_A^{sw} > C_A > 0.8C_D$) shown in Figure V-6 as follows,

$$\tau_1 \propto C_A^{*-5} C_D^{-2} \qquad (V\text{-}6)$$

$$\tau_2 \propto C_A^{*-2} C_D^{0} \qquad (V\text{-}7)$$

Figure V-6 also shows, for the sake of comparison, similar double-logarithmic plot of τ_m vs C_S^* for the CTAB:NaSal/W systems. We see that the values of τ_2 with varying C_A^* agree well with that of τ_m on C_S^* in the region of relatively low C_A^* or C_S^*, where $\tau_m \propto C_S^{*-2} C_D^{0}$. On the other hand, since

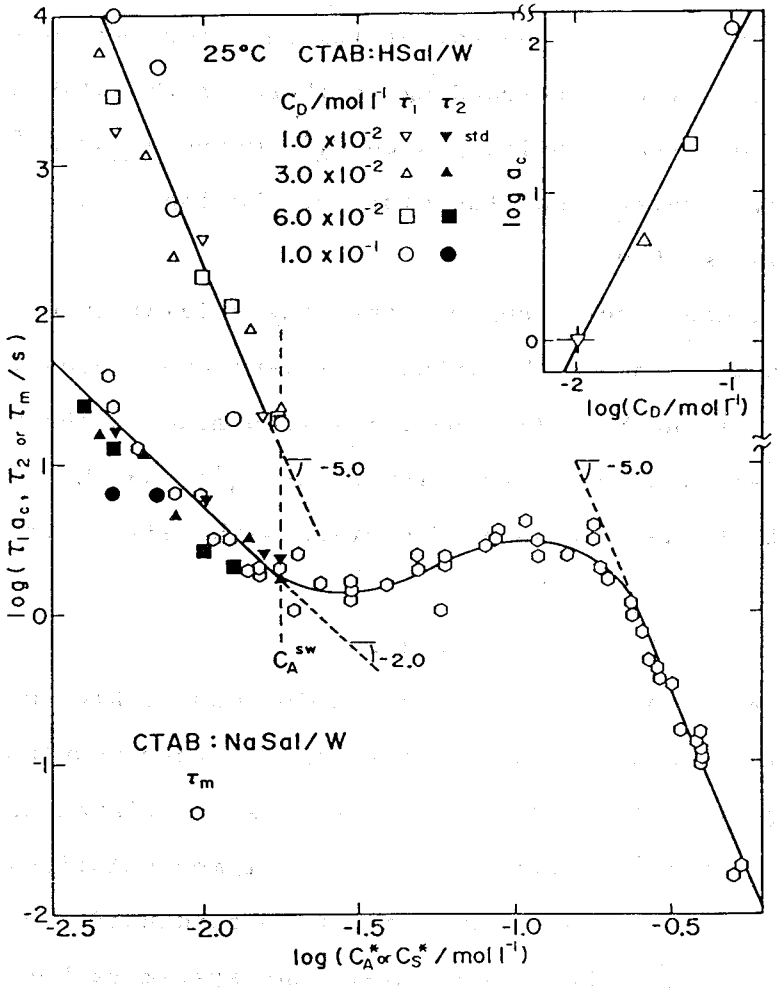

Figure V-6. Double-logarithmic plots of the reduced relaxation times $\tau_1 a_c$ of the slow mode and that τ_2 of the fast mode on the concentration C_A^* for CTAB:HSal/W systems at 25°C. Hexagonal symbols represent the τ_m vs C_S^* for CTAB:NaSal/W systems in the previous Chapter IV. An insert shows double-logarithmic plots of the shift factor a_c vs the detergent concentration C_D.

HSal has the limited solubility in water, we could not observe the behavior corresponding to those of the CTAB:NaSal/W systems with relatively high C_A^*, where $\tau_m \propto C_S^{*-5} C_D^0$. We note, however, that the slope of the $\log(\tau_1 a_C)$ vs $\log(C_A^*)$ curve is -5.0.

These results suggest that the relaxation mechanism of the fast mode in the CTAB:HSal/W systems are basically the same as that of the Maxwell-type relaxation mode in the CTAB:NaSal/W systems with relatively low C_S or C_S^*; and that the slow mode, that of the CTAB:NaSal/W systems with relatively high C_S^*.

V-3-5 Relaxation Mechanisms

For concentrated polymer solutions of high-molecular weight M and concentration C, the plateau modulus G_N^0 is proportional to $M^0 C^{2.2}$ and the longest relaxation time, to $M^{3.4} C^{1.5}$.[2,5] Obviously, in the polymer solutions, the relaxation is far slower in a more condensed and fully entangled, higher molecular-weight system rather than in a dilute and less fully entangled, lower molecular-weight system. In terms of the tube theory of polymer dynamics,[4] the relaxation in such a system is governed by diffusion of the polymer molecules along their own contour through the entanglement network with the mesh size dependent on the polymer concentration.[1,4]

However, in the micellar solutions, diffusion of the micelles along their contour appears to be nothing to do with the relaxation of the entanglement network. The relaxation

appears to be taking place via actual break down of the entanglement network of the thread-like micelles presumably by passing through each other at the entanglement points.[6,7] As we discussed in Chapter IV, in the concentrated CTAB:NaSal/W systems with high $C_S C_D^{-1}$ ratio, exchange between the immobilized Sal^- ions at the entanglement points of the micelles and free Sal^- ions in the bulk aqueous phase appears to promote dissociation of the complex at the entangled sites, leading to the relaxation in the CTAB:NaSal/W systems. The relaxation time τ_m was accordingly a function of C_S^* alone.

In the present CTAB:HSal/W systems, on the other hand, free HSal molecules in the medium may play the same role as the free Sal^- ions are playing in the CTAB:NaSal/W systems. If such the case, the HSal molecules in the different immobilized sites of the micelles presumably contribute to the relaxation of the CTAB:HSal/W systems in different manners. The fact that the CTAB:HSal/W systems exhibited two relaxation modes might reflect this situation. The HSal molecules in the (c) state might contribute to the slow relaxation mode with τ_1, while those in the (b) state may contribute to the fast mode with τ_2.

A striking fact is that the relaxation time τ_1 of the slow mode becomes shorter as $\tau_1 \propto C_D^{-2}$, while the relaxation strength G_1 varies as $G_1 \propto C_D^{2.2}$, when C_A^* is not very high or $C_A C_D^{-1}$ is in the range of 0.8 to 1.0. The slow relaxation mode proceeds much faster, as the system becomes more and more condensed: This behavior is just opposite to that usually

seen in concentrated polymer solutions, and is not seen even in the CTAB:NaSal/W systems.

A possible explanation on these features is as follows: Disentanglement of network junctions in the system in which free HSal molecules or Sal^- ions are not abundant must be taking place through the reaction involving collisions, fusion and separation between the segments of the thread-like micelles at the entanglement junctions, as depicted in Figure IV-7 of the Chapter IV. Electrostatic repulsion between the thread-like micelles, especially between those composed of CTA^+:HSal complex, may retard primarily the collisions involved in such a reaction. Under such a mechanism, the relaxation time should be inversely proportional to the frequency of such collisions, while the relaxation strength or the modulus must be proportional to the density of the entanglement junctions, both of which are in turn proportional to C_D^2.

This speculation may explain the difference and similarity in the relaxation modes between the CTAB:NaSal/W and CTAB:HSal/W systems. Namely, the surface of the thread-like micelles in the former should be electrically neutral, because the micelles are essentially 1:1 complexes of CTA^+ cations and Sal^- anions, while that in the latter is presumably positively charged, because the micelles are essentially 1:1 complexes between CTA^+ cations and neutral HSal molecules. The electrostatic repulsion between the neutral micelles in the CTAB:NaSal/W systems should be weak, and consequently, the

collisions may not be the rate determining process. On the other hand, the electrostatic repulsion between the charged micelles in the CTAB:HSal/W systems should be much stronger especially in those with low C_D and C_A concentration, thereby retarding the relaxation more severely in the systems with low C_D and low C_A^* rather than that in those with high C_D and high C_A^*.

V-3-6 Effect of Added NaBr

The speculation mentioned above on the electrostatic effects in the micellar solutions may be tested by examining effects of adding a simple electrolyte such as NaBr to the systems.

The effects of adding NaBr on the viscoelastic behavior of the micellar solutions are demonstrated in Figures V-7A and V-7B: The figures show the G' and G" curves of CTAB:NaSal:NaBr/W and CTAB:HSal:NaBr/W systems, respectively, in both of which C_D and C_S (or C_A) were 6.0×10^{-2} mol l^{-1} and the concentration C_{AS} of NaBr varied from 0 upto 6.0×10^{-2} mol l^{-1}.

As seen in Figure V-7A, the G' and G" curves of the CTAB:NaSal:NaBr/W systems are hardly altered, while as seen in Figure 11B those of the two modes merge into one with the strength $(G_1 + G_2)$ and the time τ_2, as C_{AS} of added NaBr is increased. The same feature was observed for all other systems with different C_D, C_S (or C_A) and C_{AS}: The CTAB:NaSal/W systems are practically unaffected, but the

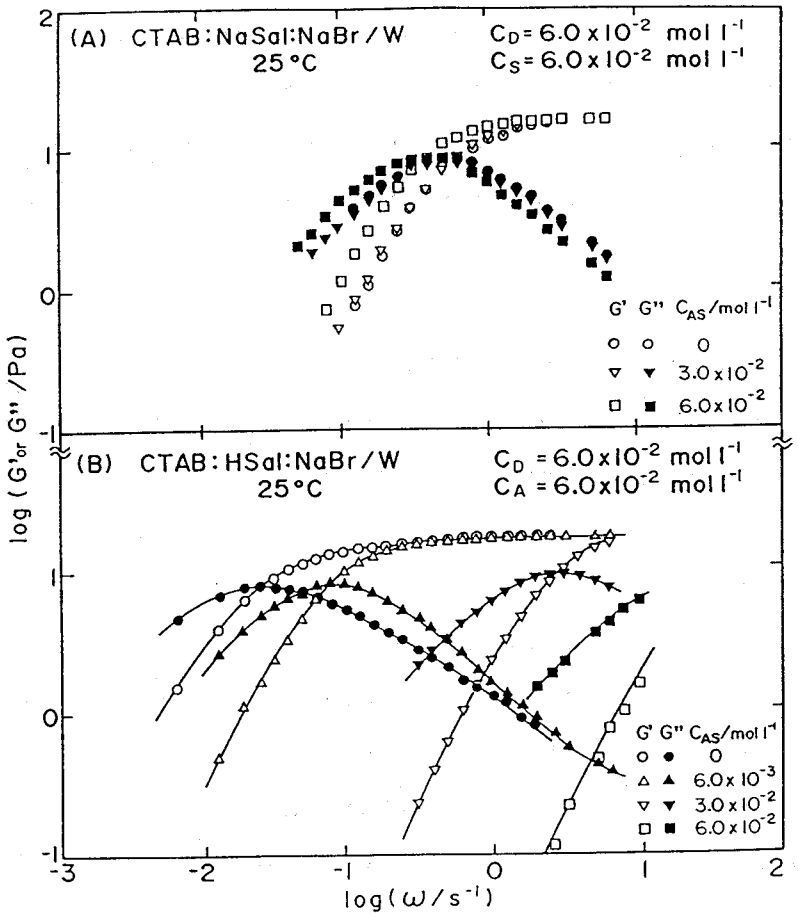

Figure V-7. Frequency ω dependence of storage G' and loss G" moduli for CTAB:NaSal:NaBr/W (A) with C_D = 6.0 x 10^{-2}, C_S = 6.0 x 10^{-2} mol l^{-1} and several C_{AS} of NaBr, and CTAB:HSal:NaBr/W (B) solutions with C_D = 6.0 x 10^{-2}, C_A = 6.0 x 10^{-2} mol l^{-1} and several C_{AS}.

CTAB:HSal/W systems become to exhibit the behavior similar to the former systems. Evidently, the excess Br^- ions from the added NaBr shield the electrostatic repulsion among the CTA^+:HSal micelles so that the collision frequency is increased to accelerate the slow mode of the CTAB:HSal/W systems. On the other hand, electrically neutral micelles of the CTAB:NaSal/W systems are unlikely to be affected by adding a simple electrolyte.

REFERENCES

1) Ferry, J. D. Viscoelastic Properties of Polymers; 3rd ed. John Wiley: New York, 1980.

2) Rouse, Jr., P. E. J. Chem. Phys. 1953, 21, 1272.

3) Zimm, B. H. J. Chem. Phys. 1956, 24, 269.

4) Doi, M.; Edwards, S. F. The Theory of Polymer Dynamics; Oxford Univ. Press: Oxford, 1986.

5) Tobolsky, A. V.; Murakami, K. J. Polym. Sci. 1959, 40, 433.

6) Nilsson, P. G.; Wennerström, H.; Lindman, B. J. Phys. Chem. 1983, 87, 1377.

7) Kato, T.; Anzai, S.; Seimiya, T. J. Phys. Chem. 1987, 91, 4655.

8) Yamamoto, Y. Buttai no Henkeigaku; Seibundoshinkousha: Tokyo, 1962.

Chapter VI

Nonlinear Viscoelastic Behavior of Aqueous Solutions of Cetyltrimethylammonium Bromide with Sodium Salicylate and with Salicylic Acid

VI-1 Introduction

In Chapters IV and V, we discussed the dynamic viscoelastic behavior of aqueous solutions of cetyltrimethylammonium bromide (CTAB) complexed with sodium salicylate, CTAB:NaSal/W, and with salicylic acid, CTAB:HSal/W, respectively. The CTAB:NaSal/W systems with high salt-to-detergent ratio exhibited only one relaxation mode, while the corresponding CTAB:HSal/W systems exhibited two distinct relaxation modes. We demonstrated that such a difference has resulted from the difference in the structural features of the thread-like micelles existing in these systems as revealed in Chapter III.

In this chapter, we examine their nonlinear viscoelastic behavior such as stress relaxation at finite strain, steady shear flow, stress growth and decay at inception and after cessation of steady shear flow on the CTAB:NaSal/W and CTAB:HSal/W systems. The results of both systems are compared with each other and also with those of concentrated polymer systems. We discuss the characteristic features of their

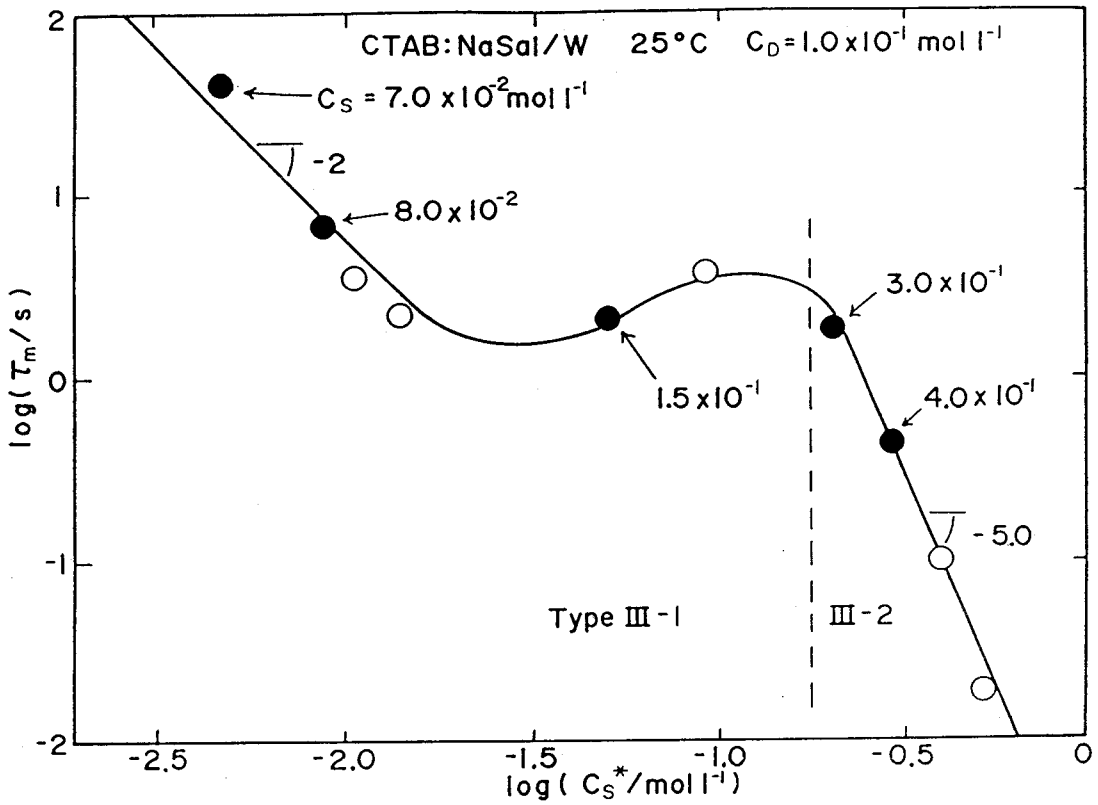

Figure VI-1. Relationship between the relaxation time τ_m determined from dynamic measurements and free Sal^- ion concentration C_S^* in bulk aqueous phase for type III CTAB:NaSal/W systems. Filled circles represent the systems studied in this chapter.

nonlinear rheological behavior to elucidate the nature of entanglement in these micellar systems in relation with that of concentrated polymer systems.

VI-2 Experimental

VI-2-1 Sample Solutions

Figure V-1 reproduces the plots, shown in Figure IV-6, for the relaxation time τ_m vs the concentration C_S^* of free salicylate ions of CTAB:NaSal/W systems with CTAB concentration C_D of 1.0×10^{-1} mol l^{-1} and salt concentration C_S varied from 7.0×10^{-2} to 4.0×10^{-1} mol l^{-1}. The filled circles distinguish the solutions examined in this Chapter. All of them belong to the type III solutions that exhibit the Maxwell-model behavior with the single relaxation time τ_m and the strength G_N^0, as described in the previous Chapter IV. The CTAB:HSal/W solutions examined in this Chapter are those with $C_D = 6.0 \times 10^{-2}$ and 1.0×10^{-1} mol l^{-1} and the acid concentration C_A varied in the range of the acid-to-detergent ratio $C_A C_D^{-1}$ from 0.8 to 1.2. The latter combination is close to the saturation of HSal in the bulk aqueous phase (cf. Chapter III-3-1).

VI-2-2 Rheological Measurements

Nonlinear stress relaxation measurement at finite shear strain[1] was carried out in the range of shear strain γ from 0.5 to 5.0 beyond which the measurement could not be performed.

Measurement of steady shear flow, stress response at inception of steady shear flow, and stress relaxation after cessation of steady shear flow were carried out in the range of shear rate $\dot{\gamma}$ varied from 1.2 $x10^{-1}$ to 4.61 x 10^{2} s^{-1}. All the rheological measurement was carried out at room temperature (about 20 - 25°C).

VI-3 Results for the CTAB:NaSal/W Systems

VI-3-1 Stress Relaxation

Figure VI-2 shows the stress relaxation behavior of the system with C_D = 1.0 x 10^{-1} and C_S = 1.5 x 10^{-1} mol l^{-1}. Up to the shear strain γ of 2.0, the relaxation modulus $G(t,\gamma)$ does not depend on γ. When γ exceeds 3.0, the $G(t,\gamma)$ in the short times suddenly increase but fall off rapidly with time. At γ above 4.0, the solution slipped on the surface of the cone and plate, and we could not carry out the measurement any longer. Each of the two lines drawn for the strain $\gamma < 0.2$ and $\gamma = 3.6$ can be cast into a single exponential decay function. The relaxation time for $\gamma = 3.6$ is slightly smaller than that for the $\gamma < 0.2$. The latter agrees with the Maxwell model relaxation time τ_m found in the dynamic measurement. Qualitatively the same results were obtained for the solutions with C_S = 7.0 x 10^{-2} and 8.0 x 10^{-2} mol l^{-1}.

Figure VI-3 shows the relaxation modulus $G(t,\gamma)$ for the solution with C_D = 1.0 x 10^{-1} and C_S = 3.0 x 10^{-1} mol l^{-1}. For $\gamma < 1.5$, this system also shows complete linearity: The

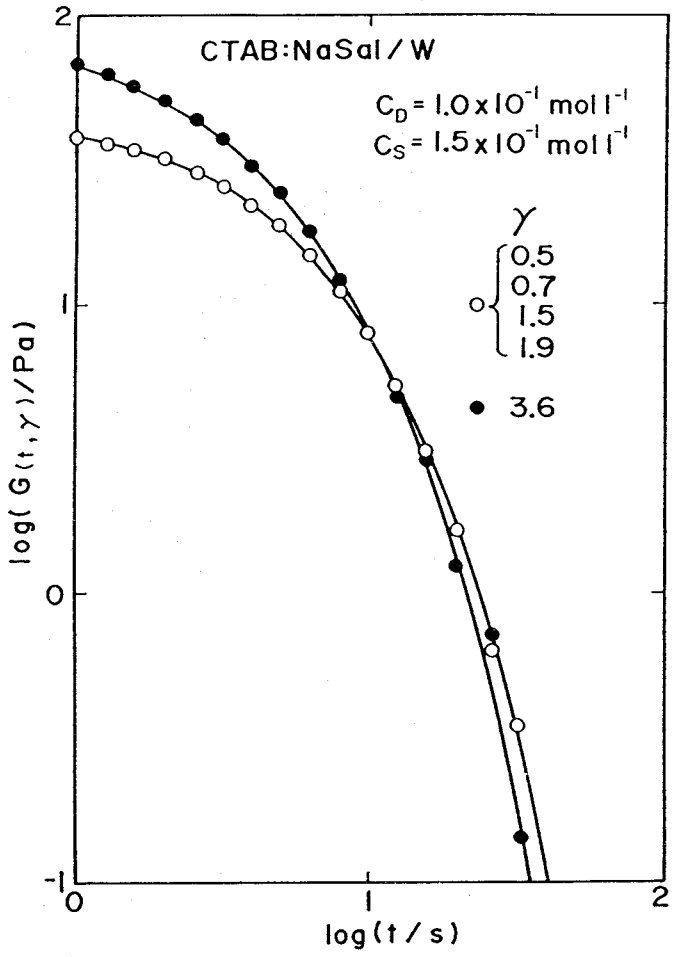

Figure VI-2. Shear stress relaxation modulus $G(t,\gamma)$ for a type III-1 solution with $C_D = 1.0 \times 10^{-1}$ and $C_S = 1.5 \times 10^{-1}$ mol l^{-1}.

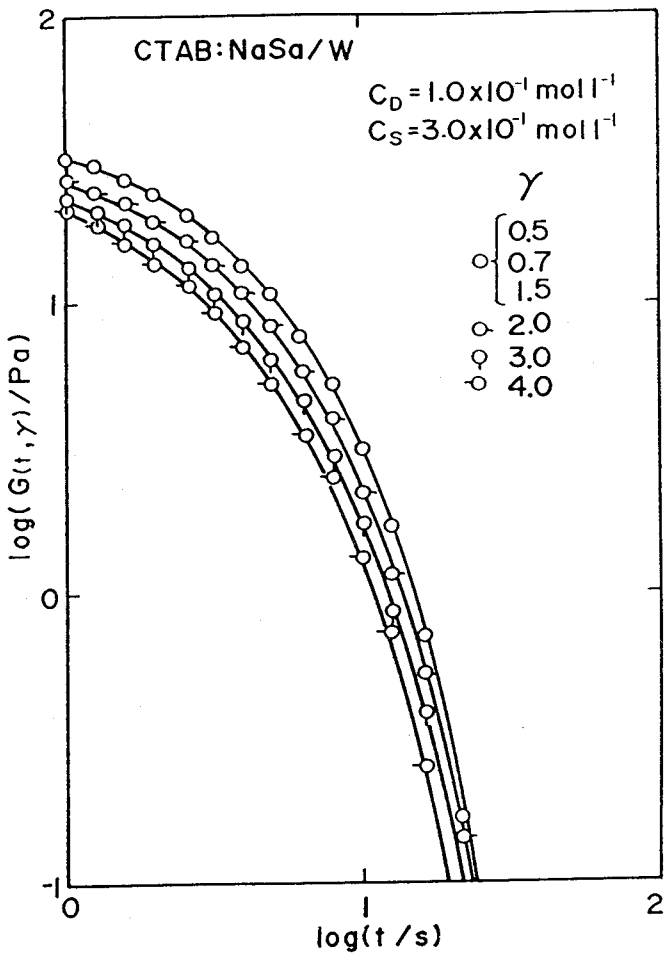

Figure VI-3. Shear stress relaxation modulus $G(t,\gamma)$ for a type III-2 solution with $C_D = 1.0 \times 10^{-1}$ and $C_S = 3.0 \times 10^{-1}$ mol l^{-1}.

relaxation modulus $G(t,\gamma)$ was independent of γ. Beyond γ > 1.5 the relaxation modulus $G(t,\gamma)$ decrease with increasing γ in all the range of t and γ examined, as opposed to the feature of the system with C_S = 1.5 x 10^{-1} mol l^{-1} shown in Figure VI-2. Again we could not determine the $G(t,\gamma)$ for γ > 5.0, because of sample slippages. For the solution with C_S = 4.0 x 10^{-1} mol l^{-1}, we could not determine the $G(t,\gamma)$ precisely, because its longest relaxation time τ_m was too short (< 1 s) to be determined accurately with the apparatus employed. For the systems with C_S = 1.5 x 10^{-1} and 3.0 x 10^{-1} mol l^{-1}, the range of γ where $G(t,\gamma)$ is independent of γ is relatively wide, and the γ dependence at higher γ is rather weak.

The remarkable difference in the γ dependence of $G(t,\gamma)$ between the systems with C_S = 1.5 x 10^{-1} and 3.0 x 10^{-1} mol l^{-1} shown in Figure VI-2 and VI-3, respectively, may indicate difference in the mechanisms of entanglement relaxation which cannot be detected in their linear (dynamic) viscoelastic behavior. The dashed line in Figure VI-1 shows the boundary dividing the systems into two groups that show typically different nonlinear relaxation behavior mentioned above. The increase in $G(t,\gamma)$ with γ is characteristic of the systems found in the region of low C_S^*, where τ_m is proportional to C_S^{*-2} and then τ_m increase with C_S^*: We call it the type III-1 behavior. Contrarily, the decrease in $G(t,\gamma)$ with γ is characteristic of the systems in the other region of high C_S^*, where τ_m is proportional to C_S^{*-5}: We call it type III-2.

VI-3-2 Steady Shear Flow

Figure VI-4 shows the steady shear viscosity $\eta(\dot{\gamma})$ as a function of the reduced shear rate $\tau_m\dot{\gamma}$ for the CTAB:NaSal/W systems with $C_D = 1.0 \times 10^{-1}$ mol l^{-1} and with $C_S = 1.5 \times 10^{-1}$ (type III-1), 3.0×10^{-1} and 4.0×10^{-1} mol l^{-1} (type III-2). All the solutions in this figure exhibit pronounced non-Newtonian flow behavior. In the range of $\tau_m\dot{\gamma} >> 1$, the $\eta(\dot{\gamma})$ decreases as $(\tau_m\dot{\gamma})^{-1}$. The system exhibits significant stress overshoot in the stress response at inception of steady shear flow and a tendency of two-stage decrease in stress relaxation after cessation of the steady shear flow (cf. Chapter VI-3-4, eq VI-3) especially in the strongly non-Newtonian region of high shear rates.

For the solutions with $C_S = 1.5 \times 10^{-1}$ and 3.0×10^{-1} we cannot determine the zero shear viscosity η_0 within the measurable shear rate range. However, we assumed from the curvatures of the $\eta(\dot{\gamma})$ curves for the three solutions that the three curves can be superposed by shifting them vertically. The reduced viscosity $\eta(\dot{\gamma})/\eta_0$ is probably a function only of the reduced shear rate $\tau_m\dot{\gamma}$ for all the systems regardless of whether they belong to the type III-1 or type III-2 groups.

The same figure also shows the frequency ω dependence of the absolute value of the complex viscosity $|\eta^*| = (\eta'^2 + \eta''^2)^{1/2}$ for the solution with $C_S = 4.0 \times 10^{-1}$ mol l^{-1}. The data for $\eta(\dot{\gamma})$ and $|\eta^*|$ coincide each other. This behavior is known as the Cox-Merz law, which well describes

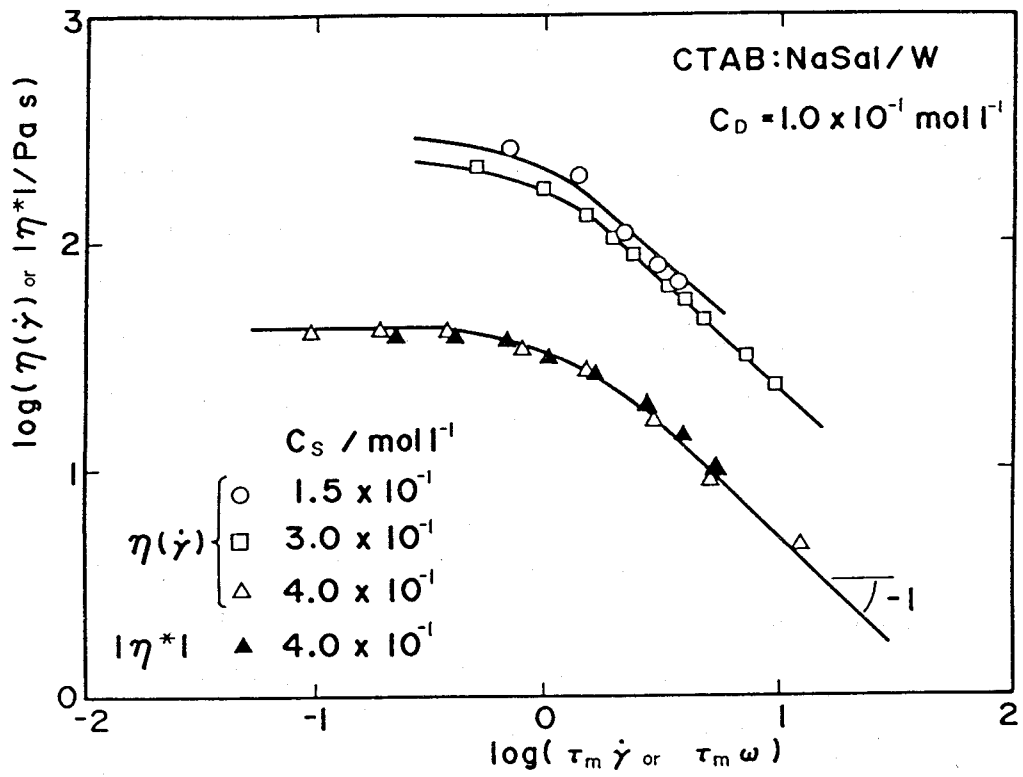

Figure VI-4. Relationship between steady shear viscosity $\eta(\dot{\gamma})$ and the reduced shear rate $\tau_m \dot{\gamma}$ for the solutions with C_D = 1.0 x 10^{-1}, and C_S = 1.5 x 10^{-1}, 3.0 x 10^{-1}, and 4.0 x 10^{-1} mol l^{-1}.

the behavior of concentrated polymer systems.[2,3] From eqs IV-1 and IV-2, the complex viscosity $|\eta^*|$ is expressed with the Maxwell model as

$$|\eta^*| = \eta_0 / \{1 + (\tau_m \omega)^2\}^{1/2} \qquad \text{(VI-1)}$$

Thus, the steady shear viscosity $\eta(\dot{\gamma})$ is also expressed with the same equation by replacing ω by $\dot{\gamma}$. Interestingly, the Cox-Merz law is valid for these CTAB:NaSal/W thread-like micellar systems as well as for concentrated polymer systems, although their constitutive equations should be quite different.

VI-3-3 Stress Response at Inception of Steady Shear Flow

Here, we examine the shear stress response $\sigma_I(t,\dot{\gamma})$ at inception of steady shear flow as a function of time t and shear rate $\dot{\gamma}$. We define the viscosity growth function as $\overline{\eta}(t,\dot{\gamma}) = \sigma_I(t,\dot{\gamma}) / \dot{\gamma}$.

Figure VI-5 shows the result for a type III-1 solution with $C_D = 1.0 \times 10^{-1}$ and $C_S = 1.5 \times 10^{-1}$ mol l^{-1}. At low shear rate $\dot{\gamma} = 1.2 \times 10^{-1}$ s^{-1}, the function $\overline{\eta}(\dot{\gamma},t)$ monotonously increase with t to the steady state value $\eta(\dot{\gamma})$ in a manner

$$\overline{\eta}(t,\dot{\gamma}) = \eta(\dot{\gamma})\{1 - \exp(-t / \tau_m)\} \qquad \text{(VI-2)}$$

At higher $\dot{\gamma} = 0.24$ s^{-1}, the viscosity growth function

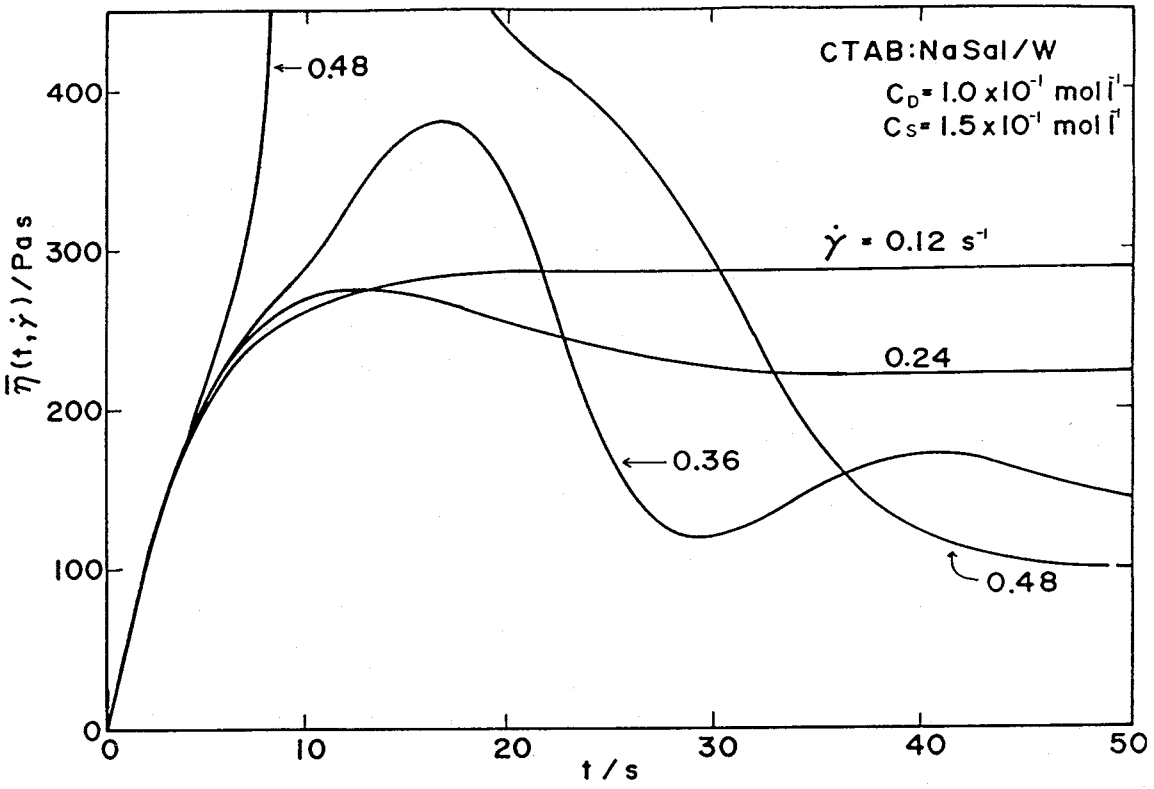

Figure VI-5. Viscosity growth function $\overline{\eta}(t,\dot{\gamma})$ at inception of steady shear flow at various shear rates $\dot{\gamma}$ for the (type III-1) solution with C_D = 1.0 x 10^{-1} and C_S = 1.5 x 10^{-1} mol l^{-1}.

$\overline{\eta}(t,\dot{\gamma})$ exhibits a maximum, the phenomenon known as the stress overshoot.[2,4] At still higher $\dot{\gamma} \geqq 0.36\ s^{-1}$, the maximum is followed by a minimum, and another maximum, and finally the viscosity approaching to the steady state value $\eta(\dot{\gamma})$. The process looks like damping oscillation.[5]

When $\dot{\gamma}$ was increased beyond $4.8 \times 10^{-1}\ s^{-1}$, the viscosity increased very rapidly, and slippage occurred at the stress level of about 10^3 Pa. After the slippage, the viscosity approached the steady state values accompanying irregular damping oscillation. The viscosity growth function at $\dot{\gamma}$ = 3.6×10^{-1} and $4.8 \times 10^{-1}\ s^{-1}$ have an inflection point at around 8 s, suggesting that the increase in stress occurs in two separate stages. The maximum of the viscosity growth curves at $\dot{\gamma}$ = 0.36 and 0.48 s^{-1} exceed that of the curve at the lowest $\dot{\gamma}$ = 0.12 s^{-1} examined here. Presumably, this feature of the type III- 1 behavior is related to the increase in the relaxation modulus with increasing strain as seen in Figure VI-2.

Figure VI-6 shows the viscosity growth function $\overline{\eta}(t,\dot{\gamma})$ for a type III-2 solution with $C_D = 1.0 \times 10^{-1}$ and $C_S = 3.0 \times 10^{-1}$ mol l^{-1}. This system shows no slippage even at rather high shear rates and the viscosity growth function varies systematically with increasing $\dot{\gamma}$: A monotonous increase for the function at low $\dot{\gamma}$ ($< 0.12\ s^{-1}$) according to eq VI-2; one peak for those at $\dot{\gamma}$ around 0.36 to 0.48 s^{-1}; and two peaks in the curves at $\dot{\gamma} > 0.72\ s^{-1}$. With increasing $\dot{\gamma}$, the maximum and minimum become appreciable, and the damping oscillation

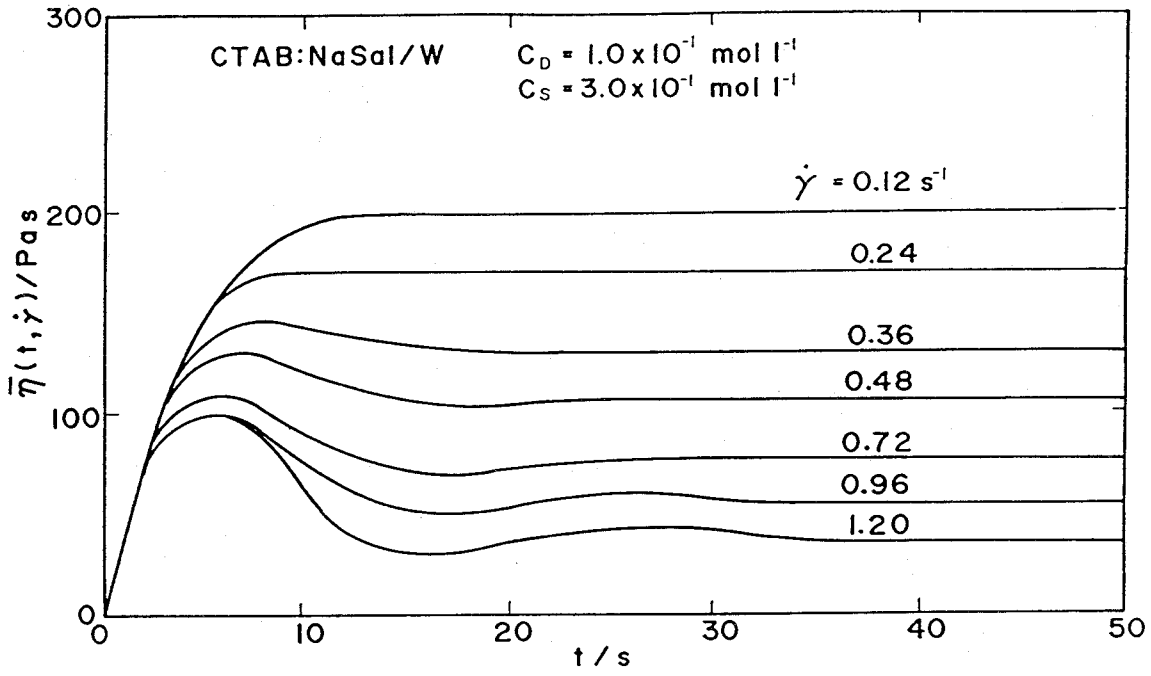

Figure VI-6. Viscosity growth function $\bar{\eta}(t,\dot{\gamma})$ at inception of steady shear flow at various shear rates $\dot{\gamma}$ for the (type III-2) solution with $C_D = 1.0 \times 10^{-1}$ and $C_S = 3.0 \times 10^{-1}$ mol l^{-1}.

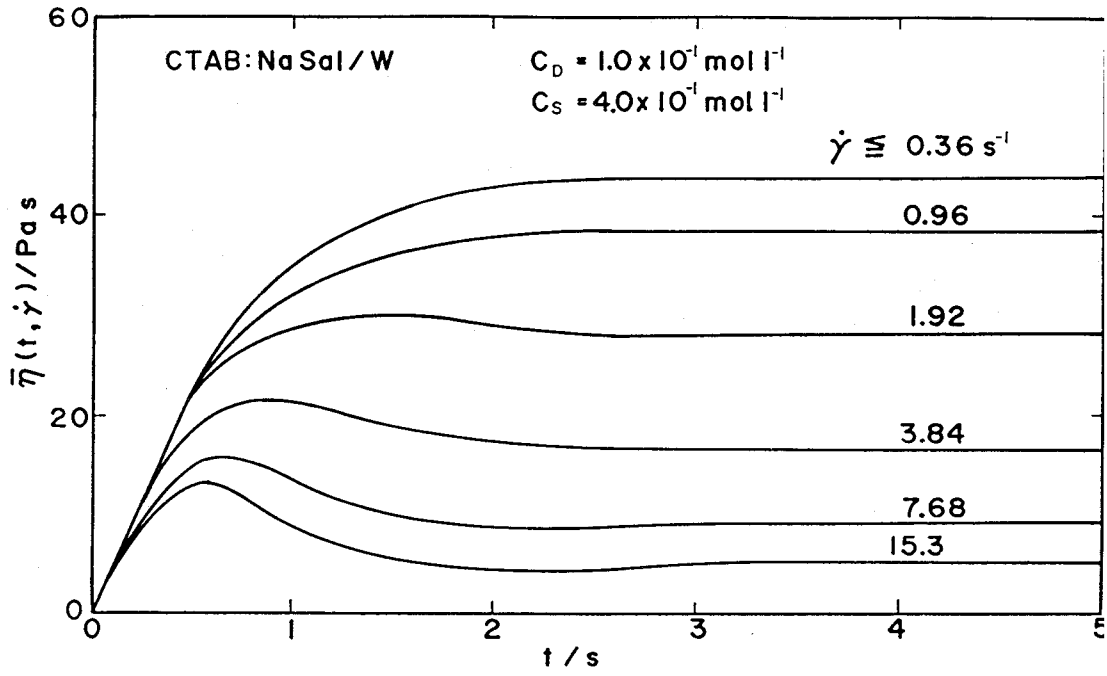

Figure VI-7. Viscosity growth function $\overline{\eta}(t,\dot{\gamma})$ at inception of steady shear flow at various shear rates $\dot{\gamma}$ for the (type III-2) solution with C_D = 1.0 x 10^{-1} and C_S = 4.0 x 10^{-1} mol l^{-1}.

also becomes striking, while the frequency of the damping oscillation is independent of $\dot{\gamma}$. The time t_M, at which the viscosity exhibits the first maximum, approaches a certain value close to τ_m asymptotically with increasing $\dot{\gamma}$.

Interestingly, the solutions shown in Figures VI-5 (type III-1) and VI-6 (type III-2), possess roughly the same relaxation time τ_m, but their viscosity responses at the same $\dot{\gamma}$ are quite different.

Figure VI-7 shows the viscosity growth function $\overline{\eta}(t,\dot{\gamma})$ of another type III-2 solution with C_D = 1.0 x 10^{-1} and C_S = 4.0 x 10^{-1} mol l^{-1}. The shape of the function $\overline{\eta}(t,\dot{\gamma})$ is similar to but the damping oscillatory decay is not so pronounced as that of the solution with C_S = 3.0 x 10^{-1} mol l^{-1}. The time t_M decreases with increasing $\dot{\gamma}$.

VI-3-4 Stress Relaxation after Cessation of Steady Shear Flow

Figure VI-8 shows typical results of the reduced stress relaxation $\sigma_C(t,\dot{\gamma})/\sigma_C(0,\dot{\gamma})$ after cessation of steady shear flow for the system with C_D = 1.0 x 10^{-1} and C_S = 3.0 x 10^{-1} mol l^{-1}. The system of this figure belongs to the type III-2. The qualitative feature of the reduced stress relaxation function $\sigma_C(t,\dot{\gamma})/\sigma_C(0,\dot{\gamma})$ curves is essentially the same for all the CTAB:NaSal/W systems studied here. For $\dot{\gamma}$ < 4.8 x 10^{-1} s^{-1}, the stress relaxes with a single relaxation time τ_α . The relaxation time τ_α estimated from the slope of log $\sigma_C(t,\dot{\gamma})$ vs t curves is identical with the τ_m evaluated from the linear viscoelastic behavior.

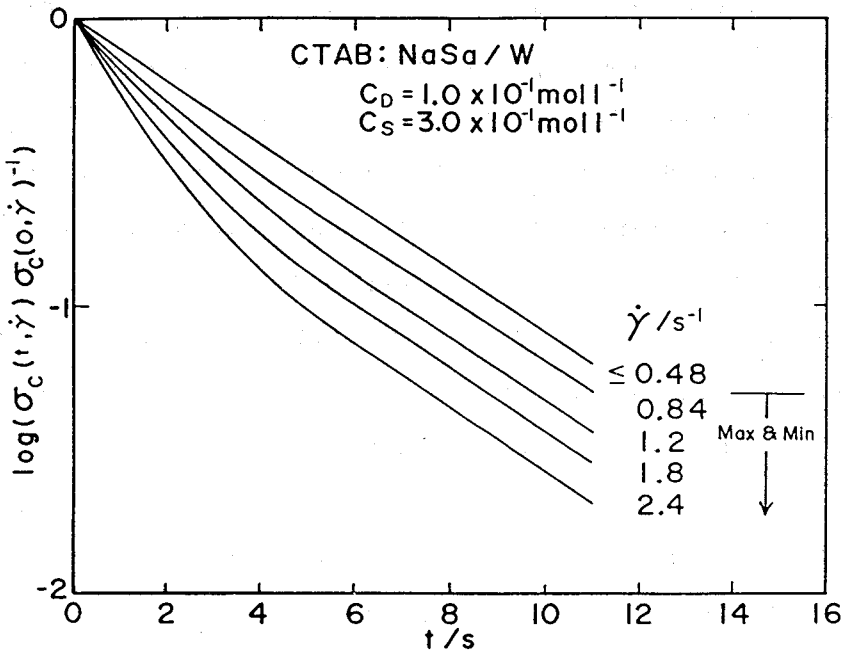

Figure VI-8. Stress relaxation functions $\sigma_C(t,\dot{\gamma})/\sigma_C(0,\dot{\gamma})$ after cessation of steady shear flow at various shear rates $\dot{\gamma}$ for the (type III-2) solution with C_D = 1.0 x 10^{-1} mol l^{-1} and C_S = 3.0 x 10^{-1} mol l^{-1}.

As $\dot{\gamma}$ was increased for this type III-2 system, a maximum appeared in the stress response after inception of steady shear flow and the stresses after cessation of flow did not relax with a single time but in at least two stages. Thus, the curves for $\dot{\gamma} > 0.84\ s^{-1}$ shown in Figure VI-8 can be fitted to the sum of two exponential decay functions with two time constants τ_α and τ_β ($< \tau_\alpha$) as

$$\sigma_C(t,\dot{\gamma})/\sigma_C(0,\dot{\gamma}) = P_\alpha \exp(-t/\tau_\alpha) + (1 - P_\alpha)\exp(-t/\tau_\beta) \quad \text{(VI-3)}$$

We estimated τ_α, τ_β and the fraction P_α of the stress component with τ_α. The results are shown in Figure VI-9A and VI-9B. Interestingly, both τ_α and τ_β are independent of $\dot{\gamma}$. On the other hand, the fraction P_α decreases with increasing $\dot{\gamma} > 0.84\ s^{-1}$ beyond which the fast relaxation mechanism with τ_β becomes prevailing.

The relaxation time τ_β probably corresponds to the time necessary for the system to heal the inner structure disturbed by the steady shear flow at $\dot{\gamma}$ to recover the state responsible to the linear viscoelasticity.[6]

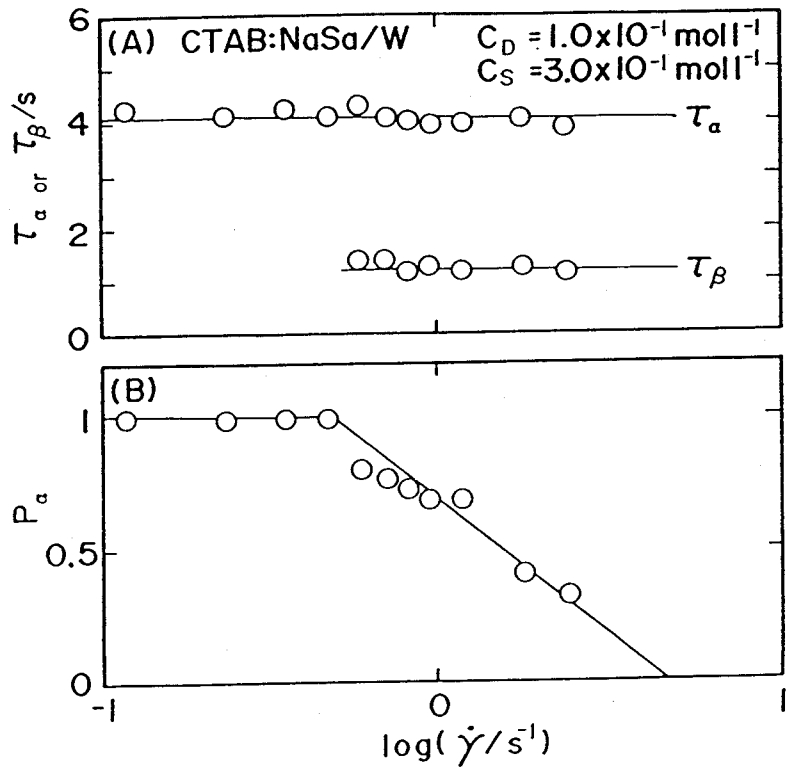

Figure VI-9. (A):Shear rate $\dot{\gamma}$ dependence of the relaxation times τ_α and τ_β obtained from Figure 8. (B):Shear rate $\dot{\gamma}$ dependence of fraction P_α of the component with τ_α in the stress relaxation functions after cessation of steady shear flow obtained from Figure VI-8.

VI-4 Results for the CTAB:HSal/W Systems

VI-4-1 Stress Relaxation

Now we turn our attention to the CTAB:HSal/W systems with high acid-to-detergent ratio $C_A C_D^{-1}$, which exhibited two distinct relaxation modes in their linear viscoelastic responses.

Figure VI-10 shows typical results of the strain dependent relaxation modulus $G(t,\gamma)$ for the solution with C_D = 6.0 x 10^{-2} and C_A = 6.0 x 10^{-2} mol l^{-1}. At short times, the strain γ dependence of $G(t,\gamma)$ is not large but becomes increasingly pronounced with time.

Corresponding to the two-mode linear viscoelastic behavior described in Chapter V, this system also exhibits two modes in the nonlinear behavior: The characteristic time τ_1 is about 50 s, but τ_2, about 6.3 s, which exactly agree with those determined from the linear behavior (cf., Table V-1 in Chapter V). The slow relaxation mode with τ_1 appears to have stronger strain dependence with its strength decreasing with γ than the fast relaxation mode with τ_2. Other solutions with different C_A behaved essentially in the same manner.

This two-stage change in $G(t,\gamma)$ and its γ dependence of the CTAB:HSal/W systems are in quite a contrast to those of the CTAB:NaSal/W systems. To see the time t and strain γ dependence of $G(t,\gamma)$ more precisely, we replotted the data of the same system in a semi-logarithmic scale and in a linear scale in Figures VI-11A and VI-11B, respectively. The broken lines in these figures express the linear relaxation modulus

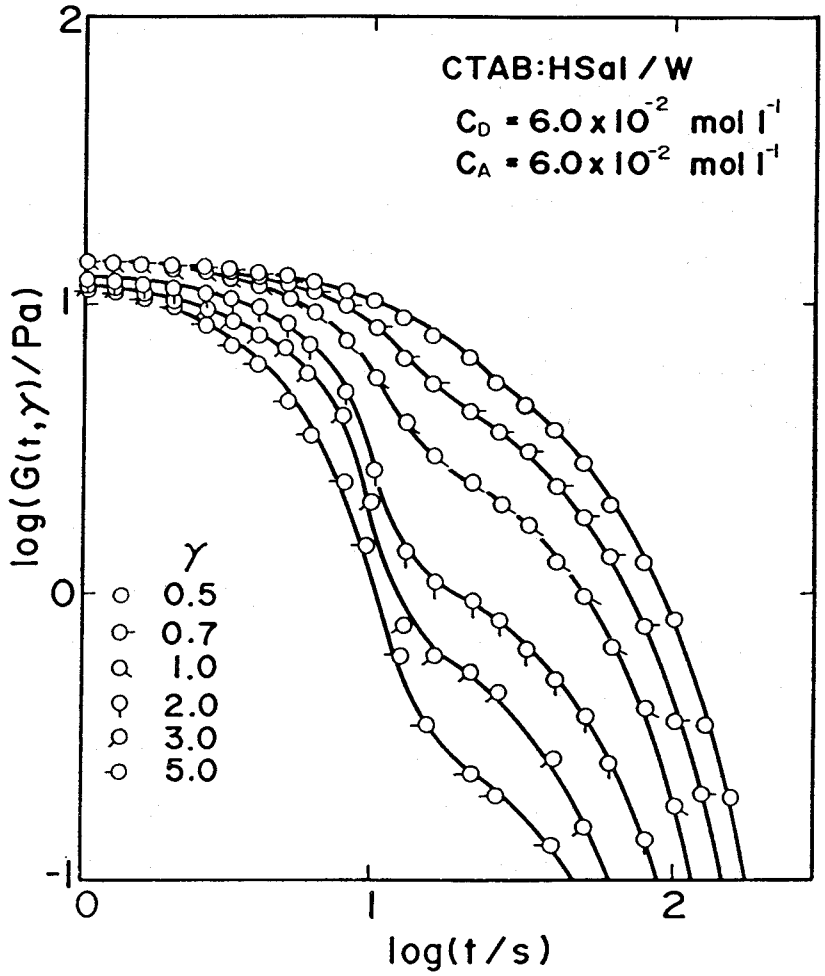

Figure VI-10. Double-logarithmic plots of shear relaxation modulus $G(t,\gamma)$ vs time t at various strain γ for the solution with C_D = 6.0 x 10^{-2} mol l^{-1} and C_A = 6.0 x 10^{-2} mol l^{-1}.

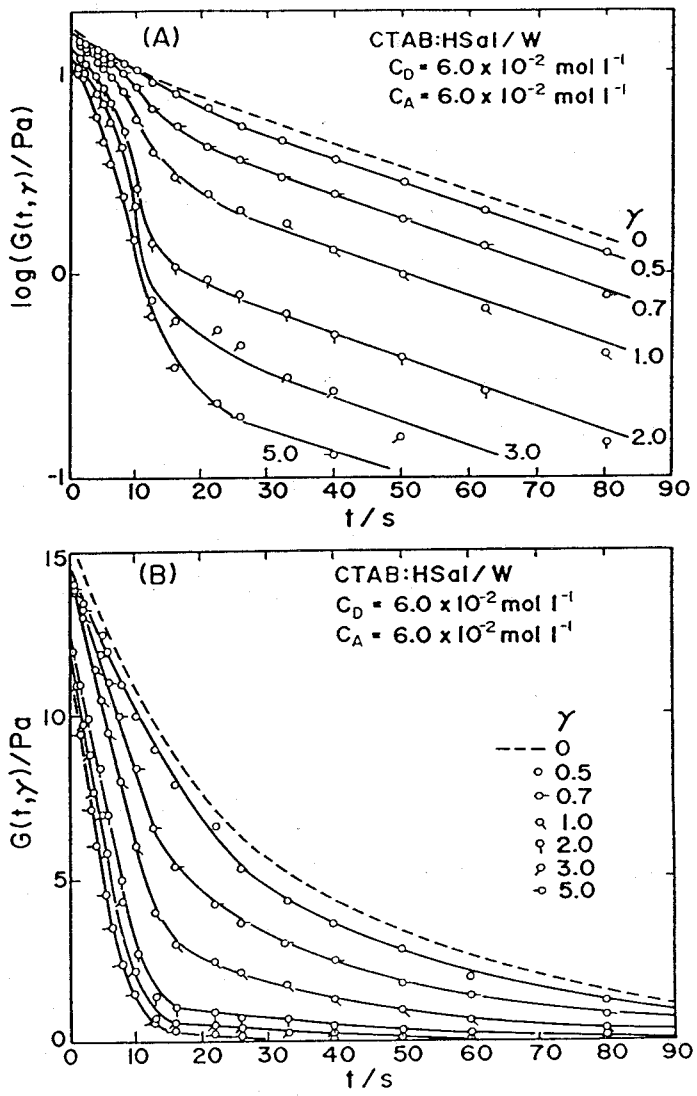

Figure VI-11. Semi-Logarithmic (A) and linear (B) plots of the shear relaxation modulus $G(t,\gamma)$ vs time t for the same data in Figure VI-10. The broken lines in the figures represent the curves for the linear limit estimated from the dynamic measurements in the Chapter V.

G(t) estimated from the dynamic moduli with a small strain amplitude (γ_0 = 0.33) described in the previous Chapter V.

As seen in Figure VI-11A, all the log $G(t,\gamma)$ vs t curves possess at the long time ends (t > 30 s) a straight line portion with nearly the same slope. The result implies that the relaxation time τ_1 of the slow mode is nearly independent of γ, but its strength, rapidly decreasing with γ. These relaxation times and the strength should correspond to the τ_1 and G_1, respectively, of the slow mode in the linear viscoelastic response at the limit of infinitesimally small strain. Thus, the modulus G_1 should be a nonlinear function $G_1(\gamma)$ of γ.

The log $G(t,\gamma)$ vs t curves of this system at relatively high strain are upward convex in the short time region (t < 20 s) as seen in Figure V-11A. Since other solutions tested have also shown more or less the same tendency, this peculiar behavior of $G(t,\gamma)$ appears to be characteristic of the CTAB:HSal/W systems. This behavior means that the nonlinear relaxation modulus $G(t,\gamma)$ of the present systems cannot be given as a sum of exponential functions with the strain dependent strength $G_i(\gamma)$ and relaxation time $\tau_i(\gamma)$ as

$$G(t,\gamma) = \sum_i G_i(\gamma) \exp\{- t / \tau_i(\gamma)\} \qquad \text{(VI-4)}$$

Most of the nonlinear relaxation moduli reported so far especially for polymer solutions are known to be cast into

this eq VI-4.[2,4]

Figure VI-11B shows linear scale plots of the $G(t,\gamma)$ data for the same system. From this figure, we read that $G(t,\gamma)$ at relatively high strain ($\gamma > 1.0$) decreases roughly proportionally to time t in the short time region. The slope of the straight line portions of the $G(t,\gamma)$ vs t curves depends slightly on the strain γ. Then, from these two Figures VI-11A and VI-11B we can cast the $G(t,\gamma)$ curves at the relative high strain into the following form,

$$G(t,\gamma) = \{G^0 - G_1(\gamma)\} - k\,t + G_1(\gamma)\exp(-t/\tau_1) \qquad \text{(VI-5)}$$

$$\begin{cases} k = K(\gamma) & t < \{G^0 - G_1(\gamma)\}/K(\gamma) \\ k = 0 & t \geqq \{G^0 - G_1(\gamma)\}/K(\gamma) \end{cases}$$

where G^0 is the modulus at $t = 0$ and $K(\gamma)$ is a proportional constant slightly dependent on γ, respectively. Under an infinitesimally small strain the fast relaxation mode with τ_2 was observed around $t < 10$ s in the linear viscoelastic response. Under high strain, however, this strange nonlinear behavior completely obscures the τ_2 mode.

To see the γ dependence of $G(t,\gamma)$ quantitatively, we define a damping function,

$$h(\gamma) = G_1(\gamma)/G^0$$
$$(= G(t,\gamma)/G(t) \quad \text{for the long time side}) \qquad \text{(VI-6)}$$

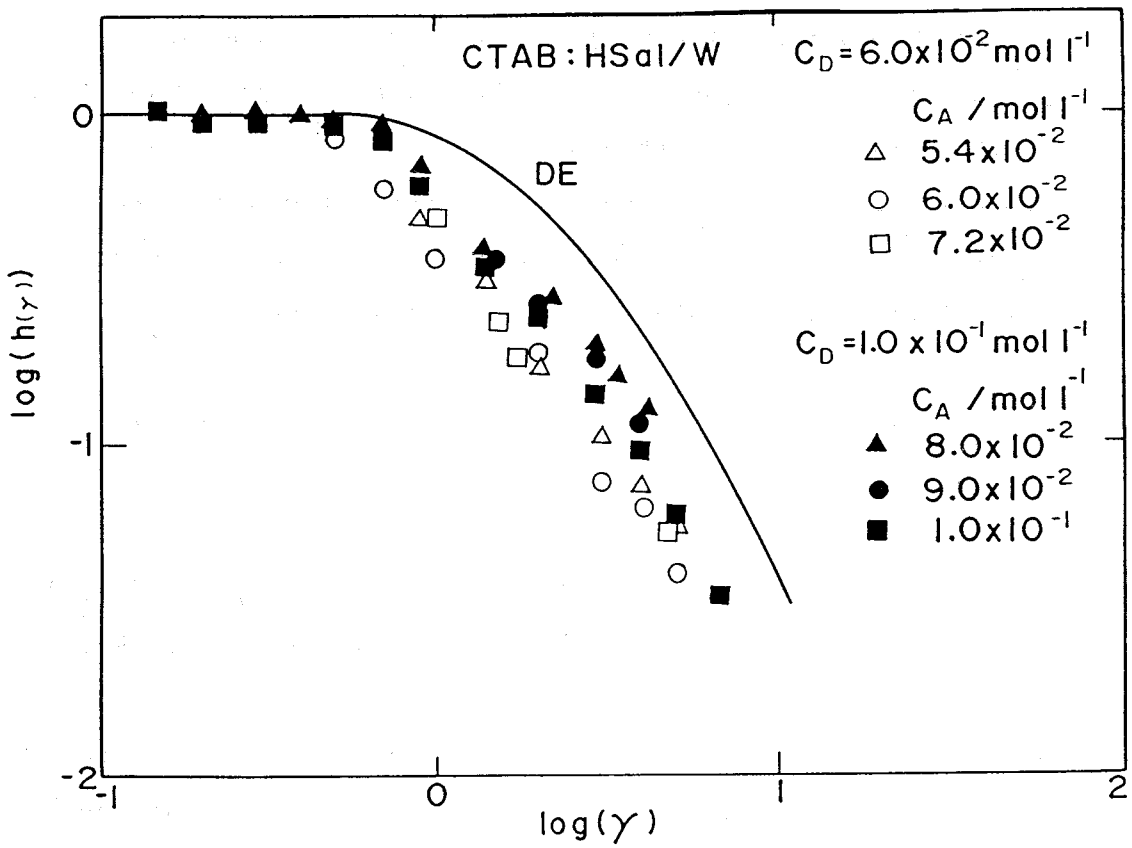

Figure VI-12. The damping function h(γ) for the solutions with C_D = 6.0 x 10^{-2} and 1.0 x 10^{-1} mol l^{-1} and with several C_A. The solid line represents the damping function h(γ) predicted by the Doi and Edwards for concentrated polymer systems.[7]

Figure VI-12 shows the γ dependence of $h(\gamma)$ for the solutions with C_D = 6.0 x 10^{-2} and 1.0 x 10^{-1} mol l^{-2} and with several C_A. The function $h(\gamma)$ rapidly decreases with increasing γ.

VI-4-2 Steady Shear Flow

Figure VI-13 shows the normalized steady shear viscosity $\eta(\dot{\gamma})/\eta_0$ as a function of the reduced shear rate $\tau_1\gamma$ for the solutions with C_D = 6.0 x 10^{-2} and C_A = 5.4 x 10^{-2}, 6.0 x 10^{-2} and 7.2 x 10^{-2} mol l^{-1}. Here, η_0 is the zero shear viscosity estimated from the results of dynamic measurements described in the Chapter V. The slope of all the curves is about -1. All the systems showed pronounced non-Newtonian flow behavior in all the range of measured shear rates.

The normalized dynamic viscosity $|\eta^*|/\eta_0$ for the solution with C_A = 7.2 x 10^{-2} mol l^{-1} is also plotted with the solid line against the reduced frequency $\tau_1\omega$ in the same Figure VI-13. The data of $\eta(\gamma)/\eta_0$ and of $|\eta^*|/\eta_0$ do not coincide with each other. On the other hand, we already saw that $\eta(\dot{\gamma})$ and $|\eta^*|$ of the CTAB:NaSal/W systems coincided with each other, satisfying the Cox-Merz law[3] just like polymer systems.[2] The disagreement between $\eta(\dot{\gamma})$ and $|\eta^*|$ seen in Figure VI-13 appears to be characteristic of the CTAB:HSal/W systems.

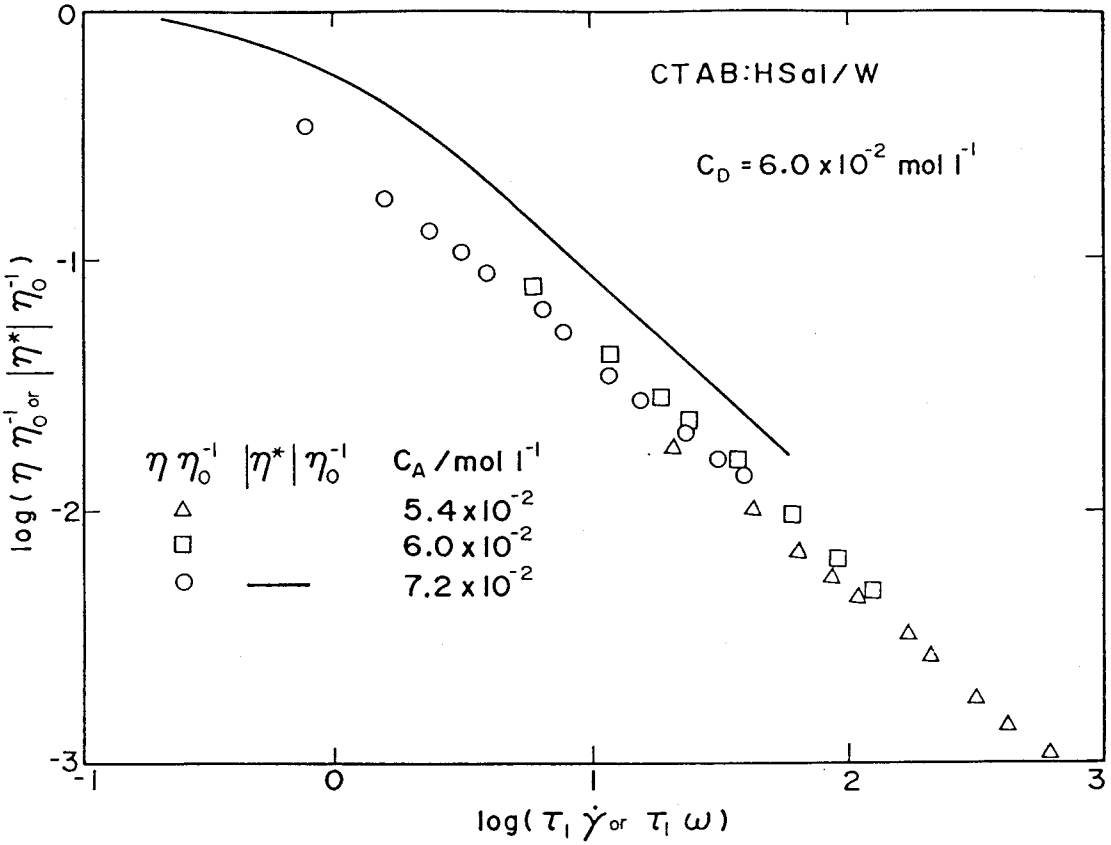

Figure VI-13. Flow curves for the solutions with C_D = 6.0 x 10^{-2} and C_A = 5,4 x 10^{-2}, 6.0 x 10^{-2} and 7.2 x 10^{-2} mol l^{-1}. This figure also contains the dependence of dynamic viscosities $|\eta^*|$ on the frequency for the system with C_D = 6.0 x 10^{-2} and C_A = 7.2 x 10^{-2} mol l^{-1}.

VI-4-3 Stress Response at Inception of Steady shear

Figure VI-14 shows the viscosity growth function $\overline{\eta}(t,\dot{\gamma})$ at inception of steady shear flow at several shear rates γ on the solution with C_A = 6.0 x 10^{-2} mol l^{-1}. This system is strongly non-Newtonian in all the shear rate range examined here (cf., Figure VI-13). Correspondingly, the viscosity growth function exhibits significant stress overshoot even at the shear rate level of as low as 0.12 s^{-1}. Moreover, after the first stress maximum at t_M after the inception of the steady shear, small minima and maxima follow alternately: The process also looks like damping oscillation as seen in Figure VI-14.

On the other hand, as shown in Figures VI-6 and VI-7 for CTAB:NaSal/W systems, their viscosity growth function at low shear rate level monotonously increased to the steady state value, and only that at high shear rates, where significant non-Newtonian behavior was seen, exhibited stress overshoot and following damping oscillation. Still another striking differences between these two systems are as follows: (i) Although the time t_M of the CTAB:NaSal/W systems gradually decreased with increasing $\dot{\gamma}$ to the characteristic time τ_m of the linear response regime, the time t_M of the CTAB:HSal/W systems became much shorter than τ_1 (or even than τ_2) with increasing $\dot{\gamma}$. (ii) The time of the first stress minimum of the CTAB:NaSal/W systems was independent of $\dot{\gamma}$, while the corresponding time of the CTAB:HSal/W systems rapidly decreased with increasing $\dot{\gamma}$.

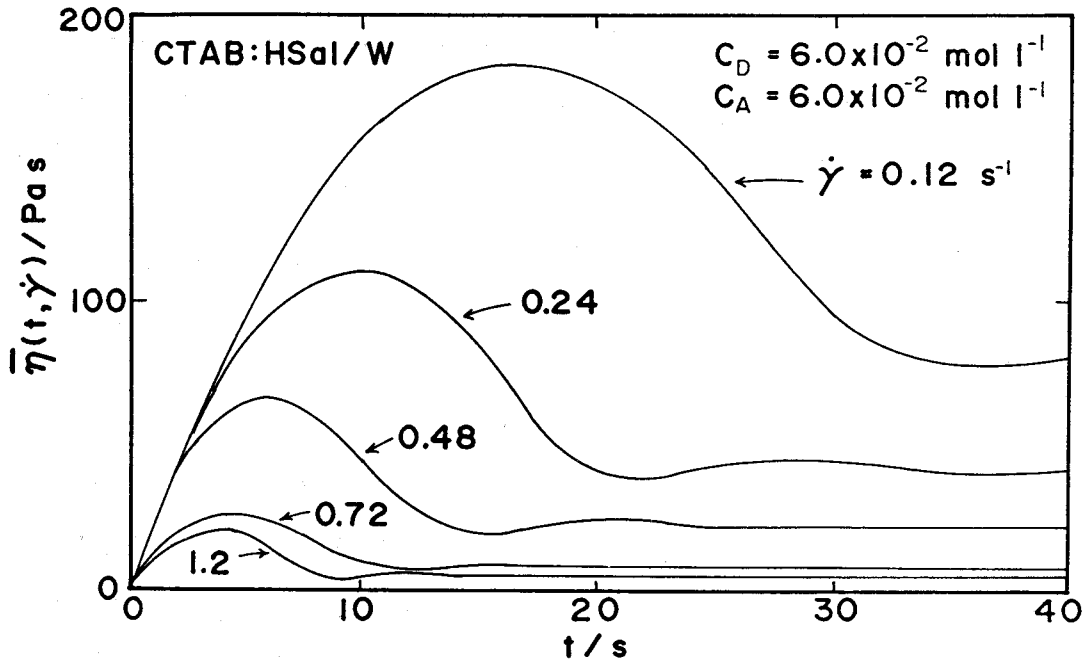

Figure VI-14. Viscosity growth function $\bar{\eta}(t,\dot{\gamma})$ at inception of steady shear flow at various rate of shear $\dot{\gamma}$ for the solution with $C_D = C_A = 6.0 \times 10^{-2}$ mol l^{-1}.

VI-4-4 Stress Relaxation after Cessation of Steady Shear Flow

Figure VI-15 shows stress relaxation behavior after cessation of steady shear flow at various shear rates for the solution with $C_D = C_A = 6.0 \times 10^{-2}$ mol l^{-1}. When the shear rate is relatively low ($\dot{\gamma} \leqq 0.36\ s^{-1}$), the slope of the reduced relaxation functions $\sigma_C(t,\dot{\gamma})/\sigma_C(0,\dot{\gamma})$ vs t in the long time side is the same. The time constant for the decay functions corresponds to the characteristic time τ_1 for the slow mode. The reduced relaxation functions at higher shear rates ($\dot{\gamma} \geqq 0.48\ s^{-1}$) also possess a straight portion in the long time side. However, the slope becomes steeper with increasing shear rate. For other CTAB:HSal/W solutions, similar results were observed.

As described in Chapter VI-3-4, the reduced relaxation functions after cessation of steady shear flow for the CTAB:NaSal/W systems were expressed as a sum of two exponential functions as given in eq VI-3 with i=1 and 2. For the CTAB:NaSal/W systems, the times τ_α and τ_β were independent of, but the fraction P_α, dependent on the shear rate. The reduced relaxation functions of the present CTAB:HSal/W systems, however, could not be expressed in the same manner because not only the fraction P_α but also the time τ_α are dependent on the shear rate in the range of $\dot{\gamma} \geqq 0.48\ s^{-1}$.

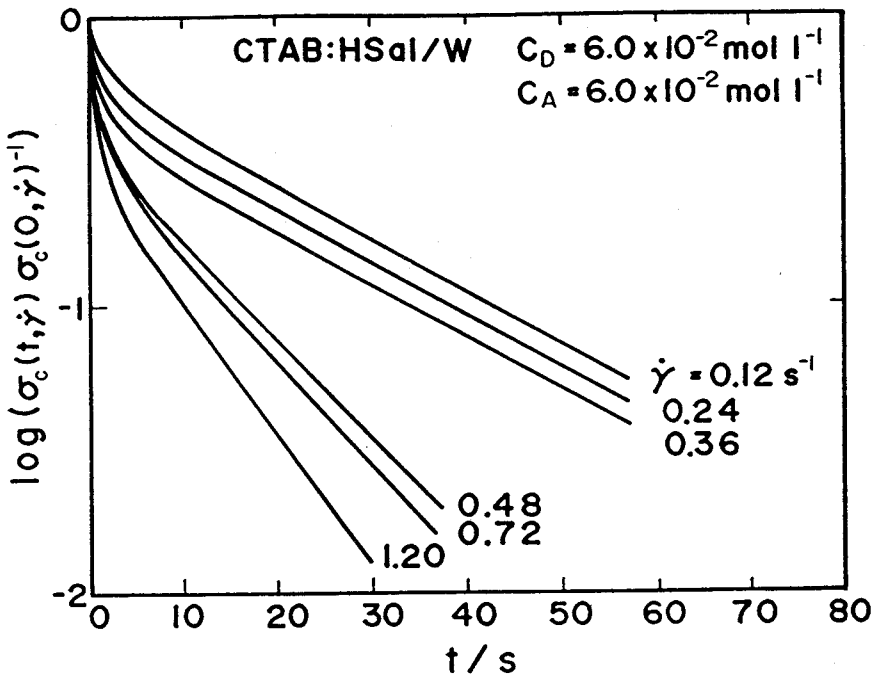

Figure VI-15. Stress relaxation function $\sigma_C(t,\dot{\gamma})/\sigma_C(0,\dot{\gamma})$ after cessation of steady shear flow at various rate of shear for the solution with C_D = 6.0 x 10^{-2} and C_A = 6.0 x 10^{-2} mol l^{-1}.

VI-5 Discussion

VI-5-1 Comparison of the Nonlinear Behavior of CTAB:NaSal/W, CTAB:HSal/W and Concentrated Polymer Solutions

Here, we compare the features of the nonlinear viscoelastic behavior of the micellar systems with those of concentrated polymer systems. Figure VI-16 schematically summarizes the features of the nonlinear stress relaxation moduli $G(t,\gamma)$ and the viscosity growth function $\overline{\eta}(t,\dot{\gamma})$ for concentrated polymer solution.

For concentrated polymer systems, the feature of the stress relaxation modulus at finite (large) strains has been well established by Osaki et al.[2,4] Polymer systems exhibit broad box-type relaxation spectra with their terminal relaxation modes strongly dependent on the molecular weight M and polymer concentration C. The nonlinear relaxation moduli are strongly dependent on strain as well: Their strength decreases, but the relaxation times stay unchanged with increasing amplitude of strain as schematically shown in Figure VI-16A.[2,4,7]

For polymer systems, the nonlinear relaxation modulus of the terminal mode can be expressed as

$$G(t,\gamma) = h(\gamma)G(t) \qquad \text{(VI-7)}$$

The function $h(\gamma)$ is however independent of the molecular weight M and polymer concentration C over a wide range.[2,4,7] The molecular theory proposed by Doi and Edwards successfully

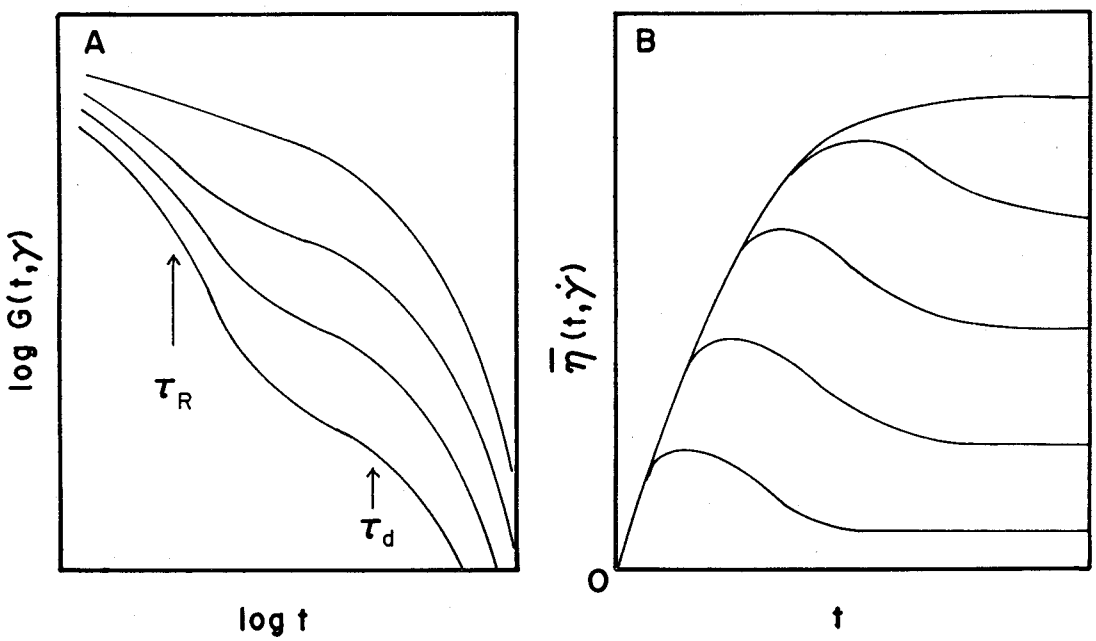

Figure VI-16. Schematic representation of the typical nonlinear behavior of concentrated polymer systems.[2,4,7] (A); the stress relaxation modulus $G(t,\gamma)$. Strain γ increases from top to bottom. (B); the viscosity growth function $\bar{\eta}(t,\dot{\gamma})$. Rate of shear $\dot{\gamma}$ increases from right to left.

explained this feature of the polymer system.[4,7] The solid line in the previous Figure VI-12 represent the prediction of the Doi-Edwards theory[4,7] for the function $h(\gamma)$.

According to the Doi-Edwards theory, topological constraints around a primitive polymer chain caused by other surrounding chains is represented as a tube, and stress is calculated from the amount of deformed part of the tube.[7] Situations of the primitive chain and the tube under the stress relaxation after large step strain are schematically illustrated in Figure VI-17.[7] Before deformation the conformation of the primitive chain is in equilibrium. After deformation the primitive chain is affinely deformed immediately. After characteristic time τ_R, the primitive chain contracts along the tube and recovers the equilibrium contour length. After another time τ_d, the primitive chain leaves the deformed tube by reptation. The oblique lines in Figure VI-17 indicates the deformed part of the tube. The times τ_R and τ_d under the nonlinear stress relaxation modulus $G(t,\gamma)$ are illustrated schematically in Figure VI-16A.

The viscosity growth function $\overline{\eta}(t,\dot{\gamma})$ of concentrated polymer systems monotonously increases with time in the Newtonian flow region at low shear rates, but it exhibits a maximum and approaches to the steady state value in the non-Newtonian flow region at high shear rates. The $\overline{\eta}(t,\dot{\gamma})$ of concentrated polymer systems rarely show any tendency of damping oscillation. The time t_M corresponding to the stress overshoot maximum decreases in proportion to $\dot{\gamma}^{-1}$.[8-10] These

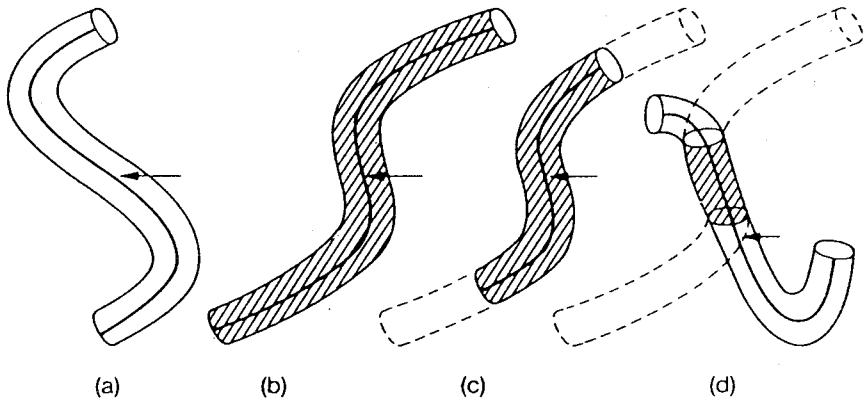

Figure VI-17. Schematic illustrations representing the primitive polymer chain and its tube under the stress relaxation after large step strain.[7] (a); $t = -0$ (before deformation), (b); $t = +0$ (at deformation), (c); $t \cong \tau_R$, (d); $t \cong \tau_d$.

features for the $\overline{\eta}(t,\dot{\gamma})$ of concentrated polymer systems are described schematically in Figure VI-16B. The features of the $G(t,\gamma)$ and rate-dependent t_M of the polymer systems are well described with a BKZ type constitutive equation with a strain-dependent memory function.[11,12]

As seen in Figure VI-2, the $G(t,\gamma)$ of the type III-1 CTAB:NaSal/W systems increases with γ in quite contrast to that of a concentrated polymer system described schematically in Figure VI-16A. On the other hand, the $G(t,\gamma)$ of the type III-2 CTAB:NaSal/W systems always decreases with γ as seen in Figure VI-3. This behavior is qualitatively similar to that of the polymer system. However, the γ dependence of their $G(t,\gamma)$ is weaker than that of the polymer systems. Both of the two CTAB:NaSal/W systems have a much wider range of γ where the $G(t,\gamma)$ is independent of γ than the polymer systems.

For the type III-2 CTAB:NaSal/W systems, the time t_M approaches to the relaxation time τ_m with increasing $\dot{\gamma}$ as seen in Figure VI-6. These features of the weak γ dependence of $G(t,\gamma)$ and the rate-independent t_M for the type III-2 CTAB:NaSal/W systems may be related to the constitutive equation with a rate-dependent memory function, which has extensively been studied but has not been found to fit well to any real systems.[13-15]

Now we turn our attention to the CTAB:HSal/W systems. When one compares the typical γ dependent $G(t,\gamma)$ of the CTAB:HSal/W systems shown in Figure VI-10 is compared with

that of a concentrated polymer system shown in Figure VI-16, one finds that the γ dependent $G(t,\gamma)$ of the former qualitatively resembles that of the concentrated polymer system. However, their quantitative features are quite different. Obviously, as seen in Figure VI-12 the γ dependence of $h(\gamma)$ of the CTAB:HSal/W system is much stronger than the prediction of the Doi-Edwards theory[7] that well represents the concentrated polymer systems.

As described previously, according to the Doi-Edwards theory the origin of the nonlinear stress relaxation is a contraction process of the primitive chain, in other words, the presence of terminals in polymer molecules. However, in the CTAB:HSal/W systems with the ratio $C_A C_D^{-1}$ of about 1, the thread-like micelles would not have terminals so that the systems can not relax with the contraction nor the reptation processes like polymer systems.

The time t_M of the CTAB:HSal/W systems also decreases with increasing $\dot{\gamma}$ as seen in Figure VI-14. However, the rate $\dot{\gamma}$ dependence of t_M is weaker than that of the polymer systems. These features of the $G(t,\gamma)$ and t_M of the CTAB:HSal/W systems mean that the suitable constitutive equation must contain a strain-dependent memory function, which is different from the strain-dependent memory function good for polymer systems.

VI-5-2 Rate-Dependent Nonlinear Behavior of the CTAB:NaSal/W Systems

In the previous Chapter IV, we modified the quasi-network model proposed by Yamamoto[16] and Lodge[17,18] to describe the linear viscoelastic behavior with a single relaxation mode of the CTAB:NaSal/W entangled micellar solutions. We called it the type III behavior. For the model, we assumed that relaxation of its entanglement network takes place by mutual passing through of the thread-like micelles at the entanglement sites as a result of the reaction between micelle subunits M to form an entanglement site E with the rate constants dependent only on the concentration C_S^* of free salicylate ions in the bulk aqueous phase. We thus obtained a memory function $\mu(t-t')$ of the form,

$$\mu(t-t') = L \exp\{-(t-t')/\tau\} \qquad \text{(VI-8a)}$$

with

$$L = \{K/(2\tau)\}[M]^2 \qquad \text{(VI-8b)}$$

and

$$\tau_m = k_3^{-1}(C_S^*)^{-n} \qquad \text{(VI-8c)}$$

as defined in eq IV-12.[18] Supposing L is independent of either the strain γ or the rate of shear $\dot{\gamma}$, we obtain from

this eq VI-8 a viscoelastic functions never show the nonlinear viscoelastic behavior. Thus, L should be dependent on γ or $\dot{\gamma}$ or both.

If we assume that the front factor L of the memory function depends only on shear rate, because as we pointed out in the preceding section a rate-dependent memory function appears to be more adequate to the CTAB:NaSal/W systems. Then, eq VI-8 can be written as follows.[13,18]

$$\mu\,(t-t';\dot{\gamma}\,) = L(\dot{\gamma}\,)\,\exp\{-(t-t')/\tau\,\} \qquad \text{(VI-9)}$$

From this eq VI-9, we can calculate the stress growth function $\overline{\eta}\,(t,\dot{\gamma}\,)$ and the stress relaxation function $\sigma_C(t,\dot{\gamma}\,)/\sigma_C(0,\dot{\gamma}\,)$ after cessation of steady shear flow as functions of time t and shear rate $\dot{\gamma}$.

However, the calculated $\overline{\eta}\,(t,\dot{\gamma}\,)$ can not reproduce at all the unique experimental results such as damping oscillatory decay shown in Figures VI-6 and VI-7. The calculated $\sigma_C(t,\dot{\gamma}\,)/\sigma_C(0,\dot{\gamma}\,)$ also can not reproduce the two-mode relaxation process with τ_α and τ_β shown in Figure VI-8. Although the nonlinear viscoelasticity of the type III-2 CTAB:NaSal/W systems is essentially rate-dependent, the memory function of the systems can not be expressed in such a simple form as eq VI-9.

VI-5-3 Strain-Dependent Nonlinear Behavior of the CTAB:HSal/W Systems

The CTAB:HSal/W systems showed unique nonlinear viscoelastic behavior which is quite different from that of the CTAB:NaSal/W systems and also from concentrated polymer systems as described previously.

Under stress relaxation measurements with sufficiently small strains the systems exhibited a linear stress relaxation modulus G(t) as described in Chapter V.

$$G(t) = G_1 \exp\{-t/\tau_1\} + G_2 \exp\{-t/\tau_2\} \qquad \text{(VI-10)}$$

However, the relaxation modulus of the CTAB:HSal/W systems showed pronounced strain γ dependence with increasing γ in contrast to the CTAB:NaSal/W systems as seen in Figures VI-11 and VI-12.

If we assume that the memory function of these systems depends on strain γ but not on the shear rate, we can write it as $\mu(t;\gamma)$. According to the general theory,[2,15] the memory function can be evaluated from the relaxation modulus $G(t,\gamma)$ as

$$\mu(t;\gamma) = - \partial G(t,\gamma)/\partial t \qquad \text{(VI-11)}$$

The $G(t,\gamma)$ for the CTAB:HSal/W systems already has given as eq VI-10 for the linear region and eq VI-5 for the nonlinear region. Then, we can obtain memory functions for each regions

with eq VI-11 as follows.

$$\mu(t) = \{G_1/\tau_1\}\exp(-t/\tau_1) + \{G_2/\tau_2\}\exp(-t/\tau_2) \qquad \text{(VI-12)}$$

for the linear region.

$$\mu(t;\gamma) = \{G_1(\gamma)/\tau_1\}\exp(-t/\tau_1) + k \qquad \text{(VI-13)}$$

$$\begin{cases} k = K(\gamma) & t < \{G_N^0 - G_1(\gamma)\}/K(\gamma) \\ k = 0 & t \geq \{G_N^0 - G_1(\gamma)\}/K(\gamma) \end{cases}$$

for the nonlinear region. When the system belongs to the nonlinear regime, G_1 of the first term in eq VI-12 has strong γ dependence and the second term is replaced by the constant k as eq VI-13. At relatively large strain and for $t < \{G^0 - G_1(\gamma)\}/K(\gamma)$, the first term in above eq VI-13 might have little contribution. Then, the memory function $\mu(t;\gamma)$ should be a constant k. This implies that the stimulation caused the CTAB:HSal/W systems through sudden imposition of the strain γ do not fade out for $t < \{G^0 - G_1(\gamma)\}/K(\gamma)$. This feature is characteristic of the CTAB:HSal/W systems.

The relaxation mechanisms in the thread-like micellar systems should be the processes involving chemical reactions which break down the entanglement junctions, as discussed in Chapters IV and V. For the present CTAB:HSal/W systems, when the strain is small enough such as in the dynamic measurement with small strain amplitudes or in the stress relaxation

measurement under very small strain, the systems may have the rate constant k_e ($= 1/\tau_1$) for the reaction of entanglement scission. Then, the memory function decays in the first order kinetics with the constant k_e.

On the other hand, when the CTAB:HSal/W systems are subjected to large strain and are strongly deviated from the equilibrium state, the memory function presumably becomes $K(\gamma)$ for $0 < t < \{G^0 - G_1(\gamma)\}/K(\gamma)$. Then, the CTAB:HSal/W systems recover the equilibrium state quickly, or almost elastically.

According to the discussion in Chapter V, the rate constant k_e is proportional to $C_D{}^2 C_A{}^{*5}$. This suggested that the frequency of collisions or contacts between the thread-like micelles govern the slow relaxation mode of τ_1. The number of collisions or contacts between the micelles might suddenly increase at the start (t=0) of the relaxation measurement under the large strain γ, and some of the entanglement junctions might be broken down by the contacts or the collisions. This process might be the cause of the rapid decrease of $G_1(\gamma)$ with γ as seen Figure VI-12.

Interestingly, the thread-like micellar systems alter their nonlinear viscoelastic behavior from rate-dependent to strain-dependent one when the structure of their micelles is changed from a 1:1 complex between cetyltrimethylammonium cations CTA^+ and salicylate anions Sal^- to one between CTA^+ and salicylic acid HSal molecules.

REFERENCES

1) Tamura, M.; Kurata, M.; Osaki, K.; Einaga, Y.; Kimura, S. Bull. Ins. Chem. Res., Kyoto Univ. 1971, 49, 43.

2) Ferry, J. D. Viscoelastic Properties of Polymers 3rd edn; Wiley: New York, 1980.

3) Cox, P. W.; Merz, E. H. J. Polym. Sci. 1958, 28, 619.

4) Osaki, K.; Doi, M. Polym. Eng. Rev. 1984, 4, 35.

5) Huppler, J. D.; Macdonald, I. F.; Ashare, E.; Spriggs, T. W.; Bird, R. B.; Holmes, L. A. Trans. Soc. Rheol. 1967, 11, 181.

6) Malkin, A. Ya.; Yarlykov, B. V.; Virogradov, G. V. Rheol. Acta 1970, 9, 323.

7) Doi, M.; Edwards, S. F. The Theory of Polymer Dynamics; Oxford University Press: Oxford, 1986.

8) Zapas, L. J.; Phillips, J. C. J. Res. Natl. Bur. Stand. 1971, 75A, 33.

9) Chen, I-J.; Bogue, D. C. Trans. Soc. Rheol. 1972, 16, 59.

10) Meissner, J. J. Appl. Polym. Sci. 1972, 16, 59.

11) Berstein, B.; Kearsley, E. A.; Zapas, L. J. Trans. Soc. Rheol. 1963, 7, 391.

12) Berstein, B.; Kearsley, E. A.; Zapas, L. J. Trans. Soc. Rheol. 1965, 9, 27.

13) White, J. L. Rubber Chem. Technol. 1969, 42, 257.

14) Bird, R. B.; Armstrong, R. C.; Hassager, O. Dynamics of Polymeric Liquids Vol.1; Wiley: New York, 1977.

15) Yamamoto, M. Buttai no Henkeigaku; Seibundoshinkousha: Tokyo, 1962.

16) Yamamoto, M. J. Phys. Soc., Japan 1956, 11, 413.

17) Lodge, A. S. Trans. Faraday Soc. 1956, 52, 120.

18) Lodge, A, S. Elastic Liquids; Academic Press: London, 1964.

Chapter VII

Summary and Conclusion

In this thesis, unique viscoelastic properties of aqueous solutions of cetyltrimethylammonium bromide (CTAB) with sodium salicylate (NaSal) or with salicylic acid (HSal) were studied in detail in conjunction with the structure of the thread-like micelles formed in the systems. The principal results of this study and the conclusion derived are summarized as follows.

In Chapter III, electron microscopic observation was carried out on CTAB:NaSal/W and CTAB:HSal/W systems. When the concentration C_S of NaSal (or C_A of HSal) higher was than the concentration C_D of CTAB in the systems, we found long and stable rod-like or thread-like micelles densely entangling. Spherical micelles and/or short thread-like micelles were found in the systems with C_A lower than C_D. The former systems exhibited strong viscoelasticity, whereas the latter showed low viscosity.

^1H NMR measurement on CTAB:NaSal/D_2O and CTAB:HSal/D_2O systems was carried out with varying concentrations C_D of CTAB, C_S of NaSal or C_A of HSal, respectively, to determine the structure of the micelles and the concentration C_S^* of free salicylate ions (Sal^-) or C_A^* of free salicylic acid (HSal) molecules in these systems. The thread-like micelles

of the CTAB:NaSal/W systems are 1:1 complexes between cetyltrimethylammonium cation (CTA^+) and Sal^-. The relation $C_S^* = C_S - C_D$ was obtained in the condition $C_S > C_D$. On the other hand, the thread-like micelles of the CTAB:HSal/W systems are 1:1 complexes between CTA^+ and HSal, and HSal assumes two different immobilized states in the thread-like micelles: One is the state equivalent to that occupied by Sal^- in the CTAB:NaSal micelles, and another has the location of much deeper position in the micelles than that of the former. C_A^* also approaches the relation $C_A^* = C_A - C_D$ with increasing C_A beyond C_D.

In Chapter IV, dynamic viscoelastic properties of CTAB:NaSal/W systems were examined with varying the concentrations C_D of CTAB and C_S of NaSal. The viscoelastic behavior was classified into tree types. When $C_D >> C_S$ (type I), the systems behaved like low-molecular-weight polymer solutions without entanglement. When $C_D > C_S$ (type II), they behaved like semi-dilute or concentrated polymer systems with full entanglements. When $C_D \leqq C_S$ (type III), they behaved just like a Maxwell model having only one relaxation time τ_m and plateau modulus G_N^0. The τ_m varied complicatedly with a ratio $C_S C_D^{-1}$. The G_N^0 was not dependent on C_S but was proportional to $C_D^{2.2}$. The relaxation time τ_m was dependent only on C_S^* but independent of C_D. Thus, the factor controlling τ_m was C_S^*. This finding implied that the mechanism for the entanglement relaxation of the type III

micellar systems was not controlled through the diffusion of the micelles along their contour, as opposed to polymer systems. Consideration based on a quasi-network model led to an idea that the free Sal^- is behaving as a catalyst for the disentanglement reaction in the type III behavior.

In Chapter V, dynamic viscoelastic properties of CTAB:HSal/W systems were examined with varying the concentrations C_D of CTAB and C_A of HSal. Effects of adding NaBr were also examined. The results were compared with those of the CTAB:NaSal/W systems described in the Chapter IV. Under the condition in which thread-like micelles of CTAB:HSal were fully entangling, the systems exhibited two distinct relaxation modes, while under the same condition the CTAB:NaSal/W systems were approximated by a Maxwell model with G_N^0 and τ_m. The slow mode, specific to the CTAB:HSal/W systems, has the relaxation time $\tau_1 \propto C_A^{*-5} C_D^{-2}$ which becomes shorter with increasing C_D; and the fast mode, the relaxation time $\tau_2 \propto C_A^{*-2} C_D^{0}$, similar to the τ_m of the CTAB:NaSal/W systems. The corresponding relaxation strengths G_1 and G_2 were approximately $(G_1 + G_2) \cong G_N^0 \propto C_D^{2.2} C_A^0$. Addition of NaBr produced little effects on the CTAB:NaSal/W systems, but led to significant reduction in the relaxation time of the CTAB:HSal/W systems, especially of their slow mode, which merged to the fast mode with increasing NaBr concentration.

In Chapter VI, the nonlinear viscoelastic behavior of the CTAB:NaSal/W and CTAB:HSal/W systems was examined. The relaxation modulus $G(t,\gamma)$ for the CTAB:NaSal/W systems did not exhibit γ dependence for a wide range of γ (< 2). The nonlinear behavior varied with the concentration C_S^* of free Sal^-. At low C_S^*, $G(t,\gamma)$ increased with increasing γ. On the other hand, at high C_S^*, $G(t,\gamma)$ slightly decreased with increasing γ. The stress response function at inception of steady shear flow exhibited a pronounced overshoot and damped oscillatory before reaching the steady state value. The viscoelastic behavior of this micellar system could not be described with the integral constitutive equation with a strain-dependent memory function, which is suitable for the polymer system.

The relaxation modulus $G(t,\gamma)$ for the CTAB:HSal/W systems was strongly dependent on γ even at small γ in quite contrast to that of CTAB:NaSal/W. $G(t,\gamma)$ was rapidly decreased with γ. At relatively high γ, $G(t,\gamma)$ decreased in proportion to time t in the initial stage, and then decayed in an exponential manner with the relaxation time τ_1 in the long time end. This feature is qualitatively similar to that of concentrated polymer systems, but γ dependence of $G(t,\gamma)$ of this CTAB:HSal/W was stronger than that of the polymer systems. This strange strain-dependent nonlinear behavior of the CTAB:HSal/W systems would be attributed by the relaxation mechanism with the relaxation time τ_1 which was never observed in the CTAB:NaSal/W systems.

LIST OF PUBLICATIONS

The contents of this thesis have been published or will be published in the following original papers:

1. Shikata, T.; Sakaiguchi, Y.; Urakami, H.; Tamura, A.; Hirata, H., "Enormously Elongated Cationic Surfactant Micelles Formed in CTAB-Aromatic Additive Systems", J. Colloid Interface Sci., 1987, 119, 291.
2. Sakaiguchi, Y.; **Shikata, T.**; Urakami, H.; Tamura, A.; Hirata, H., "Electron Microscopic Observation on the Elongated Micelle in Cationic Surfactant with Some Aromatic Additives", J. Microsc., 1987, 36, 168.
3. Sakaiguchi, Y.; **Shikata, T.**; Urakami, H.; Tamura, A.; Hirata, H., "Electron Microscopic Study of Viscoelastic Cationic Surfactant Systems", Colloid Polym. Sci., 1987, 265, 750.
4. Shikata, T.; Hirata, H.; Kotaka, T., "Micelle Formation of Detergent Molecules in Aqueous Media: Viscoelastic Properties of Aqueous Cetyltrimethylammonium Bromide Solutions", Langmuir, 1987, 3, 1801.
5. Shikata, T.; Hirata, H.; Kotaka, T., "Micelle Formation of Detergent Molecules in Aqueous Media 2: Role of Free Salicylate ions on Viscoelastic properties of Aqueous Cetyltrimethylammonium Bromide-Sodium Salicylate Solutions", Langmuir, 1988, 4, 354.

6. Shikata, T.; Hirata, H.; Takatori, E.; Osaki, K., "Nonlinear Viscoelastic Behavior of Aqueous Detergent Solutions", J. Non-Newtonian Fluid Mech., 1988, 28, 171.
7. Shikata, T.; Hirata, H.; Kotaka, T., "Micelle Formation of Detergent Molecules in Aqueous Media 3: Viscoelastic Properties of Aqueous Cetyltrimethylammonium Bromide-Salicylic Acid Solutions", Langmuir, submitted.
8. Shikata, T.; Hirata, H.; Kotaka, T., "Micelle Formation of Detergent Molecules in Aqueous Media 4: Influence of Addition of NaBr on Viscoelastic Properties of Aqueous Cetyltrimethylammonium Bromide Solutions", in preparation for publication.
9. Shikata, T.; Hirata, H.; Takatori, E.; Osaki, K., "Nonlinear Viscoelastic Behavior of Aqueous Cetyltrimethylammonium Bromide-Salicylic Acid Solutions", in preparation for publication.

Other Related Papers

1. Shikata, T.; Kotaka, T., "State of Dispersion and Rheological Properties of Silica-Gel/Polyoxyethylene System", Nihon Reoroji Gakkaishi, 1983, 11, 82.
2. Shikata, T.; Kotaka, T., "Rheopexy of Silica Gel/Silicone Oil Systems", Nihon Reoroji Gakkaishi, 1984, 12, 98.
3. Shikata, T.; Hirata, H., "Fluorescence Behavior of Aqueous Cetyltrimethylammonium Bromide-Sodium Salicylate Solutions", in preparation for publication.